The transcriptional regulator SpxA1 impacts the virulence, morphology, and redox response of *Listeria monocytogenes*

Monica R. Cesinger

A dissertation
submitted in partial fulfillment
of the requirements for the degree of

Doctor of Philosophy

University of Washington
2022

Reading Committee:
Michelle Reniere, Chair
Carrie Harwood
Joseph Mougous

Program authorized to offer degree:
Microbiology

©Copyright 2022
Monica R. Cesinger

University of Washington

Abstract

The transcriptional regulator SpxA1 impacts the virulence, morphology, and redox response of *Listeria monocytogenes*

Monica R. Cesinger

Chair of Supervisory Committee:
Michelle Reniere
Department of Microbiology

Bacterial pathogens require precise transcriptional regulation to effectively cause disease. Using a complex regulatory strategy, the model intracellular pathogen *Listeria monocytogenes* grows successfully as a saprophyte and can rapidly initiate an infectious lifecycle upon ingestion by a host. This dissertation presents a comprehensive analysis of the redox responsive transcriptional regulator SpxA1, which is required for both *L. monocytogenes* virulence and environmental growth. Whole-cell proteomics and transcriptomics provide evidence that SpxA1 regulates peroxidase abundance, heme biosynthesis, and motility. Subsequent experiments reveal that SpxA1 directly regulates genes via a conserved promoter motif and this interaction is necessary for aerobic growth. Our data further suggest that SpxA1-regulated heme biosynthesis and catalase are essential for aerobic growth in rich broth but dispensable for virulence. While investigating the role of SpxA1 in virulence, we discovered that the Δ*spxA1* mutant forms elongated cells with inappropriate frequencies and distributions of division septa. However, critical proteins involved in cell wall biosynthesis, cell division, and DNA damage-regulated elongation were unchanged between wt and Δ*spxA1*, a result that diverges from previously described homologs. Finally, we demonstrated that both elongation and decreased motility impact the phagocytosis of Δ*spxA1*. Together, these results describe a novel role for the highly conserved SpxA1 regulator in *L. monocytogenes*.

Table of Contents

Acknowledgements

I have many people to thank for their support. First, thank you to my advisor Dr. Michelle Reniere for being my mentor and challenging me to grow as a scientist. I am so grateful to the Reniere lab for their empathy and support through thick and thin. I am lucky to have met not only remarkably intelligent scientists in this lab but also friends for life.

I would also like to thank the UW community, including my thesis committee and reading committee for providing useful scientific feedback. In particular, thank you to Dr Michelle Reniere, Dr. Paul Wiggins and Dr. Carrie Harwood for writing many letters of recommendation. Thank you to the UW Micro labs for generosity with advice, reagents, and lab equipment. For assistance with specific experiments, thank you to Dr. Qing Tang, Dr. Yaxi Wang, Dr. Andi Liu, Emily Pruit, and Dr. Ellen Lavoie. An especially big thank you to Dr. Maureen Thomason, Amy Gundlach, and Andrea Pardo for keeping the department running. Thank you to the Merrikh lab for teaching me that change is not only possible but can be evolutionarily beneficial. Finally, I couldn't ask for a better graduate student family: Rochelle, Shivam, Neel, Lyndsey, Robin, Brittany, and many others.

I would also like to thank my community outside of UW. Scott, Jenna, Sean, and Ethan, thank you for literally living with me through all the highs and lows. Thanks also to Ben, Christie, Aleena, and rest of my Seattle family for making this place home. Especially big thanks to Justin for your whole deal! Thank you to Dr. Sheryl Dickman, Dr. Steve Cook, Penney Sconzo, Dr. Heidi Gilpin, and Dr. Alix Purdy for always believing in me as a scientist. Thank you to Rainer for all the chaos, anarchy, and fractals, and a big thanks to all the other out-of-town friends and family who brightened my time in Seattle. Thank you to my mom Janna, whose creativity and resiliency makes thinking outside the box look easy, and thank you to my dad Steve for being my strongest, longest, and loudest cheerleader. Finally, thank you Grandma Joey and Great-Grandma Wagner for always looking over me.

This work was funded by NIH R01 A132356, the UW MBTG fellowship (NIH T32GM008268), and the Howard Hughes Medical Institute through the James H. Gilliam Fellowship for Advanced Study (GT11030). The funders had no role in study design, data collection and interpretation, or the decision to submit the work for publication.

List of Tables and Figures

Chapter 6

Chapter 1: Background

Introduction to *Listeria monocytogenes*

The gram-positive bacterium *Listeria monocytogenes* is the causative agent of the foodborne disease listeriosis and a well-described model intracellular pathogen. *Listeria monocytogenes* lives ubiquitously as an environmental saprophyte until consumed by a susceptible mammalian host, where it is taken up into host cell cytosol and initiates a well characterized intracellular lifecycle (1). While most well-studied for its role in human disease, *L. monocytogenes* can be harbored by at least 37 species of mammals, including common pets, food production animals, laboratory model organisms, and several species found only in the wild (2). *L. monocytogenes* has also been isolated from 17 different avian species as well as several species of fish. First described in 1926 in a laboratory outbreak in rabbits and guinea pigs, the role of *L. monocytogenes* as the etiological factor of listeriosis has been investigated for nearly a century (3). A majority of listeriosis cases are caused by the ingestion of contaminated food such as deli meat, soft cheeses, and fresh vegetables and fruits, although other forms of transmission have been reported (4). *L. monocytogenes* can survive in these ready-to-eat foods partially because this organism tolerates high salt and heat and can grow in anaerobic and refrigerated environments with ease (5).

While not a common source of food borne illness, *L. monocytogenes* causes one of the deadliest foodborne infections. Immunocompetent individuals typically experience non-invasive infections resulting in gastroenteritis. However, listeriosis can manifest as bacteremia and meningitis in immunocompromised individuals, as well as result in maternal neonatal infection and spontaneous abortion (6). Over 80% of pregnant people

infected with *L. monocytogenes* experience major neonatal or fetal complications, and only 39% of neurolisteriosis patients survive and fully recover (7). The rate of listeriosis incidence in the United States has remained stable since the early 2000s, emphasizing the need for new breakthroughs in *L. monocytogenes* outbreak control and treatment (8).

The *L. monocytogenes* intracellular life cycle

The success of *L. monocytogenes* as a food borne pathogen has been attributed to its ability to rapidly rewire transcriptional programs upon transitioning from saprophyte to pathogen. The virulence factors employed by *L. monocytogenes* during its intracellular lifecycle have been extensively studied (Fig. 1) (5). Once ingested, *L. monocytogenes* is phagocytosed by professional phagocytes or induces its own uptake into non-phagocytic cells. *L. monocytogenes* transiently resides in the highly oxidized phagosome and secretes the pore-forming toxin listeriolysin O (LLO) (9). This protein damages the phagosomal membrane and allows bacteria to escape into the highly reduced host cytosol where *L. monocytogenes* rapidly replicates. Upon entering the cytosol, *L. monocytogenes* produces the surface-associated protein ActA, which recruits host actin and propels the bacteria throughout the cell and into neighboring cells (10). This intracellular lifecycle requires that *L. monocytogenes* adapt quickly to changing conditions, including the drastic change from the oxidizing phagosome to the reduced cytosolic environment within as little as 30 minutes. While genetic data suggest a link between redox sensing and virulence gene regulation, the molecular mechanisms by which *L. monocytogenes* senses the host environment and adapts appropriately are not well-understood (11–13).

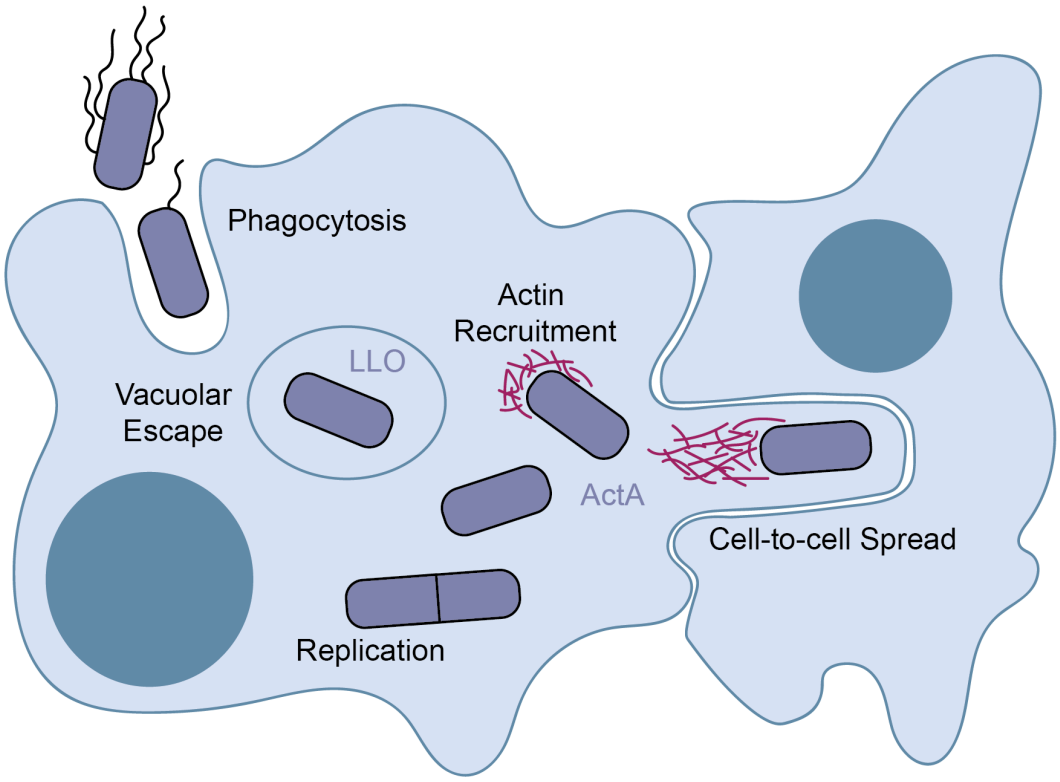

Figure 1. The intracellular lifecycle of *L. monocytogenes*. In order to cause disease, *L. monocytogenes* must carry out a highly regulated intracellular lifecycle which begins with either receptor mediated entry or phagocytosis into a host cell (10). Upon entry, *L. monocytogenes* is enclosed in a vacuole, where it can experience a highly oxidative environment with increased levels of reactive oxygen and nitrogen species. *L. monocytogenes* can escape the vacuole in under 15 minutes by secreting Listeriolysin O (LLO), a cholesterol dependent cytolysin. Once in the cytosol, *L. monocytogenes* simultaneously begins replicating and producing the surface associated protein ActA, which can recruit host actin. *L. monocytogenes* can take advantage of a polarized actin cloud to push itself around host cytosol and initiate cell-to-cell spread. Upon entering a neighboring cell, this intracellular life cycle begins again.

Regulation of virulence in *L. monocytogenes*

To successfully disseminate and colonize a host, *L. monocytogenes* requires precise regulation of several critical virulence factors. The “master virulence regulator” of these factors is PrfA, which directly activates 9 virulence factors essential for pathogenesis, including the internalins necessary for receptor-mediated endocytosis (InlA, InlB, and InlC), phagocytic vacuole damaging factors LLO, PclA, and PclB, sugar

uptake permease Hpt, and the inducer of host actin polymerization ActA. (14). Accordingly, precise activation and regulation of PrfA are critical to virulence as well. A *prfA* deletion mutant is attenuated four logs in a mouse model, while constitutive PrfA activation significantly decreases growth rate in broth (15, 16). Regulation of PrfA activation is multifactorial; activation requires binding to reduced glutathione as well as the reduction of four cysteine residues to bind DNA. Thus, the transcription of the major proteins involved in execution of the *L. monocytogenes* lifecycle is likely dependent in part on the redox status of the bacterial cytosol where PrfA is found (12, 17). However, little is known about how changes to the internal redox state of bacterial cytosol might influence expression of PrfA-regulated genes in conditions of endogenous or exogenous redox stress.

One of the hallmarks of *L. monocytogenes* is the relatively unique capacity of this pathogen to enter non-phagocytic cells by coopting cellular receptor-dedicated endocytosis machinery. *L. monocytogenes* produces over 25 proteins called internalins (18). Two of these proteins, InlA and InlB, have been extensively studied for their roles in entry via interactions with the host receptors E-cadherin and the receptor for hepatocyte growth factor Met (19). Met is ubiquitously expressed, leading to InlB-mediated endocytosis in a wide variety of cell types. E-cadherin, on the other hand, is only expressed in a limited set of epithelial cell types, resulting in a stringent cell tropism for InlA. Furthermore, InlA interaction is specific to a set of E-cadherin orthologs. InlA binds readily to the E-cadherin of humans, dogs, gerbils, rabbits, and Guinea pigs, but not with that of mice or rats, decreasing the efficiency of InlA-mediated uptake in these species (18).

Once in host cytosol, *L. monocytogenes* recruits and polarizes host actin using the virulence factor ActA, which previous research determined is produced less in an *spxA1*-deficient mutant (13). The ActA protein is anchored to the bacterial membrane and exposed on the *L. monocytogenes* surface, where its polar distribution dictates the direction of actin comet trail formation. While its role in cell-to-cell spread has been studied most extensively, ActA has been proposed to contribute to bacterial attachment and entry, escape from the phagosome, and avoidance of cytosolic autophagy (20). ActA is essential for cell-to-cell spread, and a Δ*actA* mutant will remain sequestered in the cytosol of an invaded cell and is completely avirulent. Consequently, proper ActA regulation and distribution is also critical for *L. monocytogenes* virulence.

The master regulator PrfA is responsible for the rapid induction of *actA* transcription in host cytosol. PrfA activation of genes is dependent on PrfA abundance, promoter sequence specificity (presence of a PrfA box) and activation via cofactor binding (1, 11). The activation of PrfA requires allosteric binding to reduced glutathione, but this can be bypassed by a version of PrfA, PrfA*, which lock the protein in the active confirmation (16). Bacteria producing PrfA* express *actA* and other virulence factors to a high level regardless of environment, although broth-grown PrfA* mutants still cannot recapitulate the levels of *actA* expression seen in intracellular bacteria. While PrfA has been rigorously studied, there are still many questions about what trans-acting factors could impact the expression of PrfA-activated genes such as *actA*.

After protein production, the polarization of ActA along the bacterial cell surface is itself an important point of regulation. Distribution of ActA is tightly coupled to the bacterial cell cycle and necessary for motility initiation, comet tail formation, and steady-state

bacterial movement rates within host cytosol (Rafelski and Theriot 2005). *L. monocytogenes* can express ActA and begin recruiting actin as early as 30-60 minutes post-infection (10). However, bacteria can spend several hours surrounded by a uniform actin cloud before breaking this symmetric association, polarizing actin into comet tails, and finally becoming motile (21) Experiments with spherical ActA-coated beads in cytosol and cell-free environments support that the rod-shape of *L. monocytogenes* promotes the breaking of actin cloud symmetry and subsequent actin polarization within host cytosol (22–24). Thus, both the quantity of ActA and its organization as dictated by bacterial shape and cell cycle matter for actin-based motility and resultant cell-to-cell spread.

Redox stress encountered by bacteria

A change in redox environment can present an important signal for pathogens as well as a significant challenge to survival. Bacteria frequently encounter abundant redox stressors present in the environment and during infection of a mammalian host. While replicating in in aerobic environments, bacteria must contend with reactive oxygen species (ROS) such as superoxide (O_2^-), hydroxyl radicals ($HO\cdot$), and hydrogen peroxide (H_2O_2) (25). These ROS result from the incomplete reduction of molecular oxygen and are both produced by the bacteria (endogenously) and encountered extracellularly (exogenous) (Fig. 2). During aerobic growth, ROS forms continuously in bacterial cells due to a basal level of redox enzyme autooxidation, as well as the autooxidation of redox-active molecules like menaquinone (26, 27). ROS can also accumulate exogenously to high levels and is formed by chemical and photochemical processes under many experimental conditions (28). Mutants that lack scavenging systems for ROS frequently

exhibit growth defects attributed to subsequent oxidation and disabling of iron-using proteins necessary for core metabolic processes (26). Accumulated H_2O_2 can also react with free iron inside cells, generating hydroxyl radicals that damage DNA and can lead to mutagenesis and death(29).

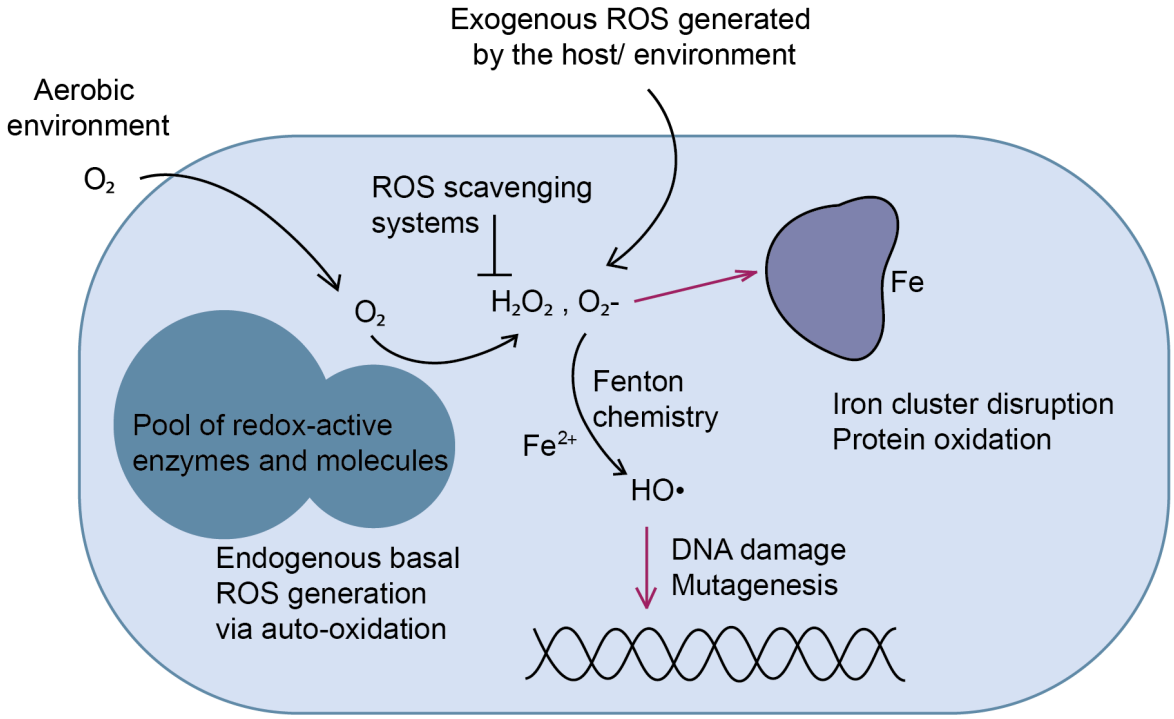

Figure 2. The impact of ROS on bacteria. ROS encountered by bacteria can be generated exogenously or endogenously. Molecular oxygen can quickly and freely diffuse into bacterial cytosol. Redox-active enzymes and molecules can oxidize in the presence of molecular oxygen, generating peroxide and superoxide, which can oxidize and disable iron-using proteins. These ROS can be depleted via ROS scavenging mechanisms. However, if not detoxified, peroxide can interact with free iron to generate hydroxyl radicals that damage DNA. Figure adapted from (25).

In light of these deleterious effects, it is perhaps unsurprising that the mammalian immune system uses ROS, including superoxide, hydrogen peroxide, and hypochlorous acid to defend against invading pathogens (30). This defense includes a respiratory burst, a period of increased oxygen consumption observed during phagocytosis due to

the activity of NADPH oxidase (31). NADPH oxidase generates ROS in the phagosome and is critical to the innate immune response, as evidenced by the increased susceptibility of patients with chronic granulomatous disease (CGD) to severe infections. CGD is an inherited immunodeficiency caused by deletions or mutations in the genes encoding NADPH oxidase (32). Without this immune defense mechanism, CGD patients suffer from invasive and recurrent infections (33). Upon infection, host cells also use nitric oxide synthase also produces nitric oxide, resulting in the development of several toxic reactive nitrogen species within the vacuole. Neutrophils can also generate the strong oxidant hypochlorous acid and use reactive oxygen species as a part of extracellular traps to kill bacterial invaders (12). To combat these assaults, bacteria produce many enzymes that detoxify ROS as well as regulators to sense ROS and induce the appropriate responses as redox stress arises (17).

Spx-Family Transcriptional Regulators

In order to control the response to oxidative stress, many Firmicutes possess at least one copy of transcriptional regulator and arsenate reductase (ArsC)-family protein Spx (34, 35). Spx homolog function has been investigated in *L. monocytogenes*, *Staphylococcus aureus*, *Streptococcus sanguinis*, *Streptococcus mutans*, and *Enterococcus faecalis*, but is most well-characterized in *Bacillus subtilis* (36–41). Spx-family proteins can sense redox stress via an amino-terminal cysteine-x-x-cysteine (CXXC) motif that forms an intramolecular disulfide bond upon oxidation. Upon interacting with the alpha-C-terminal domain (α-CTD) of RNA polymerase (RNAP), *B. subtilis* Spx regulates hundreds of genes (42). Oxidized *B. subtilis* Spx stabilizes the Spx-RNAP-DNA

interaction, which allows for the activation of genes encoding proteins required to resolve oxidative stress such as thioredoxins and bacillithiol biosynthesis machinery (34, 39, 42, 43). Additionally, reduced *B. subtilis* Spx is important for basal expression of redox homeostasis genes in the absence of oxidative stress (42). Spx has also shown anti-alpha factor activity in *B. subtilis*, where it represses 170 genes, of which several encode for vitamin, amino acid, and nucleic acid biosynthesis.

L. monocytogenes encodes two Spx paralogues, *spxA1* and *spxA2*. SpxA1 shares 83% amino acid similarity with *B. subtilis* Spx and 53% amino acid similarity with SpxA2. Initially thought to be an essential gene, *spxA1* can only be deleted under anaerobic conditions and dies upon exposure to oxygen (36, 44). Consequentially, SpxA1 was first studied in the context of a promoter-region transposon insertion which reduced expression of the protein 10-fold but still allowed for slowed aerobic growth. A *L. monocytogenes* strain with reduced SpxA1 abundance also demonstrated reduced *actA* transcription, increased sensitivity to oxidative stress, and severely attenuated infection in a murine model (13). Further research on a complete deletion mutant revealed that *spxA1* is essential for aerobic growth and pathogenesis while *spxA2* is dispensable in both conditions (26, 34). Both proteins possess a CXXC motif, and data suggests that oxidation of this motif on SpxA1 promotes aerobic growth. However, the precise conditions under which the SpxA1 CXXC motif is oxidized, as well as how oxidation changes SpxA1 function during broth growth and infection, is unknown. Interestingly, complementation with *B. subtilis spx* can restore Δ*spxA1* aerobic growth and pathogenesis, suggesting that the protein structure necessary for RNAP-Spx interactions

are conserved (36). However, it is not known whether SpxA1 interacts with RNAP using the same residues important for *B. subtilis* Spx-RNAP interaction.

While it is unclear exactly the conditions that positively promote *spxA1* expression, the degradation of SpxA1 via posttranslational regulation by YjbH is well-understood (Fig. 3). Highly conserved in the Firmicutes, YjbH was first characterized in *B. subtilis* as a protease adaptor that maintains low steady-state levels of Spx through direct binding and subsequent enhancement of ClpXP-mediated degradation (45–47). YjbH aggregates during disulfide stress, hindering its ability to aid in Spx degradation and allowing for downstream activation of Spx-regulated thiol stress response genes (48). The YjbH protein contains a disulfide-stress sensitive CXXC motif, although a role of this CXXC motif for function in *B. subtilis* has not been described.

YjbH was first investigated in *L. monocytogenes* after being found in the same forward genetic screen as SpxA1. This screen isolated mutants that could not produce wt levels of ActA (13). Similarly to *B. subtilis*, a *L. monocytogenes* Δ*yjbH* mutant is deficient in thiol stress response, and deficiencies can be complemented by the addition of either *B. subtilis* or *L. monocytogenes yjbH* (49). In agreement with this data, *L. monocytogenes* YjbH has 39% amino acid identity with *B. subtilis* and contains a CXXC motif. Recent data demonstrate that *L. monocytogenes* YjbH and SpxA1 interact directly and this interaction is dependent on a functional YjbH CXXC motif. Consequently, SpxA1 abundance and nitrosative stress tolerance increases significantly in a YjbH mutant (49). In *B. subtilis*, YjbH facilitates ClpXP degradation of Spx, but the precise mechanism of YjbH-mediated SpxA1 degradation has yet to be elucidated (48).

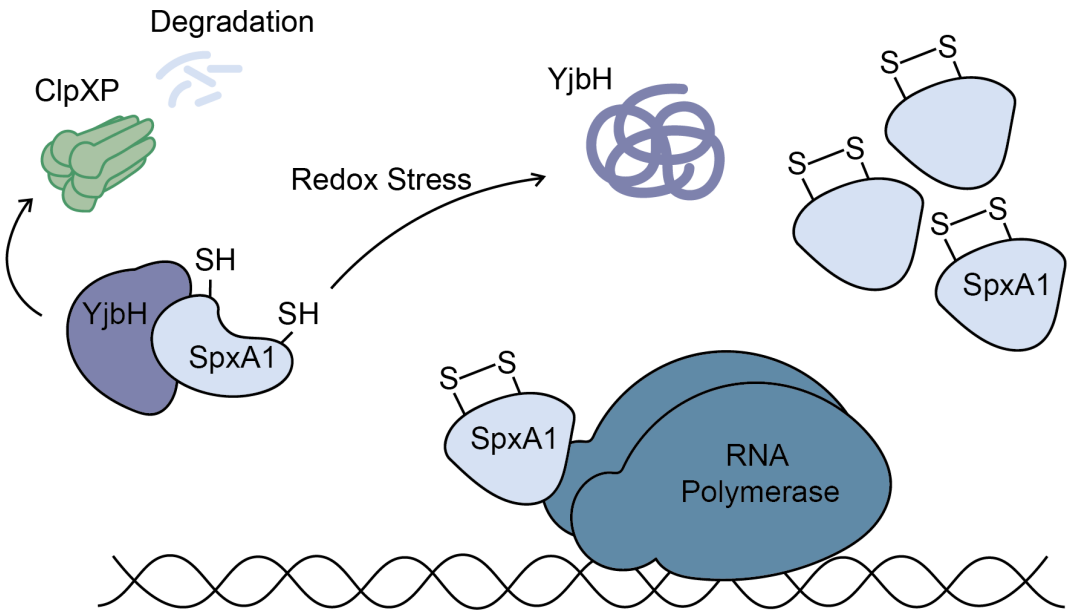

Figure 3. A working model of SpxA1 regulation by the protease adaptor YjbH. The conserved protease adaptor YjbH keeps basal SpxA1 abundance low in a reduced redox environment by chaperoning SpxA1 to the ClpXP protease for degradation. Disulfide and other stressors can induce YjbH aggregation, impeding adaptor function and therefore increasing SpxA1 concentrations. Upon oxidation, SpxA1 undergoes a structural change that facilitates its binding to RNAP and the downstream activation of hundreds of genes. Figure adapted from (17).

Presentation of main questions

Much is still unknown about how *L. monocytogenes* uses a highly complex transcriptional network to rapidly respond to the transition from living in the environment to infecting a host. While *L. monocytogenes* must contend with ROS in both the environment and host, the role of peroxide stress tolerance during infection is unclear. One of the regulators important for both *L. monocytogenes* pathogenesis and aerobic growth in the environment is SpxA1. However, the specific SpxA1-regulated factors necessary for these phenotypes had not been elucidated at the onset of this study. This work first establishes how SpxA1 directly regulates genes in *L. monocytogenes*, as well as how this direct regulation impacts aerobic growth and virulence (Chapter 2). Next, this

study characterizes the impact of all annotated *L. monocytogenes* peroxidases on growth and virulence, including several impacted by SpxA1 (Chapter 3). Next, this work examines the role of SpxA1 during infection via microscopy and subsequently investigates the impact of SpxA1 on cell shape and motility during both extracellular and intracellular growth (Chapter 4). Together, these analyses find that SpxA1 plays a multifaceted role in virulence and aerobic growth through the activation of peroxide stress response, heme biosynthesis, motility, and cell septation.

Chapter 2: Listeria monocytogenes SpxA1 is a global regulator required to activate genes encoding catalase and heme biosynthesis enzymes for aerobic growth

Introduction

Bacterial pathogens are challenged with abundant redox stressors present in the environment and during infection of a mammalian host. The innate immune system attempts to eliminate invading pathogens after phagocytosis by activating the respiratory burst, bombarding pathogens with ROS. In addition to exogenous ROS, bacteria must also manage the endogenous ROS generated during aerobic respiration from the reaction of oxygen with free metals, quinones, or flavoproteins (12, 50). To combat these assaults, bacteria produce many enzymes that detoxify ROS as well as regulators to sense ROS and induce the appropriate responses as redox stress arises (17).

One transcriptional regulator that controls the response to oxidative stress is the ArsC-family protein Spx, which is conserved in low G+C *Firmicutes* (34, 35). In this work, we identified SpxA1-regulated genes in *L. monocytogenes* and ascertained those that are required for aerobic growth and virulence. We demonstrated that although SpxA1 regulates hundreds of genes, the severe growth defect of Δ*spxA1* in broth can be rescued simply by supplementing the media with exogenous heme or catalase. While catalase and heme biosynthesis enzymes were required for aerobic growth *in vitro*, neither was necessary for intracellular growth in macrophages. Collectively, these results support a model in which SpxA1 directly activates genes required for aerobic growth and distinguish its role *in vitro* from its role during infection.

This chapter represents a collaborative effort by Monica Cesinger, Maureen Thomason, Mauna Edrozo, Cortney Halsey, and Michelle Reniere. My contributions to this paper included performing experiments described in Figures 10, 13, and 14. I also contributed to the writing and preparation of the final manuscript.

Results

Transcriptomics to identify SpxA1-regulated genes

SpxA1 is essential for *L. monocytogenes* aerobic growth and pathogenesis (36). To investigate the mechanisms behind these phenotypes, we took a global approach and analyzed the SpxA1-dependent transcriptome. RNA was harvested from *L. monocytogenes* wild type (wt) and Δ*spxA1* strains grown anaerobically in rich broth (brain heart infusion, BHI) and from J774 macrophages infected with either strain for 8 hours. Following rRNA depletion, Illumina sequencing of the cDNA revealed hundreds of genes were changed in abundance in an SpxA1-dependent manner (see Experimental Procedures for details). Genes that exhibited a greater than two-fold difference in abundance between wt and Δ*spxA1* samples ($P < 0.001$) were included for further analysis. Table 1 includes genes reduced in Δ*spxA1* compared to wt during infection as well as those most highly changed in BHI.

Table 1. SpxA1-Activated Genes

LMRG	Lmo	Gene	Function	Fold change in Δ*spxA1*		Spx Motif (Position relative to +1 transcription)†
				BHI	J774	
LMRG_01912	lmo2785	kat	catalase	-66.76	-11.47	-46 -32 AAGCCTTTTAGTTGA
LMRG_01620	lmo2212	hemE uroD	uroporphyrinogen decarboxylase	-15.77	-46.45	-46 -32 GGCAATTTGTTTGGT
LMRG_01621	lmo2211	hemH cpfC	ferrochelatase	-15.44	-36.79	
LMRG_01954	lmo2742	-	hypothetical protein	-12.25	-22.89	-46 -32 AAGCACATCGAAAGC
LMRG_01953	lmo2743	-	transaldolase	-8.21	-20.62	
LMRG_01781	lmo2467	-	chitin-binding protein	-12.16	-25.47	-46 -32 AGCGAATTATTTCTA
LMRG_01977	lmo2719	-	tRNA-adenosine deaminase	-11.11	-19.80	-46 -32 AGCAGATTATTCCTA
LMRG_01978	lmo2718	cydA	cytochrome bd oxidase subunit I	-9.43	-	no motif
LMRG_01980	lmo2716	cydC	ABC transporter	-9.10	-	
LMRG_01979	lmo2717	cydB	cytochrome bd oxidase subunit II	-8.69	-	
LMRG_01981	lmo2715	cydD	ABC transporter	-7.37	-	
LMRG_00292	lmo0609	-	Rhodanese Homology Domain	-9.09	-20.68	-46 -32 GAGCAGAAAATTTGT
LMRG_00833	lmo1381	-	acylphosphatase	-8.33	-6.63	-46 -32 AATGCAAATTTTTGA
LMRG_01976	lmo2720	-	acetyl-CoA synthetase	-7.67	-8.09	no motif
LMRG_02566	lmo0302	-	hypothetical protein	-7.65	-2.65	no motif
LMRG_02565	lmo0303	-	hypothetical secreted protein	-6.16	-3.89	-49 -35 TGGCATGATGAGTAT
LMRG_00343	lmo0656	-	uncharacterized membrane protein	-7.32	-16.07	-46 -32 AGCTCAATCTTTCGC
LMRG_02823	lmo1799	-	peptidoglycan binding protein	-7.16	-3.52	-46 -32 TCTAGTACTTTTTAC
LMRG_00563	lmo1121	-	hypothetical protein	-6.78	-	no TSS
LMRG_00564	lmo1122	-	hypothetical protein	-5.58	-	
LMRG_00565	lmo1123	-	hypothetical protein	-4.47	-	
LMRG_02864	lmo1120	-	hypothetical protein	-4.09	-	
LMRG_00566	lmo1124	-	hypothetical protein	-4.07	-	
LMRG_00478	lmo0790	-	Cys-tRNA(Pro) deacylase	-6.64	-11.58	no motif

LMRG_00477	lmo0789	-	DAP-epimerase Superfamily	-6.45	-9.69	
LMRG_01211	lmo2061	-	hypothetical protein	-6.14	-13.08	no TSS
LMRG_01210	lmo2060	-	hypothetical protein	-5.72	-11.35	
LMRG_01212	lmo2062	-	copper transport protein	-4.67	-16.30	
LMRG_00339	lmo0652	-	putative acetyltransferase	-6.25	-8.23	-48 -34 TGCTATTTTAAAGGT
LMRG_00340	lmo0653	-	hypothetical protein	-5.78	-8.70	
LMRG_01024	lmo1878	mntR	transcriptional regulator mntR	-5.49	-9.61	P2-46 -32 AAGGGCATACTTTTG P1-46 -32 GGGTAATTGCTTTTA
LMRG_01023	lmo1877	-	formate-tetrahydrofolate ligase	-3.85	-4.15	-46 -32 TGCATTAATAAGCCA
LMRG_00144	lmo0452	-	hypothetical protein	-5.13	-5.08	-49 -35 GCCACGTTAAATCTT
LMRG_00146	lmo0454	-	MoxR-like ATPase	-4.61	-7.28	
LMRG_00145	lmo0453	-	hypothetical protein	-4.22	-6.38	
LMRG_01925	lmo2770	gshF	glutathione synthase	-4.89	-11.79	no TSS
LMRG_01656	lmo2176	-	TetR-family transcriptional regulator	-4.83	-27.87	no TSS
LMRG_00561	lmo1117	-	glyoxalase	-4.80	-	no motif
LMRG_02738	lmo2393	-	hypothetical protein	-4.65	-7.33	-46 -32 AAACAGCTTAGTCGC
LMRG_02737	lmo2392	-	hypothetical protein	-4.00	-6.63	
LMRG_02358	lmo0109	-	AraC family transcriptional regulator	-4.62	-4.39	-46 -32 TGGTTTATATTCGCT
LMRG_02359	lmo0110	-	esterase/lipase	-4.52	-4.21	
LMRG_00128	lmo0436	-	hypothetical protein	-4.59	-3.05	no TSS
LMRG_00671	lmo1225	-	MarR family transcriptional regulator	-4.52	-10.28	-46 -32 TTCTTTTCATTTGAC
LMRG_00672	lmo1226	-	putative drug exporter	-2.53	-4.58	
LMRG_02247	lmo0822	-	SoxR-family transcriptional regulator	-4.30	-11.51	no TSS
LMRG_00464	lmo0776	-	transcriptional regulator	-4.29	-5.00	-46 -32 TCACTTTTCATTTGT
LMRG_01240	lmo2089	-	esterase/lipase	-4.26	-6.66	no motif

LMRG_02063	lmo0964	yjbH	predicted thioredoxin	-4.19	-6.09	-50 -36 GCCAATGACAATTAT
LMRG_00270	lmo0588	-	deoxyribodipyrimidine photo-lyase	-4.17	-12.07	-46 -32 AGTCCTTTGTTTTTC
LMRG_02117	lmo1017	-	glucose-specific PTS system IIA	-4.10	-6.81	-46 -32 TAGTTTCTCCGTGCC
LMRG_02101	lmo1001	-	hypothetical protein	-4.01	-6.08	-46 -32 ATGGCTTATAGTTGA
LMRG_02681	lmo2586	-	formate dehydrogenase alpha subunit	-3.94	-4.41	P2-46 -32 TGCCGTATTACTGTG P1-46 -32 TAATATAAGCGGAAA
LMRG_02248	lmo0823	-	aldo/keto reductase	-3.83	-4.23	-46 -32 GCCAAATGTTTGCCT
LMRG_02253	lmo0830	fbp	fructose-1,6-bisphosphatase class 3	-3.67	-7.20	no motif
LMRG_01398	lmo1569	fxsA	fxsA protein	-3.56	-4.82	no TSS
LMRG_01267	lmo2113	-	heme peroxidase	-3.53	-6.04	-46 -32 AAACAGCGAAACGGA
LMRG_01266	lmo2112	-	hypothetical protein	-2.44	-2.04	-50 -36 GCAATTGTTAATGTT
LMRG_01822	lmo2426	spxA2	arsenate reductase family protein	-3.48	-3.36	-50 -36 TCTAAGTGTTGCCAT
LMRG_01824	lmo2424	-	thioredoxin	-3.34	-5.97	P1, P2 no motif P3-46 -32 TCAAAGAAGAAGAAT
LMRG_01823	lmo2425	-	glycine cleavage system H protein	-3.28	-5.60	P4-48 -34 GCTTGGTTTCAAAGA P5-46 -32 AGTGACGCTTGGTTT
LMRG_00673	lmo1227	-	uracil-DNA glycosylase	-3.31	-2.64	-46 -32 GCGGTTTTTAGTTTG
LMRG_00274	lmo0592	-	hypothetical protein	-3.30	-4.30	-46 -32 TGCTATTAATTGCTA
LMRG_00489	lmo0800	-	hypothetical protein	-3.23	-6.03	-46 -32 GAGCAGTGCGGAAG
LMRG_00219	lmo0537	-	allantoate deiminase	-3.21	-5.95	-46 -32 GTTGTTTTAGCGAGC
LMRG_00220	lmo0538	-	N-acyl-L-amino acid amidohydrolase	-2.77	-4.67	
LMRG_02830	lmo1782	-	exodeoxyribonuclease III	-3.11	-8.05	-46 -32 ATCGTTTAACTACAT
LMRG_02735	lmo2390	-	hypothetical thioredoxin reductase	-3.10	-9.44	P1-46 -32 TCTTTTTCAACAATA P2-46 -32 AAACATTCTTTTTCA P3-46 -32 AATCCCGTAAACATT
LMRG_00701	-	-	hypothetical protein	-3.06	-5.14	no TSS
LMRG_01795	lmo2453	-	epoxide hydrolase	-3.06	-2.77	-46 -32 AGCTTTTTTATAGGA

LMRG_02716	lmo2371	-	ABC transporter, permease	-3.05	-7.01	-49 -35 TCTTTGGAAAGTGAA
LMRG_02717	lmo2372	-	ABC transporter, ATP-binding protein	-2.78	-5.80	
LMRG_02835	lmo1777	-	hypothetical protein	-3.05	-6.17	no TSS
LMRG_01665	lmo2167	-	hydroxyacylglutathione hydrolase	-3.03	-5.19	no motif
LMRG_01666	lmo2166	-	hypothetical protein	-2.57	-4.81	
LMRG_01667	lmo2165	-	Crp family transcriptional regulator	-2.46	-3.56	
LMRG_02624	lmo0202	hly	listeriolysin O	-3.02	-	no motif
LMRG_00527	lmo1065	-	hypothetical protein	-2.99	-7.04	-46 -32 TAGAACAAGATTCTT
LMRG_01575	lmo2256	-	protease I	-2.98	-3.03	-46 -32 AGGCGGAATAATTTA
LMRG_00845	lmo1393	-	M16 family metallopeptidase	-2.95	-4.96	-46 -32 ATGCTAGAAAATTGT
LMRG_00844	lmo1392	-	zinc metallopeptidase	-2.92	-5.37	
LMRG_00504	lmo1043	mobB	molybdopterin biosynthesis protein B	-2.94	-3.63	-46 -32 AGTCGCTTTACTTTT
LMRG_00503	lmo1042	moeA	molybdopterin biosynthesis protein A	-2.71	-5.30	
LMRG_00505	lmo1044	-	molybdopterin converting factor subunit 2	-2.85	-5.10	
LMRG_02643	lmo0221	-	type III pantothenate kinase	-2.91	-6.89	-46 -32 AGCTATATTATTCGG
LMRG_02644	lmo0222	hslO	heat shock protein 33	-2.89	-6.17	
LMRG_01161	lmo2013	-	hypothetical protein	-2.81	-3.51	no TSS
LMRG_01162	lmo2014	-	alpha-mannosidase	-2.48	-2.57	
LMRG_00821	lmo1371	-	dihydrolipoyl dehydrogenase	-2.76	-4.25	no TSS
LMRG_00820	lmo1370	-	butyrate kinase	-2.70	-5.10	
LMRG_00822	lmo1372	-	dehydrogenase	-2.62	-4.14	
LMRG_00823	lmo1373	-	dehydrogenase	-2.41	-3.35	
LMRG_00679	lmo1233	trxA	thioredoxin	-2.75	-8.25	P1-46 -32 TAGGTGCTATACTGT P2-46 -32 GAGCAAAAACATGGC

LMRG_02758	lmo1684	-	glycerate dehydrogenase	-2.74	-5.54	no TSS
LMRG_01854	lmo2844	-	Protein N-acetyltransferase	-2.73	-	-48 -34 TCACGTGAAACATTT
LMRG_00015	lmo0323	-	hypothetical protein	-2.69	-3.26	-46 -32 AAACCCAAATCGGTG
LMRG_00519	lmo1057	-	L-lactate dehydrogenase	-2.68	-5.33	-46 -32 GTCAAGTTATTTTAT
LMRG_00520	lmo1058	-	hypothetical protein	-2.37	-4.97	
LMRG_02038	lmo0939	-	hypothetical protein	-2.64	-3.35	-50 -36 GCTATGTTCTTTTGT
LMRG_02037	lmo0938	-	protein tyrosine phosphatase	-2.32	-2.94	
LMRG_01130	lmo1982	-	N-acetyltransferase	-2.62	-4.75	-47 -33 TCACACTTTAGTTGC
LMRG_02622	lmo0200	prfA	listeriolysin regulatory protein	-2.61	-	-46 -32 TGCATTTCTTTTGCG
LMRG_01576	lmo2255	-	hypothetical protein	-2.61	-3.97	-47 -33 GCGCTTTTTTATTGG
LMRG_00352	lmo0665	-	hypothetical protein	-2.61	-8.67	-48 -34 GCGATTACTTTACTA
LMRG_00351	lmo0664	-	maltose O-acetyltransferase	-2.56	-7.75	
LMRG_00353	lmo0666	-	hypothetical protein	-2.10	-5.70	
LMRG_00416	lmo0728	-	riboflavin kinase	-2.60	-6.57	-46 -32 ATCAATAAATTTGCA
LMRG_02495	lmo1776	-	hypothetical protein	-2.58	-4.56	-46 -32 TGAAGTGTTTCTTTT
LMRG_02239	lmo2692	pstA	P-II-like protein	-2.56	-7.22	-46 -32 AAGTGCATATCGCTC
LMRG_02809	lmo2131	-	Crp family protein	-2.55	-	no TSS
LMRG_01937	lmo2759	-	hypothetical protein	-2.50	-2.64	-46 -32 GATAATCGACTTGCT
LMRG_02114	lmo1014	gbuA	glycine betaine transporter, ATP-binding	-2.49	-3.59	-46 -32 CTAAGCCGAAACTTG P2 no motif
LMRG_02115	lmo1015	gbuB	glycine betaine transporter, permease	-2.48	-3.95	
LMRG_02116	lmo1016	gbuC	glycine betaine-binding protein	-2.42	-4.48	
LMRG_02762	lmo1688	-	enoyl-[acyl carrier protein] reductase III	-2.47	-8.64	-46 -32 AAGAAGAAATGAAGC
LMRG_02763	lmo1689	-	A/G-specific adenine glycosylase	-2.44	-7.85	-46 -32 CTATTCAATTAAGCC
LMRG_02767	lmo1693	recX	regulatory protein recX	-2.46	-	-47 -33 TCCCTTTTTAGTAGT
LMRG_00166	lmo0485	-	hypothetical protein	-2.45	-4.04	-47 -33 GCCCCTTTACTAGCA

LMRG_01389	lmo1578	-	X-Pro dipeptidase	-2.43	-5.33	-46 -32 AGGTGTTTATTAGCA
LMRG_02351	lmo0102	-	quinol monooxygenase YgiN	-2.42	-	no TSS
LMRG_02264	lmo0841	-	calcium-transporting ATPase	-2.41	-2.11	-46 -32 GTGTTATCAATATTA
LMRG_01235	lmo2084	-	hypothetical protein	-2.38	-2.26	no TSS
LMRG_01384	lmo1583	tpx	2-Cys peroxiredoxin	-2.36	-9.15	-46 -32 TAGCTTATCGTTTAC
LMRG_00462	lmo0774	-	diacylglycerol kinase family enzyme	-2.36	-2.85	P1-45 -31 GAATAGAGAAGATGC P2-46 -32 TTCAAGGTAAACTAG P3 no motif
LMRG_00463	lmo0775	-	hypothetical protein	-2.34	-3.11	P4-46 -32 CAAGGCTGTGACTGG
LMRG_01491	lmo2352	-	LysR family transcriptional regulator	-2.35	-3.80	no TSS
LMRG_00294	lmo0611	acpD	FMN-dependent NADH-azoreductase 1	-2.33	-27.00	-46 -32 AGCAATATGCTTGCT
LMRG_00689	lmo1243	-	hypothetical protein	-2.30	-4.16	-48 -34 TCTTTAGTTTATAAC
LMRG_02428	lmo2857	-	hypothetical protein	-2.30	-	no TSS
LMRG_02028	lmo0929	srtA	sortase A	-2.25	-2.17	P1-46 -32 ACTGATTTTCTTTGC P2 no motif
LMRG_00510	lmo1049	moeB	molybdopterin biosynthesis protein MoeB	-2.24	-5.28	-46 -32 GCCTTGCAAGTAAGC
LMRG_00355	lmo0668	-	antibiotic transport system permease	-2.23	-4.65	-46 -32 CGTAATCAGGGAGTG
LMRG_00378	lmo0690	flaA	flagellin	-2.22	-3.53	no motif
LMRG_00452	lmo0764	lplA	lipoate-protein ligase A	-2.20	-2.75	@lmo0763 TSS -46 -32 AGTAGCTGAGTAAAG
LMRG_01941	lmo2755	-	predicted acyl esterase	-2.18	-2.61	no TSS
LMRG_00703	lmo1254	-	alpha-phosphotrehalase	-2.17	-	@lmo1255 TSS -46 -32 AATTAAAGTGGTTGC
LMRG_01036	lmo1889	-	hypothetical protein	-2.15	-3.17	-46 -32 TCCTAGACCATTACC
LMRG_00331	lmo0644	mdoB	phosphoglycerol transferase	-2.11	-2.38	no motif
LMRG_02801	lmo2139	-	sodium transporter, ATP-binding protein	-2.10	-2.32	-51 -36 GCTCTTTACTTTTAGC

LMRG_02799	lmo2141	-	acetyltransferase	-2.05	-2.04	
LMRG_01842	lmo2406	-	hypothetical protein	-2.09	-3.24	-46 -32 GACCAAATTAAAGGC
LMRG_00241	lmo0559	-	hypothetical protein	-2.08	-	no motif
LMRG_01388	lmo1579	-	alanine dehydrogenase	-2.03	-4.20	P1-46 -32 TTGTGTTAGCATGGG P2 no motif P3 no motif P4 no motif
LMRG_01572	lmo2259	-	cellobiose-specific PTS system IIA	-2.03	-2.48	no TSS
LMRG_01770	lmo2478	trxB	thioredoxin-disulfide reductase	-2.01	-6.96	P1-46 -32 TTCCGTATTAGGATT P2-46 -32 TTTGCTATTCCGTAT P3 no motif P4-46 -32 GAGCAGATAAATAGA

† Highlighted genes are predicted to be in an operon. Transcription start sites identified from Listeria Viewer (51). Possible GC-motif is underlined. 'no TSS' indicates no experimental determination of a transcription start site (TSS). 'no motif' indicates lack of GC or TC sequence -30 to -50 nucleotides from the TSS.

During anaerobic growth *in vitro*, SpxA1 directly or indirectly activated 145 genes, and 87% of those also exhibited SpxA1-dependent expression during infection (Table 1). As expected from the role of Spx-family proteins in other *Firmicutes*, *L. monocytogenes* SpxA1 was required to activate genes involved in the oxidative stress response (*kat*, catalase; *gshF,* glutathione synthase; *trxA*, thioredoxin; *trxB*, thioredoxin reductase; *tpx*, thiol peroxidase; and *yjbH,* predicted thioredoxin). In the absence of *spxA1*, 72 genes exhibited increased expression during anaerobic growth *in vitro*, suggesting that SpxA1 normally functions to directly or indirectly repress those genes (Table 2). Approximately 60% of the repressed genes were also SpxA1-dependent during macrophage infection. SpxA1-repressed genes encode proteins involved in diverse functions, including: transport of amino acids (e.g. *ctaP* and *gltD*), sugars (*lmo0859-61* operon), potassium (*kdpAB*), and zinc (*znuA*); phosphotransferase (PTS) system components (*ulaA*, *bvrB*,

and fructose-specific components); and nucleotide metabolism (*guaA*, *guaB*2, and *purE*). The genes with the greatest increase in expression in Δ*spxA1* were *lmo0437*, encoding an uncharacterized protein with a predicted NAD(P)-dependent oxidoreductase domain, and the *mecA-coiA* operon, which is adjacent to *spxA1* in the genome. MecA and CoiA are proteins involved in competence in other Gram-positive bacteria (44), but their functions are unclear in *L. monocytogenes,* which is not known to be naturally competent.

Table 2. SpxA1-repressed genes

LMRG	Lmo	Gene	Function	Fold change in Δ*spxA1*		Spx Motif (Position relative to +1 transcription)†
				BHI	J774	
LMRG_00129	lmo0437	-	NAD(P)H dehydrogenase	14.16	6.12	no TSS
LMRG_01642	lmo2190	mecA	adapter protein	11.11	4.31	P1-46 -32 ATGAGCTACAATGAA P2-46 -32 CTATTTCTTAATATG P2-46 -32 AGGAAAAATGGTGGT
LMRG_02700	lmo2568	-	hypothetical protein	8.55	9.17	no TSS
LMRG_02701	lmo2567	-	hypothetical protein	8.20	8.40	
LMRG_00493	lmo1032	-	transketolase	7.68	6.39	no TSS
LMRG_00492	lmo1031	-	hypothetical protein	7.11	5.16	
LMRG_00494	lmo1033	-	transketolase	6.76	5.65	
LMRG_00495	lmo1034	glpK2	glycerol kinase	4.80	5.05	
LMRG_00496	lmo1035	-	PTS beta-glucoside transporter subunit IIABC	2.77	2.24	
LMRG_02190	-	-	hypothetical protein	6.58	6.51	no TSS
LMRG_02191	lmo2646	-	hypothetical protein	6.71	3.74	-46 -32 GGAATTGGGCTTTTT
LMRG_02192	lmo2647	-	creatinine amidohydrolase	6.25	3.20	
LMRG_02193	lmo2648	-	hypothetical protein	5.78	2.28	

LMRG_02194	lmo2649	ulaA	ascorbate-specific PTS system IIC component	4.12	2.04	
LMRG_02195	lmo2650	-	ascorbate-specific PTS system IIB component	3.15	-	
LMRG_02196	lmo2651	-	mannitol-specific PTS system IIA	4.86	-	
LMRG	lmo2210	-	hypothetical protein	5.64	-	-46 -32 TGAAGTTTTAATCAA
LMRG_02797	lmo2143	-	mannose-6-phosphate	5.20	3.60	-46 -32 AATAGATTGTAATGA
LMRG_02282	lmo0859	-	multiple sugar transport system substrate-binding protein	4.83	5.39	
LMRG_02283	lmo0860	-	multiple sugar transport system permease	4.17	5.42	
LMRG_02284	lmo0861	-	multiple sugar transport system permease	3.22	4.70	-46 -32 AAAAGTAATTATTGA
LMRG_02285	lmo0862	-	trehalose-6-phosphate hydrolase	3.15	3.68	
LMRG_02286	lmo0863	-	hypothetical protein	3.53	4.25	
LMRG_02287	lmo0864	-	Predicted glycosyl hydrolase	2.66	3.30	
LMRG_02288	lmo0865	-	phosphomannomutase	2.98	2.46	
LMRG_01896	lmo2801	-	N-acetylmannosamine-6-phosphate 2-epimerase	4.66	3.72	
LMRG_01897	lmo2800	-	predicted dehydrogenase	4.53	2.92	-46 -32 TTTAATCGATATTGA
LMRG_01898	lmo2799	-	PTS mannitol transporter IIBC	2.88	3.62	
LMRG_01643	lmo2189	coiA	competence protein	4.26	2.67	no TSS
LMRG_01762	lmo2486	-	hypothetical protein	3.80	7.45	-46 -32 GAAATCTAGCGCCGT
LMRG_01761	lmo2487	-	hypothetical protein	3.68	7.87	-46 -32 CCTCTGGTTGTATGA
LMRG_01573	lmo2258	-	hypothetical protein	3.76	3.72	-46 -32 CCTATGGAACGATGC
LMRG_00087	lmo0394	-	extracellular P60 protein	3.59	6.02	-46 -32 AAAAAAGGGGTGCGT
LMRG_02398	lmo0153	znuA	Zinc ABC transporter, periplasmic-binding protein	3.44	-	no TSS
LMRG_01726	lmo2522	-	Resuscitation promoting factor	3.22	2.11	-46 -32 TTTTTTAGTAACCAA

LMRG_00093	lmo0400	-	fructose-specific PTS system IIC	3.21	-	TSS @lmo0398 -46 -32 AATTCCTTATGTTCA
LMRG_02097	lmo0997	clpE	Clp protease ATP-binding subunit	3.14	-	-46 -32 AAGCAAAATACTTGA
LMRG_02538	lmo1733	gltD	glutamate synthase small subunit	3.08	-	no TSS
LMRG_02537	lmo1734	-	glutamate synthase large subunit	2.77	-	
LMRG_01938	lmo2758	guaB	inosine-5'-monophosphate dehydrogenase	3.00	2.35	-46 -32 AGGAAAACCTTCTTG
LMRG_02270	lmo0847	-	glutamine ABC transporter	2.99	-	-46 -32 TAAATAACTATGGTC
LMRG_02271	lmo0848	-	amino acid transporter, ATP-binding	2.94	-	
LMRG_02227	lmo2682	kdpA	K+-transporting ATPase A subunit	2.97	-	no TSS
LMRG_02226	lmo2681	kdpB	K+-transporting ATPase B subunit	2.51	-	
LMRG_01858	lmo2841	-	sucrose phosphorylase	2.90	3.24	-46 -32 AAAATTGTGTTTGAC
LMRG_01859	lmo2839	-	multiple sugar transport system substrate-binding protein	2.50	4.28	
LMRG_01910	lmo2787	bvrB	beta-glucoside-specific phosphotransferase enzyme II ABC	2.76	-	no TSS
LMRG_02496	lmo1775	purE	phosphoribosylaminoimidazole carboxylase catalytic subunit	2.67	2.96	P1-46 -32 ATCGTACCTATTGTT P2-46 -32 TCGATTTTTCGTTGA
LMRG_01018	lmo1871	-	phosphoglucomutase	2.67	2.05	P1-46 -32 TATAAGCTATAATGA P2-46 -32 TGTAAAAGCTATGTG
LMRG_00228	lmo0546	-	NAD(P)-dependent oxidoreductase	2.67	4.23	no TSS
LMRG_02617	lmo0195	-	putative ABC transporter, permease	2.53	2.77	-46 -32 CTCCGATGTACTTCA
LMRG_02615	lmo0193	-	hypothetical protein	2.33	2.50	
LMRG_01145	lmo1997	-	mannose-specific PTS system IIA	2.52	2.06	TSS @lmo2001 -46 -32 AAAAAAAGTAACCTT TSS @lmo2004 -46 -32 TAAAAAGACTATTGA
LMRG_01147	lmo1999	-	glucosamine 6-phosphate synthetase	2.26	-	
LMRG_01146	lmo1998	-	opine catabolism protein	2.18	-	
LMRG_01325	lmo1641	citB	aconitate hydratase 1	2.52	-	-46 -32 GATTCTCTTTGTTTA

LMRG_02556	lmo1713	mreB	rod shape-determining protein	2.51	-	-46 -32 TGTTTAAATAATGCT
LMRG_02234	lmo2688	-	Bacterial cell division protein	2.43	2.18	-46 -32 ACATTTTGTCTTGCG
LMRG_02233	lmo2687	-	Bacterial cell division protein	2.29	2.07	
LMRG_01623	lmo2209	-	Predicted acetyltransferase	2.41	-	no TSS
LMRG_02585	lmo0286	-	aminotransferase	2.40	-	-46 -32 AAAATCATACTGGAC
LMRG_01452	lmo1518	-	hypothetical protein	2.40	-	no TSS
LMRG_02238	lmo2691	murA	autolysin	2.36	2.59	-46 -32 TGTCGATATCAATCA
LMRG_02379	lmo0130	-	5'-nucleotidase	2.34	-	-46 -32 ATATTTCCTATTGCT
LMRG_02751	lmo0186	-	Resuscitation promoting factor	2.31	-	-46 -32 TATAAAAAATTGACA
LMRG_00498	lmo1037	-	hypothetical protein	2.30	-	no TSS
LMRG_02476	lmo0047	-	Uncharacterized membrane protein	2.26	4.92	-46 -32 ACCTAAGAAGGAAGT
LMRG_02397	lmo0152	-	peptide/nickel transport system substrate-binding protein	2.25	-	-46 -32 AAATCATTAACTTGA
LMRG_01047	lmo1900	panD	aspartate alpha-decarboxylase	2.16	2.29	no TSS
LMRG_02384	lmo0135	ctaP	cysteine transport system substrate-binding protein	2.15	-	P1-46 -32 AGTGTATCTTTAATT P2-46 -32 GTTTTCTCTTCTTGA
LMRG_00558	lmo1096	guaA	GMP synthase	2.13	-	-46 -32 AAGAAGATGAAAAGG
LMRG_00681	lmo1235	-	aspartate kinase	2.02	-	-46 -32 ATATAATAAACTTCC

† Highlighted genes predicted to be in an operon. Transcription start sites identified from Listeria Viewer (51). T/A at position -43 is highlighted. Possible GC-motif is underlined. 'no TSS' indicates no experimental determination of a transcription start site (TSS).

Promoter analysis

Spx-family proteins lack a canonical DNA-binding domain and instead directly interact with the alpha-C-terminal domain (αCTD) of RNAP to guide positive or negative regulation of genes (17). In *B. subtilis*, Spx-activated promoters exhibit extended -35 boxes with G at position -44 and C at position -43 relative to the transcription start site

(TSS) (52, 53). Here, we refer to this sequence as the 'GC-motif'. T at position -44 is also associated with Spx-activated expression, although the magnitude of regulation is reduced (42). To determine which differentially expressed genes identified in our RNA-seq analysis were directly regulated by SpxA1, the DNA sequences surrounding the TSSs of differentially expressed genes were analyzed *in silico*. Nine of the fifteen most down-regulated operons (60%) contained the GC-motif (or TC) at or near the -44/-43 position relative to the TSS. Several of the GC-motifs were shifted 1 or 2 nucleotides from the -44/-43 position. However, the TSSs were mapped in a genome-wide manner and have not been individually validated, so single-nucleotide precision of TSS mapping would not be expected (51). Four of the TSSs have not been mapped and therefore could not be analyzed for potential GC-motifs. Rochat *et al.* found 71% of the *B. subtilis* Spx-activated promoters contained C at position -43, which is similar to the frequency found here (42). In contrast, the GC-motif is not found in Spx-repressed promoters in *B. subtilis*, but instead, A or T at position -43 is correlated with repression (42). In our analysis, 29 of the 46 transcriptional units (63%) repressed by SpxA1 contained A or T at position -43 (Table 2), which is about the frequency expected by chance in a bacterium with 39% GC content. Together, these results suggested SpxA1 may directly activate a majority of the genes identified by our transcriptomics, although SpxA1-mediated repression may be direct or indirect.

The roles of SpxA1-dependent genes during infection

We hypothesized that SpxA1-dependent transcriptional changes enable aerobic growth and virulence and hence, in the absence of *spxA1*, appropriate gene induction

does not occur. Therefore, the top SpxA1-activated genes were examined to determine which may be required for virulence but were insufficiently activated in Δ*spxA1* (Table 1). Each SpxA1-dependent gene or operon was over-expressed from the constitutive HyPer promoter and stably integrated into the chromosome via the plasmid pPL2t, referred to here as pOE (13, 54). Over-expression was verified by qPCR of six of the over-expressing strains and indeed, all of the target genes were expressed at or above wt levels when integrated into the Δ*spxA1* mutant (Fig. 4).

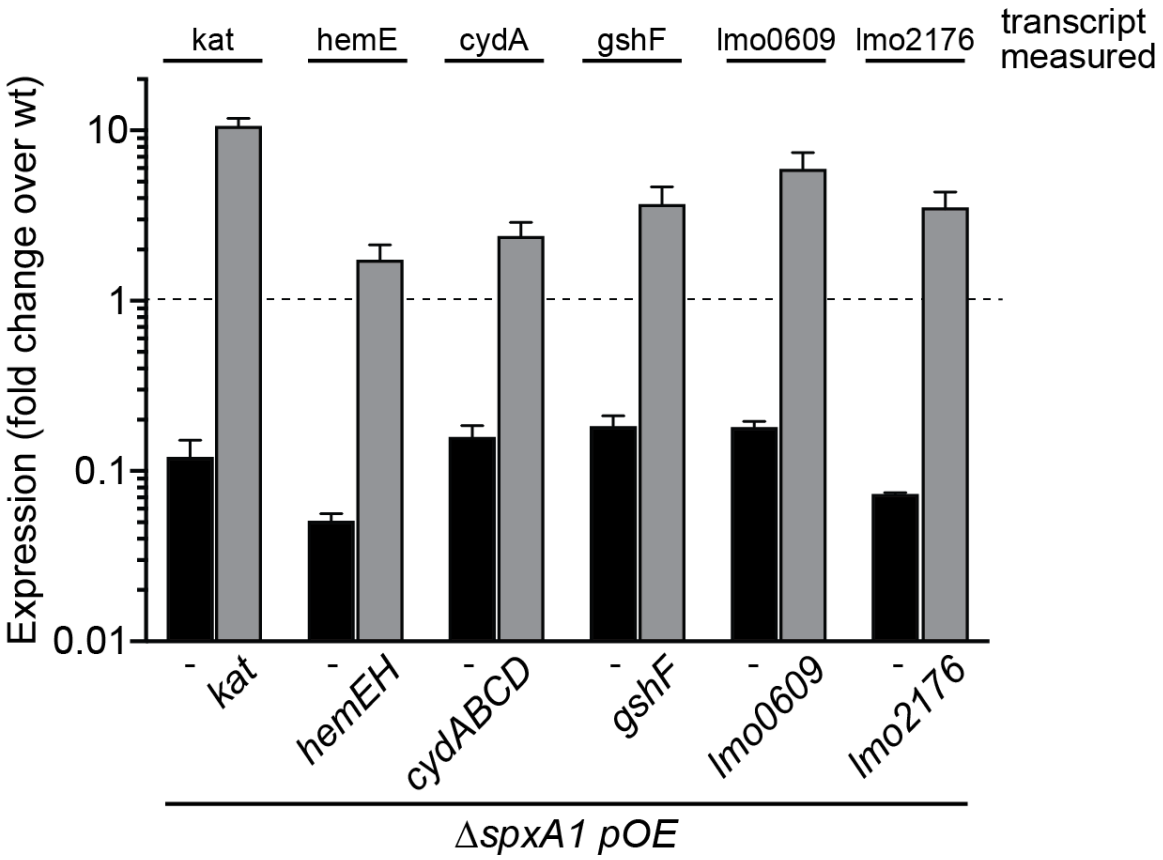

Figure 4. Verification of over-expression in Δ*spxA1 pOE* strains. Bacteria were grown anaerobically in BHI to OD_{600} = 1.0 and were harvested for RNA isolation. qPCR of selected genes in the corresponding over-expressing strain was performed. Expression was calculated as fold change over wt. Therefore, expression greater than 1 (dotted line) indicates expression greater than wt. Data are the mean and S.E.M. of three independent experiments.

L. monocytogenes Δ*spxA1* is able to replicate intracellularly and spread cell-to-cell, albeit less efficiently than wt (36). To identify the genes that contribute to these phenotypes *in vivo,* the over-expressing strains were evaluated in a plaque assay. Plaque assays measure cell-to-cell spread over three days. This requires *L. monocytogenes* be able to enter cells, escape the vacuolar compartment, replicate in the host cytosol, and use actin-based motility to spread to neighboring cells (13, 55). Hence, the ability to form a plaque is highly correlated with pathogenicity in murine models of infection. *L. monocytogenes* Δ*spxA1* formed a plaque approximately 23% the size of wt and the over-expressing strains formed similarly sized plaques, ranging from 15-37% the size of wt (Fig. 5A).

In addition to the top SpxA1-activated genes in Table 1, we investigated the roles of *spxA2* and *trxA* in the Δ*spxA1* plaque defect. SpxA1 and SpxA2 share 25% amino acid identity (56% similarity) and we hypothesized that SpxA2 may be able to compensate for the loss of *spxA1* if over-expressed. Interestingly, over-expressing either *spxA2* or *trxA* did not substantially increase the plaque size of the Δ*spxA1* parental strain (Fig. 5A).

The Δ*spxA1* mutant is not impaired in vacuolar escape or ActA production during infection of bone marrow-derived macrophages (BMDMs)(36). Therefore, we presume that the Δ*spxA1* plaque defect is primarily due to impaired intracellular growth. To test the roles of SpxA1-dependent genes in intracellular growth, BMDMs were infected with the over-expressing strains and bacteria were plated anaerobically to enumerate CFU. For these experiments, strains that formed plaques at least 25% larger than the Δ*spxA1* parental strain were included (Fig. 5A). During a six-hour infection, wt increased approximately 40-fold while the Δ*spxA1* strain increased 3-fold and the over-expressing

strains grew similarly to the Δ*spxA1* parental strain (Fig. 5B). These results demonstrated the pleiotropic nature of SpxA1 regulation, as restoring expression of a single SpxA1-dependent gene or operon was insufficient to restore virulence to the Δ*spxA1* mutant.

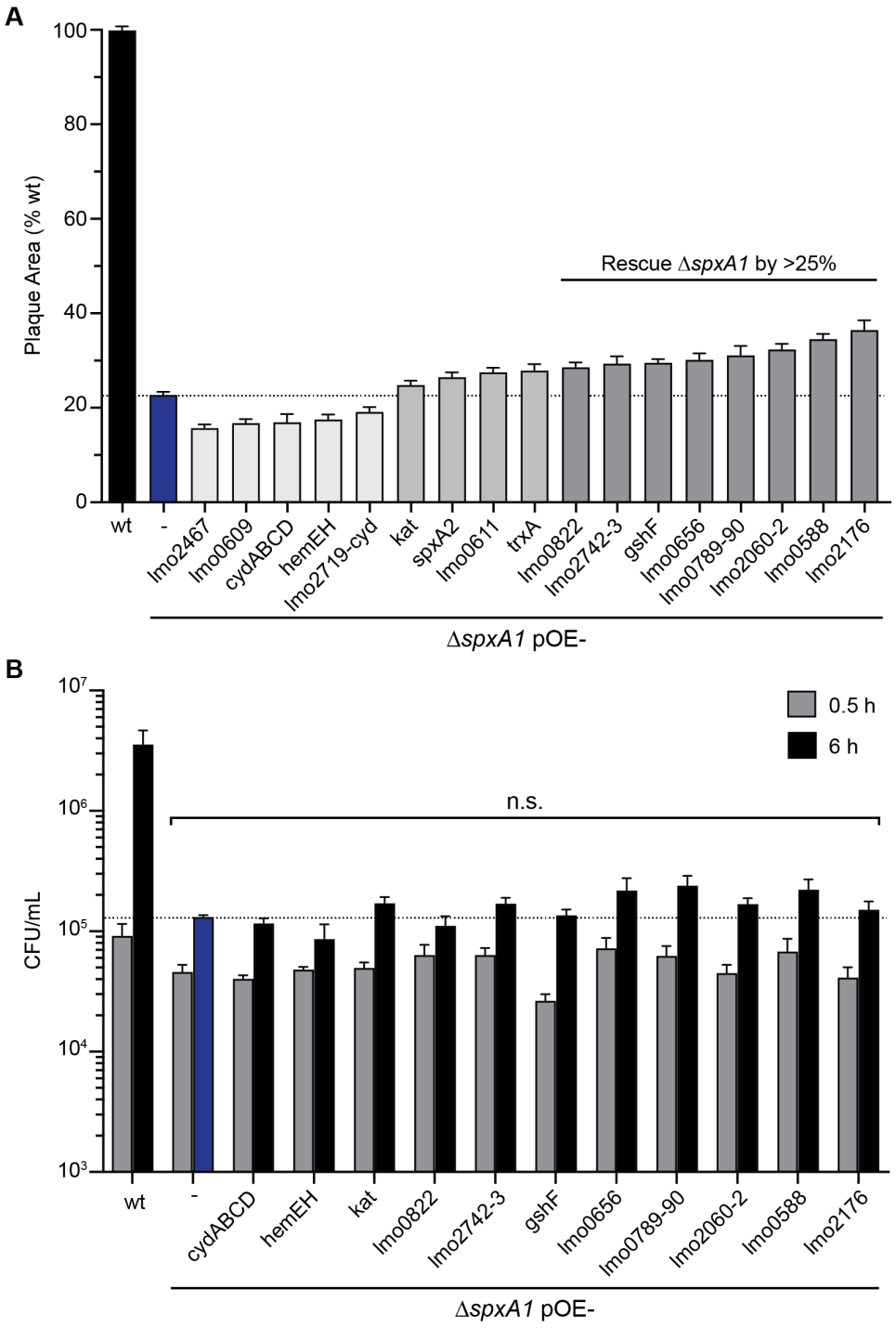

Figure 5. Intracellular replication and cell-to-cell spread of Δ*spxA1* overexpressing strains. (a) Plaque area measured as a percentage of the wt strain. (b) Intracellular growth kinetics of Δ*spxA1* overexpressing strains in BMDMs, measured at 0.5 and 6 hr post-infection. Bacteria were plated anaerobically and CFU were enumerated after 24 hr. All Δ*spxA1* overexpressing strains exhibited similar growth as the Δ*spxA1* parental strain (n.s., $p > .05$). In both panels, data are the means and standard error of the means (SEM) of three independent experiments

The roles of SpxA1-dependent genes during aerobic growth

The panel of over-expressing strains were next grown in the presence of oxygen to evaluate aerobic growth. The only over-expressing strains that formed colonies on BHI agar incubated aerobically were Δ*spxA1* pOE-*cydABCD* and Δ*spxA1* pOE-*hemEH* (Fig. 6). The Δ*spxA1* pOE-*cydABCD* strain constitutively expressed the operon encoding cytochrome *bd* oxidase, resulting in a few tiny colonies that were visible after several days on solid media, but did not grow larger. In contrast, Δ*spxA1* pOE-*hemEH* grew more robustly. This strain constitutively expressed the genes encoding uroporphyrinogen decarboxylase (HemE, also named UroD) and ferrochelatase (HemH, also named CpfC), which are two enzymes in the heme biosynthesis pathway (56). However, neither pOE-*cydABCD* nor pOE-*hemEH* rescued Δ*spxA1* aerobic growth in a shaking flask, as measured by optical density, nor did over-expression of any other gene or operon in Table 1 (data not shown).

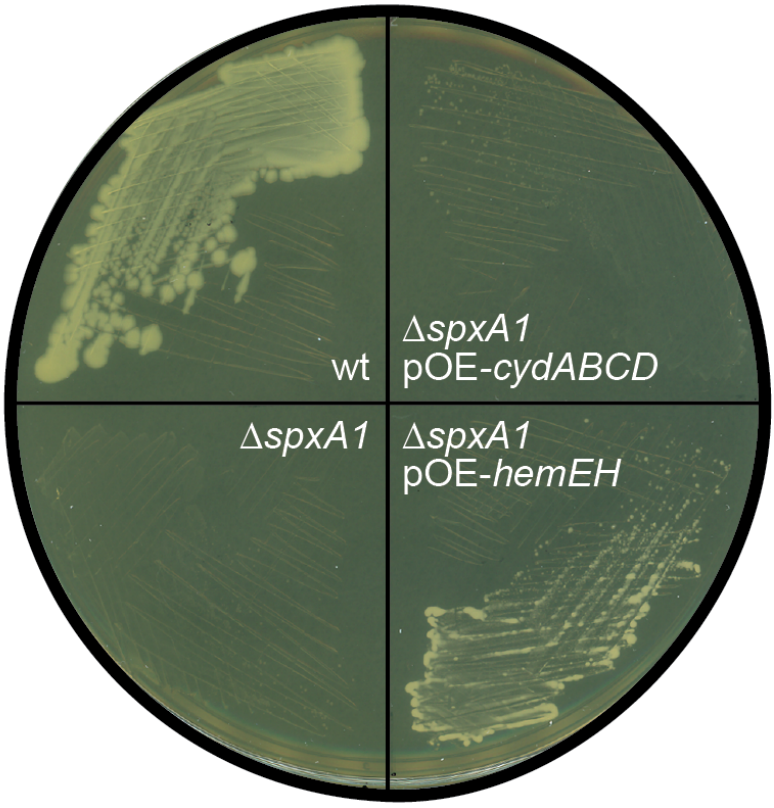

Figure 6. Overexpressing *hemEH* rescued Δ*spxA1* aerobic growth on solid media. All *L. monocytogenes* Δ*spxA1* overexpressing strains were streaked for growth aerobically and anaerobically on BHI. Only Δ*spxA1 pOE-cydABCD* and Δ*spxA1 pOE-hemEH* grew on solid media in the presence of oxygen. Colonies were visible after 3–5 days

Over-expressing *hemEH* rescued growth of Δ*spxA1* on solid media but not in aerobic liquid culture. Hence, we hypothesized that heme is necessary for growth in the presence of oxygen, but reasoned that over-expressing only two of the nine genes encoding enzymes in the heme biosynthetic pathway was insufficient. The remaining seven genes are encoded in three loci elsewhere in the chromosome, making it difficult to engineer a strain over-expressing all nine genes. Therefore, we next supplemented the growth media with exogenous heme in an attempt to restore Δ*spxA1* aerobic growth. Addition of 5 or 10 μM heme partially rescued Δ*spxA1* growth in a shaking flask, although

it did not fully restore growth to wt levels (Fig. 7A). We did not observe any effect of adding exogenous iron, suggesting that this phenotype is specific to the heme moiety (data not shown).

Heme is a redox-active molecule that is required for the function of proteins involved in electron transport, oxygen carrying, and as an enzyme cofactor (57). In addition, excess free heme is toxic due to its ability to generate reactive oxygen species and cause oxidative damage to proteins and DNA (58, 59). Surprisingly, heme rescued Δ*spxA1* growth rather than inducing additional redox stress, suggesting heme was being used as a protein cofactor. In *L. monocytogenes*, heme-binding proteins include cytochrome oxidases, catalase, heme import and biosynthesis proteins, and enzymes in the cobalamin synthesis pathway. The gene with the greatest reduction in expression in the Δ*spxA1* mutant grown in broth was *kat*, encoding the only catalase produced by *L. monocytogenes* (Table 1). *L. monocytogenes* produces two terminal cytochrome oxidases: a cytochrome *bd* oxidase (encoded by *cydABCD*) and a cytochrome aa_3-type menaquinol oxidase (encoded by *qoxABCD*). However, only the *cydABCD* operon transcripts, which is required for respiration and intracellular growth (60), were significantly less abundant in Δ*spxA1* (Table 1). The *cydABCD* operon also had a small effect on Δ*spxA1* growth when constitutively expressed (Fig. 6). We therefore postulated that exogenous heme partially rescued aerobic growth via its ability to act as a cofactor for catalase and/or cytochrome *bd* oxidase. To test this, *kat* or the *cydABCD* operon was over-expressed in Δ*spxA1* in the presence of exogenous heme and colony forming units (CFU) were measured after 24 hours of aerobic growth. Surprisingly, over-expressing *kat* significantly increased Δ*spxA1* survival in the absence of heme (Fig. 7B). However, in the

presence of exogenous heme there was no effect of over-expressing *kat* or *cydABCD* (Fig. 7B). These data suggested that *L. monocytogenes* Δ*spxA1* is unable to grow aerobically due to insufficient heme and catalase production. Moreover, the effect of exogenous heme on Δ*spxA1* aerobic growth was independent of catalase and cytochrome *bd* oxidase.

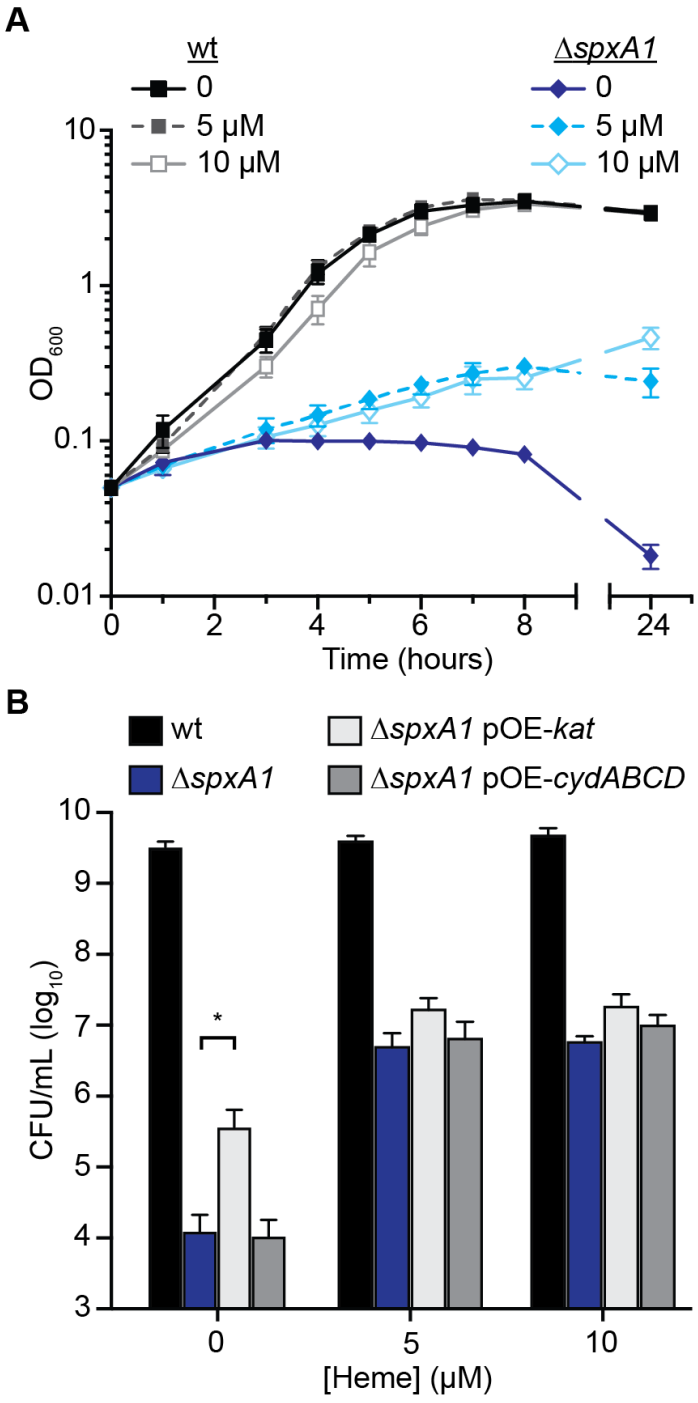

Figure 7. Exogenous heme partially rescued Δ*spxA1* aerobic growth. (a) Aerobic growth kinetics measured by optical density (OD_{600}) of *L. monocytogenes* grown in TSB alone or supplemented with heme to a final concentration of 5 or 10 μM. (b) Aerobic growth of *L. monocytogenes* strains in TSB or TSB supplemented with heme 24 hr post-inoculation with 5 × 10^7 CFU/ml. The Δ*spxA1* strain was engineered to over-express genes encoding catalase (pOE-*kat*) or the cytochrome *bd* operon (pOE-*cydABCD*), as indicated. In both panels, data are the mean and *SEM* of three independent experiments. *p* values were calculated using a heteroscedastic Student's *t* test. *$p < .05$

Catalase is required for aerobic growth *in vitro*, but not intracellular growth

Over-expressing *kat* had a small but significant effect on Δ*spxA1* aerobic growth (Fig. 7B). The *kat* over-expressing strain exhibited 10-fold higher *kat* expression than wt in anaerobic broth (Fig. 4), although we were unable to verify the protein was over-produced in this strain, as anaerobically grown bacteria did not produce detectable catalase (Fig. 8). Together, these data led to the hypothesis that additional catalase may be required to completely detoxify the endogenous ROS produced aerobically in the Δ*spxA1* mutant. Indeed, addition of catalase to the media rescued growth of Δ*spxA1* in aerobic shaking flasks (Fig. 9A). Concentrations of catalase as low as 0.01 mg/mL restored Δ*spxA1* growth over 100,000-fold (Fig. 9B). Importantly, boiled catalase did not rescue aerobic growth, indicating that enzymatic activity was required (data not shown). These data suggested that hydrogen peroxide toxicity resulting from insufficient production of catalase is the primary reason Δ*spxA1* cannot grow aerobically.

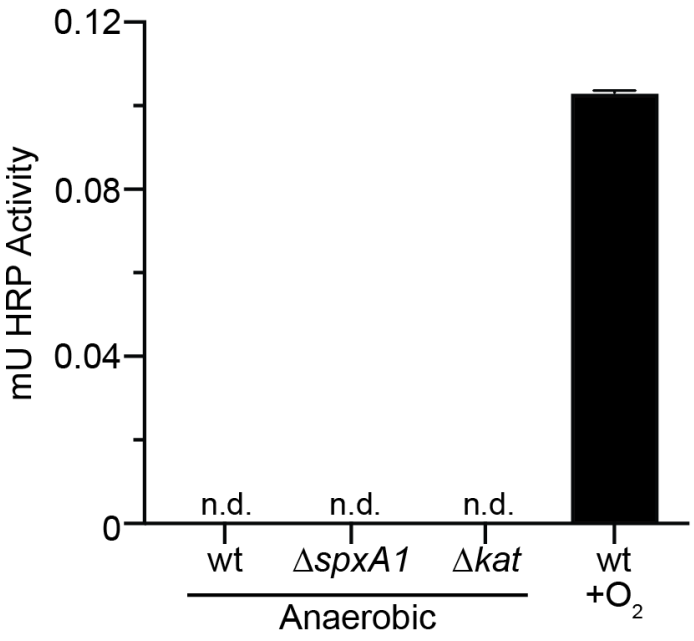

Figure 8. Anaerobic cultures do not produce detectable peroxidase activity. Bacteria were inoculated into 4 mL BHI + Strep, grown overnight in the presence or absence of oxygen, normalized to 1.5ODs in sterile PBS and assayed for peroxidase activity using Amplex Red kit (Invitrogen) according to the manufacturers instructions. Peroxidase activity was determined by generating a standard curve and reading fluorescence in a 96-well plate Biotek Flx800 plate reader (excitation 530nm, emission 590nm) 1.5h after starting the assay. Data shown are the mean and SEM of two independent biological replicates. n.d., not detected.

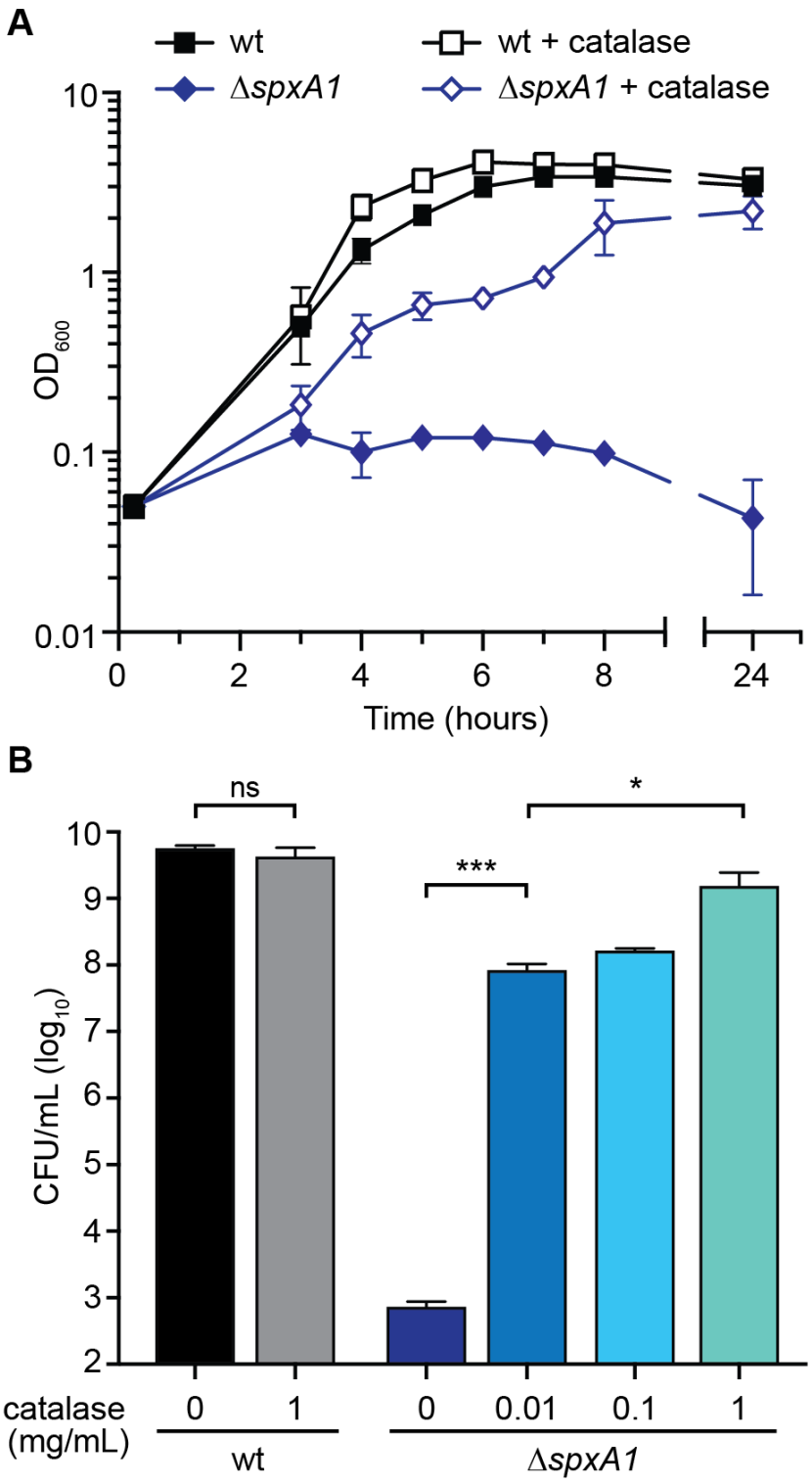

Figure 9. Exogenous catalase rescued Δ*spxA1* aerobic growth. (a) Aerobic growth kinetics of wt and Δ*spxA1* in TSB or TSB supplemented with 1 mg/ml of catalase. (b) Aerobic growth 24 hr post-inoculation in TSB alone or supplemented with various concentrations of catalase, as measured by plating for CFU and incubating anaerobically. *p* values were calculated using a heteroscedastic Student's *t* test. n.s., not significant ($p > .05$); *$p < .05$; ***$p < .001$

Catalase rescued aerobic growth of Δ*spxA1*, suggesting that toxic levels of peroxide were either present in the media or produced by the bacteria. If not specifically treated, rich media contains hydrogen peroxide from metal-catalyzed glucose oxidation. Hydrogen peroxide is also generated over time as media is exposed to light (28). To determine if Δ*spxA1* aerobic growth was inhibited by peroxide present in the media, we performed two important controls. First, TSB was degassed overnight in an anaerobic chamber prior to aerobic subculture of bacteria. Second, media was treated with catalase and then autoclaved to inactivate catalase. The media in both of these scenarios was therefore free of hydrogen peroxide at the start of the experiment, but did not contain active catalase during bacterial growth. Importantly, all media and culture flasks were kept in strict darkness to eliminate photochemical generation of hydrogen peroxide (28). We also measured peroxide concentrations in these treated media and found that degassed and autoclaved media had the same low concentration of H_2O_2 as the catalase-containing media (Fig. 10A). The only condition that supported Δ*spxA1* aerobic growth contained active catalase throughout the experiment (Fig. 10B), demonstrating that the toxic peroxide was generated by the bacteria during growth.

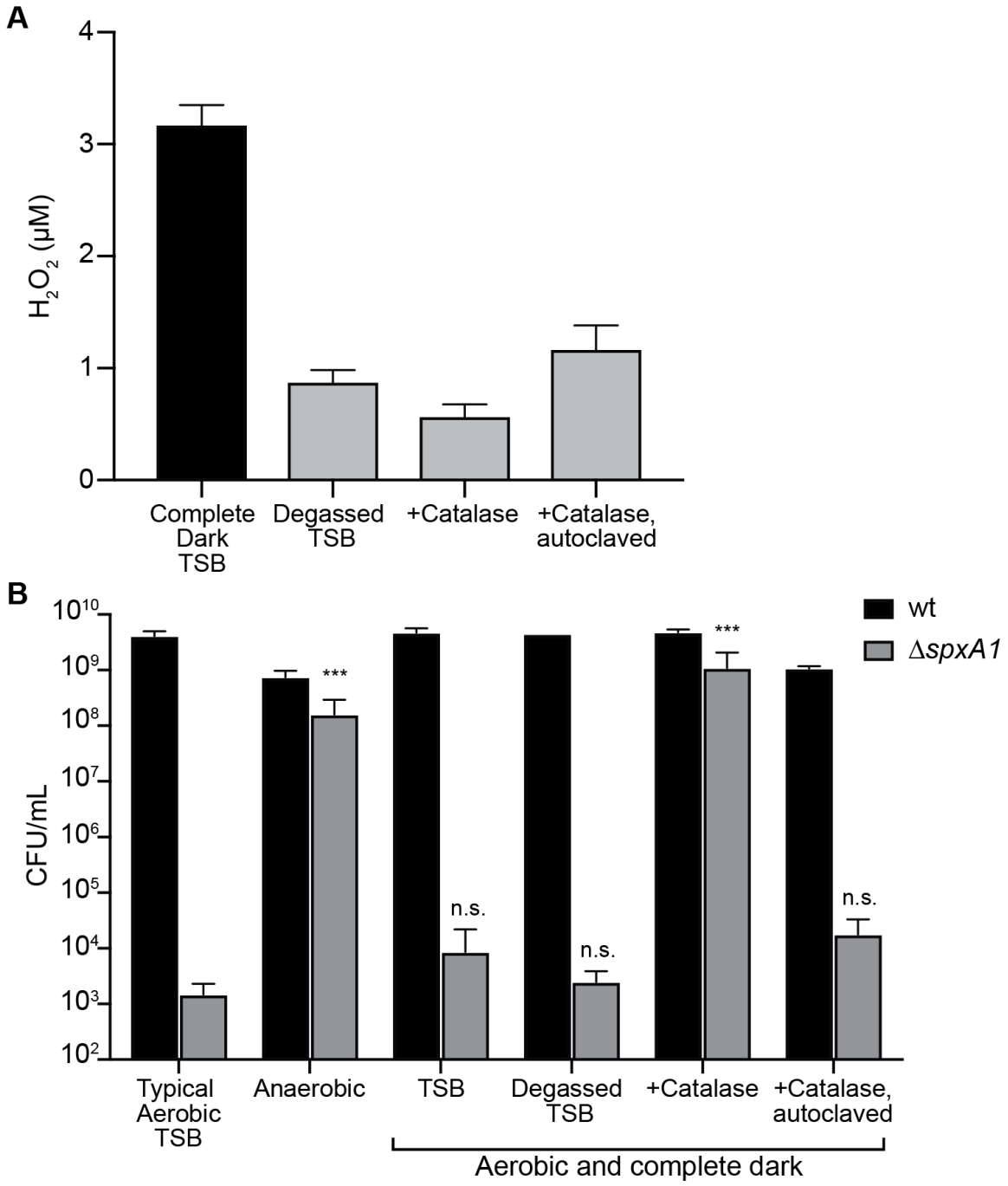

Figure 10. Toxic peroxide is not present in the media. A. Hydrogen peroxide was measured using Amplex Red kit (Invitrogen) according to the manufacturers instructions. Peroxide levels were determined by generating a standard curve and reading fluorescence. Data shown are the mean of two independent experiments with 2-4 technical replicates per experiment. **B.** Bacterial growth 24 hours post-inoculation in the media analyzed in (A). Culture flasks were grown in the dark and additionally were wrapped in foil to prevent exposure to light during bacterial growth. 'Typical aerobic TSB' was prepared without strict light precautions and used for both aerobic and anaerobic growth (first 2 sets of bars). *P* values were calculated using a heteroscedastic Student's *t* test. ***, $P < 0.001$ compared to typical aerobic TSB; n.s., not significant ($P > 0.05$).

To further explore the role of catalase in *L. monocytogenes*, a Δ*kat* mutant was constructed under anaerobic conditions and tested for growth in the presence of oxygen. To delete *kat* it was also necessary to remove the neighboring gene *lmo2784*, a putative transcriptional antiterminator, to prevent toxicity of the plasmid in *E. coli* during cloning (see Experimental Details). All phenotypes were verified to be *kat*-dependent and independent of *lmo2784* (Fig. 11A). The *L. monocytogenes* Δ*kat* strain grown anaerobically overnight and then sub-cultured into aerobic shaking flasks exhibited normal growth for the first four hours. However, after four hours, no additional growth was observed (Fig. 12A). This defect was complemented by expressing *kat* from its native promoter at an ectopic site in the chromosome (Δ*kat pPL2.kat*). To determine if Δ*kat* was killed by oxygen or if growth was merely inhibited after four hours, we tracked growth over time by enumerating live bacteria plated anaerobically. This experiment revealed that *L. monocytogenes* lacking *kat* replicated for approximately four hours, but then died over time in aerobic culture (Fig. 12B). Moreover, supplementing the media with exogenous catalase fully restored the aerobic growth of Δ*kat* (Fig. 11B), confirming that death is due to lack of functional catalase. These results demonstrated that catalase is required for *L. monocytogenes* aerobic replication.

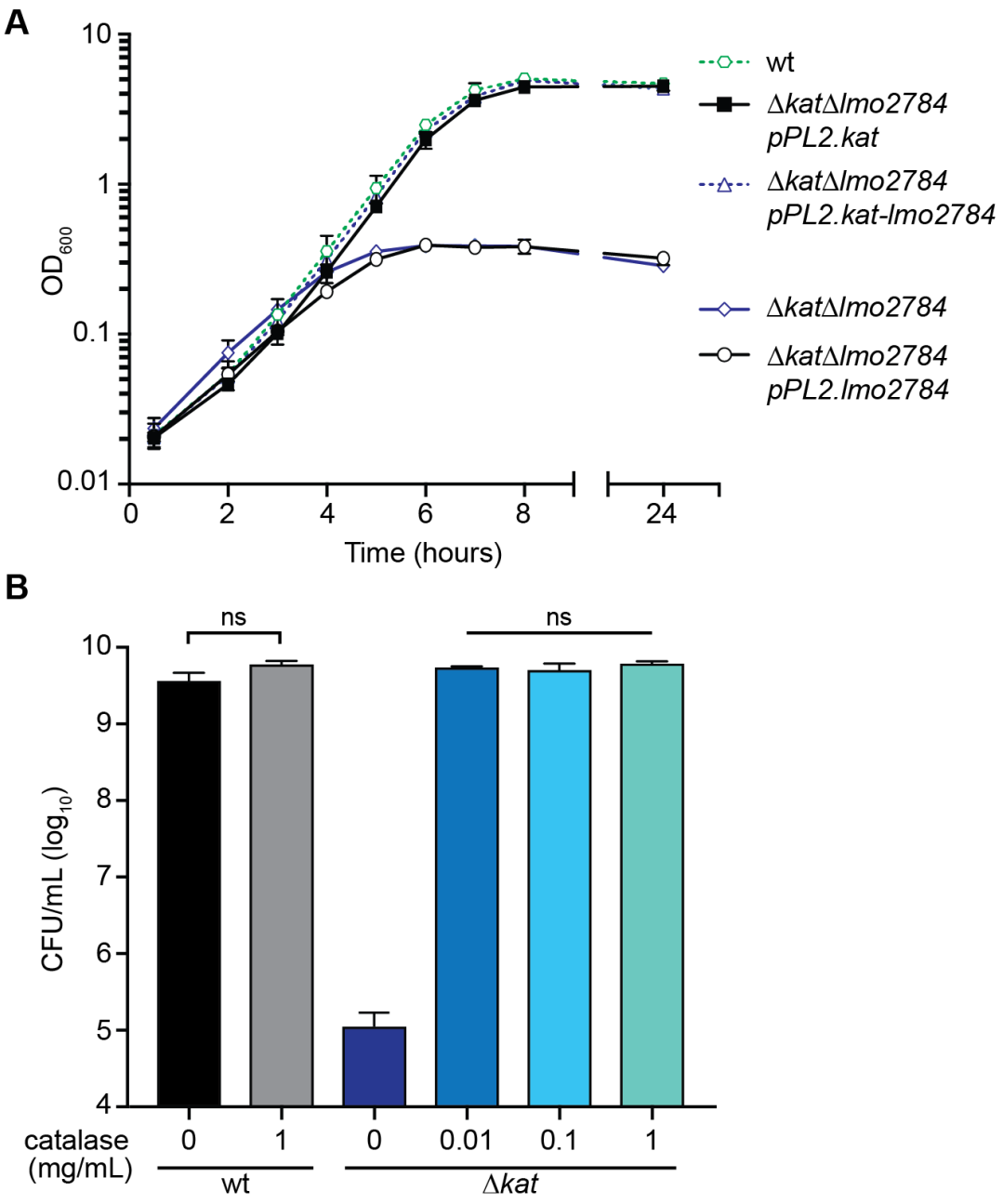

Figure 11. Strains lacking *kat* exhibit a growth defect that is rescued by exogenous catalase. A. Anaerobic overnight cultures were diluted into BHI in a shaking flask and assayed for aerobic growth. Strains lacking *kat* did not grow after 4 hours, whereas strains lacking *lmo2784* grew similarly to wt. **B.** Aerobic growth 24 hours post-inoculation in TSB alone or supplemented with various concentrations of catalase, as measured by plating for colony forming units (CFU) and incubating anaerobically. In both panels, data are the mean and SEM of three independent experiments. n.s., not significant ($P > 0.05$).

Our results showed *L. monocytogenes* requires catalase for aerobic growth and Δ*spxA1* aerobic replication requires exogenous catalase, likely for its ability to efficiently remove peroxide from the culture media. We therefore hypothesized that catalase produced by wt *L. monocytogenes* may detoxify the media and enable Δ*spxA1* growth. To test this, bacteria were washed and then co-cultured in aerobic shaking flasks at a ratio of 1:1 or 10:1 (wt:Δ*spxA1*) and differentially plated over time to enumerate CFU. The Δ*spxA1* mutant grew aerobically in the presence of equal numbers of wt if the wt bacteria were grown aerobically overnight before co-culture (Fig. 12C, open circles). Co-culture with equal wt *L. monocytogenes* grown anaerobically overnight rescued Δ*spxA1* death but did not enable growth of the mutant (Fig. 12C, closed circles). Increasing the ratio of wt-to-mutant bacteria enhanced Δ*spxA1* replication in both cases (Fig. 12C, squares). Furthermore, the Δ*kat* mutant was unable to rescue Δ*spxA1* even when co-cultured at a 10:1 ratio (Δ*kat*:Δ*spxA1*), indicating that Δ*spxA1* replication required functional catalase made by the co-cultured strain for aerobic growth. These data demonstrated that Δ*spxA1* can replicate aerobically if peroxide is detoxified by catalase, whether from purified enzyme added exogenously or bacteria in co-culture. Additionally, these results supported our finding that anaerobically grown *L. monocytogenes* does not produce measurable catalase activity (data not shown) and indicate oxygen-dependent regulation of catalase that we are currently investigating.

Considering the importance of catalase to *L. monocytogenes* growth and that mammalian host cells attack invading pathogens with ROS during the respiratory burst, we postulated that catalase might also be important for intracellular growth. BMDMs were infected with *L. monocytogenes* wt, Δ*kat*, and the complemented strain that were grown

overnight anaerobically, and intracellular growth was measured by plating bacteria anaerobically to enumerate CFU. Surprisingly, the Δ*kat* mutant was able to replicate in BMDMs at the same rate as wt (Fig. 12D), demonstrating that *kat* is completely dispensable for intracellular growth.

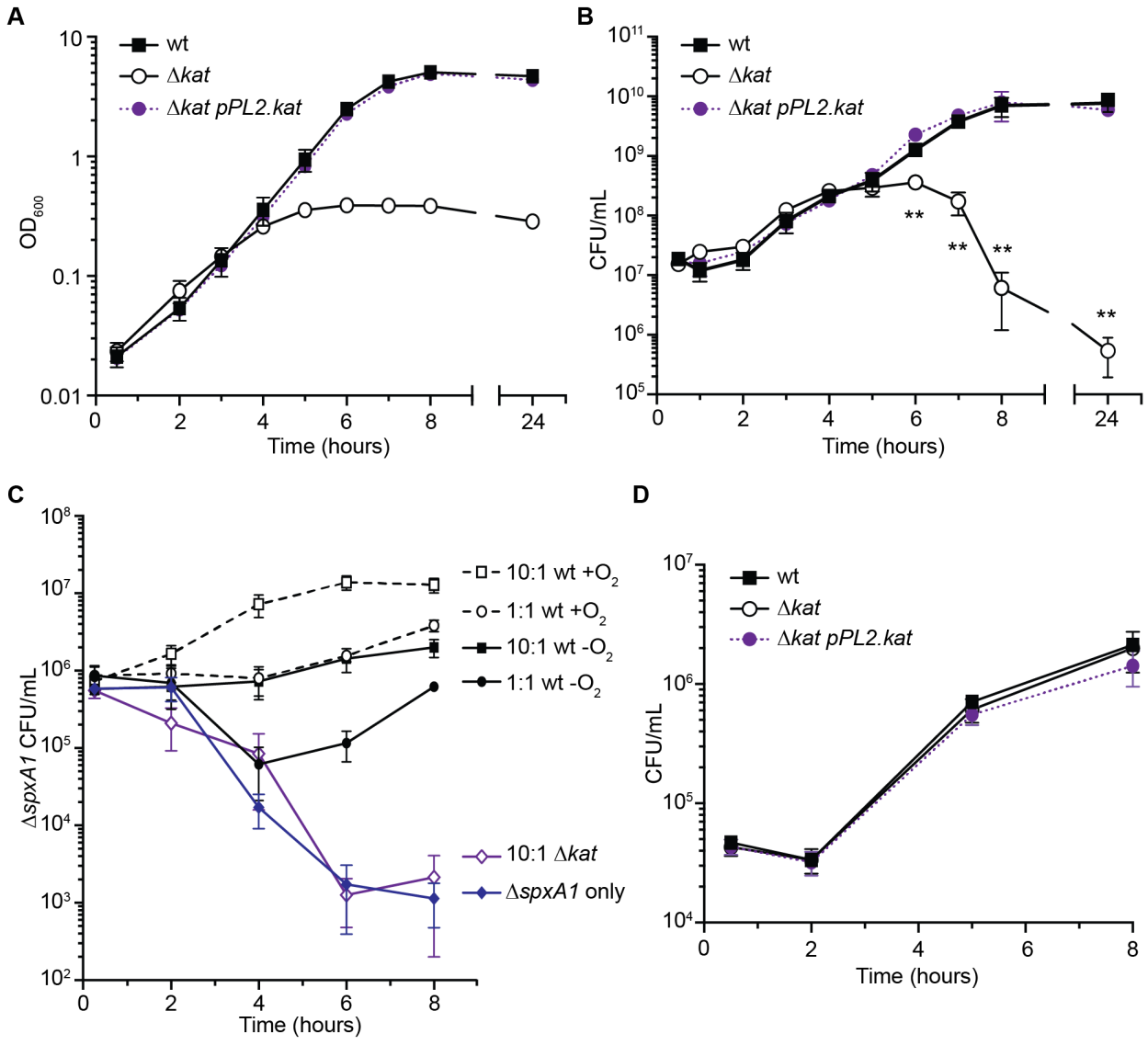

Figure 12. Catalase is required for aerobic growth, but not intracellular growth. (a) and (b) Aerobic growth kinetics of wt, Δ*kat* and the complemented strain, as measured by OD_{600} and by enumerating CFU after growth for 24 hr. (c) Co-culture of wt or Δ*kat* with Δ*spxA1* at the indicated inoculum ratios. For clarity, only Δ*spxA1* growth is shown. Wt was grown overnight aerobically or anaerobically, as indicated. (d) Intracellular growth kinetics in BMDMs of wt, Δ*kat* and the

complemented strain. *L. monocytogenes* strains were grown overnight anaerobically at 37°C before infecting BMDMs with an MOI of 0.1. Bacteria were plated anaerobically and CFU were enumerated. In all panels, data are the means and *SEM* of three independent experiments. Student's *t* test. ** $p < 0.01$

The Spx GC-motif is required for *hemEH* expression and aerobic growth

Considering the importance of heme and catalase for Δ*spxA1* aerobic growth, we sought to leverage the phenotypes of mutants in these pathways to assess direct SpxA1 activation. To this end, we anaerobically generated a Δ*hemEH* mutant, which formed small colonies on solid agar incubated aerobically and did not replicate aerobically in broth in the absence of exogenous heme (Fig. 13A). This was unsurprising, as *S. aureus* heme biosynthesis mutants are known to form small colonies on agar and exhibit a reduced growth rate when incubated in the presence of oxygen (61). Aerobic growth of *L. monocytogenes* Δ*hemEH* was rescued by addition of exogenous heme or by expressing *hemEH* from the native promoter at a neutral locus in the chromosome (Fig. 13A, *pPL2.hemEH*). Although *hemEH* was required for aerobic growth, it was dispensable for BMDM infection (Fig. 13B).

The *B. subtilis* Spx-RNAP complex recognizes a GC-motif at the -44/-43 positions relative to TSSs (42, 52), and many of the genes we identified as SpxA1-activated contain similar motifs (Table 1). To test the role of the GC-motif in SpxA1 regulation in *L. monocytogenes*, promoter regions were engineered with GC at the -44/-43 positions mutated to CA, the least represented nucleotides at those positions in *B. subtilis* Spx-activated promoters (42). The GC-motifs were disrupted in the native promoters of *kat, hemEH,* and *lmo2743* in pPL2 and integrated into the chromosomes of the respective deletion strains. These strains were grown anaerobically overnight and then sub-cultured to measure aerobic growth. Mutation of the *hemEH* GC-motif to CA at positions -44/-43

abolished aerobic growth (Fig. 13A, *pPL2.pCA-hemEH*), suggesting that SpxA1-mediated activation of *hemEH* transcription was required for aerobic replication. Consistent with this, transcript of *hemEH* was reduced approximately 20-fold when the GC-motif was mutated to CA (Fig. 14A). Similarly, *lmo2743* expression also required the GC-motif (Fig. 14B). Surprisingly, we did not see an effect of disrupting the GC-motif in the *kat* promoter (data not shown), indicating that either SpxA1-mediated *kat* regulation is indirect or that *kat* regulation is more complex. Indeed, *kat* has two annotated TSS, only one of which has a GC-motif (51), and is also transcriptionally regulated by PerR (62).

Strains lacking *hemEH* expression (both Δ*hemEH* and the GC-motif mutant) formed small colonies on solid media in the presence of oxygen and were therefore routinely cultured anaerobically to promote optimal growth (Fig. 13C, black circle). However, upon incubating the Δ*hemEH* GC-motif mutant in the presence of oxygen, large colonies spontaneously appeared after a few days at room temperature (Fig. 13C, red circle). We hypothesized that these large colonies were suppressor mutants and sequenced the *hemEH* promoters of four large colonies and four small colonies from the mixed regions. Surprisingly, all four large colonies had reverted the disrupted Spx-motif back to the wt sequence of GC at positions -44/-43 relative to the TSS and no other mutations were observed in the promoter region (Fig. 13C). The remaining small colonies retained the CA at these positions. These results validated that the GC-motif observed in Spx-activated genes in *B. subtilis* is conserved in *L. monocytogenes.* Moreover, SpxA1-dependent activation of *hemEH* and *lmo2743* required the GC-motif and the transcriptional activation of *hemEH* was required for aerobic growth of *L. monocytogenes*.

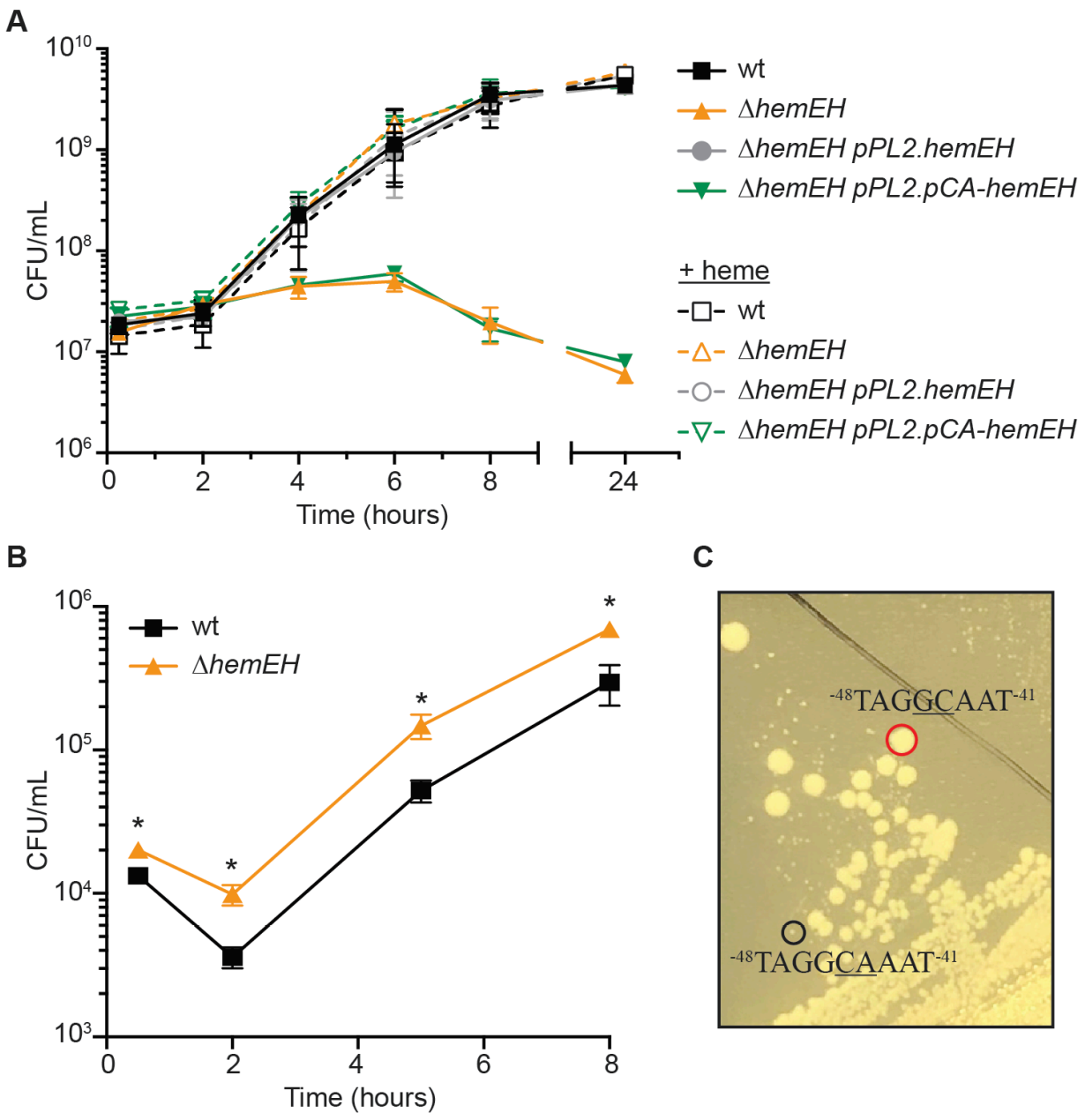

Figure 13. The GC-motif is required for SpxA1-activation of *hemEH*. (a) Aerobic growth kinetics in the absence (solid lines) or presence of 5 μM heme (dotted lines), as measured by enumerating CFU. (b) Intracellular growth kinetics in BMDMs. In panels a and b, data are the means and *SEM*s of three independent experiments. *p* values were calculated using a heteroscedastic Student's *t* test. **p* < .05. (c) Image of suppressor mutants (red circle) on rich agar incubated aerobically. Large and small colonies were sequenced and a portion of the extended −35 box of each is shown with the putative GC-motif underlined.

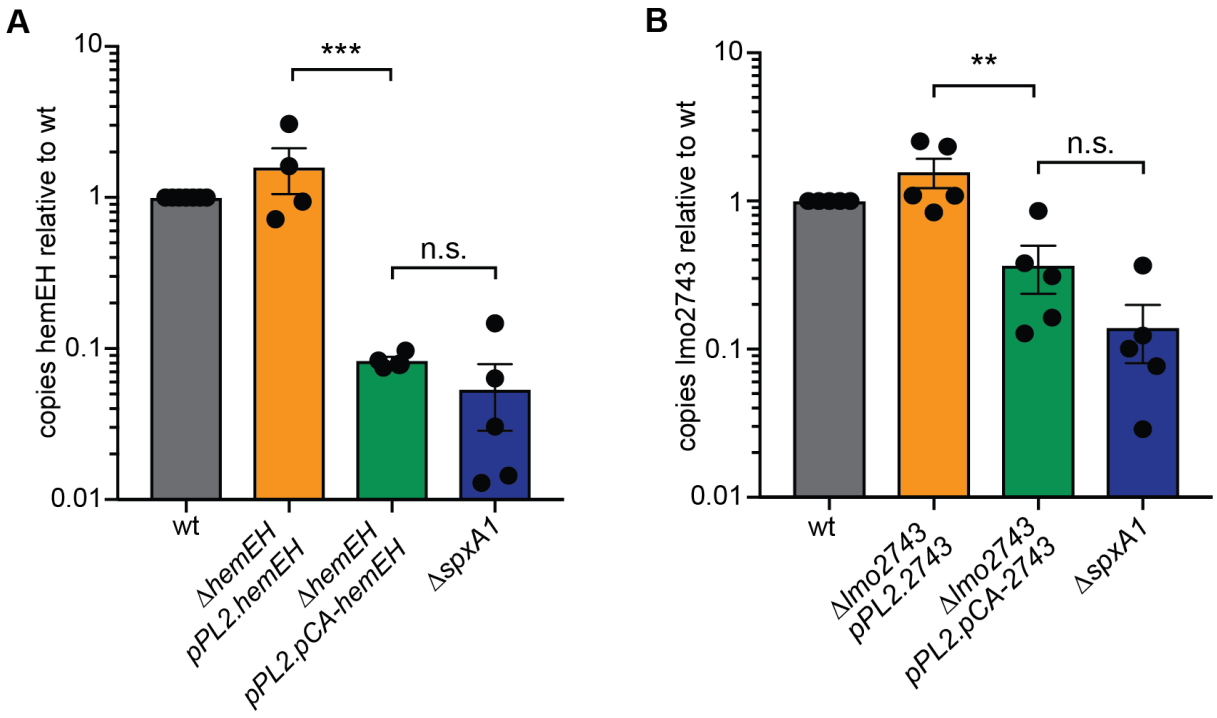

Figure 14. Expression of *hemEH* and *lmo2743* requires the GC-motif. Transcript abundance of hemEH (**A**) and lmo2743 (**B**) in strains grown anaerobically to mid-log. Cultures were back-diluted to an OD_{600} of 0.02 from anaerobic overnights and grown for four hours to an OD_{600} of 1. RNA was isolated from cultures and and transcript was measured as previously described. hemEH or lmo2743 transcript was first normalized to 16S abundance and then calculated relative to wt. Data are the mean and SEM of four or five independent experiments. *P* values were calculated using a heteroscedastic Student's *t* test. **, $P < 0.01$; ***, $P < 0.001$; n.s., not significant ($P > 0.05$).

Discussion

Redox stress is a common danger that all bacteria must be prepared to defend against. In addition to exogenous redox stress encountered during infection from the immune response or in the environment from competing bacteria, endogenous oxidative stress is generated continuously in the presence of oxygen (12, 50). To combat these stressors, bacteria basally express detoxifying enzymes and are poised to rapidly respond to an increase in oxidative stress via redox-sensing transcriptional regulators. Gram-positive bacteria employ Spx-family proteins to sense oxidative stress and regulate

cognate genes necessary to detoxify ROS and survive. Herein, we identified *L. monocytogenes* genes regulated by SpxA1 *in vitro* and during macrophage infection. The results from this study demonstrated that SpxA1 is required to activate genes for production of heme and catalase to detoxify endogenous ROS generated in the presence of oxygen. These results highlight the pleiotropic nature of SpxA1, as the top genes activated by SpxA1 (*kat* and *hemEH*) were each individually required for aerobic growth *in vitro*. Conversely, *kat* and *hemEH* were not required during macrophage infection, suggesting an alternative role for SpxA1 *in vivo*.

While this study explores important differences between the set of genes regulated by SpxA1 in *L. monocytogenes* and the Spx regulon in *B. subtilis*, RNA-seq revealed numerous similarities as well. SpxA1 activated many homologous genes, including: *fbp* (fructose-1,6-bisphosphatase), *hemH* (ferrochelatase), *lmo2256* (similar to *yraA*), *tpx* (thiol peroxidase), *trxB* (thioredoxin reductase), and the thioredoxins *trxA* and *yjbH* (39). Spx-family proteins also regulate low molecular weight thiol biosynthesis in both organisms. In *L. monocytogenes*, SpxA1 activated *gshF*, which codes for glutathione synthase. *B. subtilis* does not produce glutathione and instead synthesizes bacillithiol, production of which is regulated by Spx (63). There are also several differences between the regulons of *B. subtilis* Spx and *L. monocytogenes* SpxA1. For example, *katA*, encoding one of three catalases produced by *B. subtilis*, is repressed by Spx (39, 42). Additionally, we did not observe SpxA1-dependent changes in *sodA* expression, although it is one of the most induced genes of the *B. subtilis* Spx regulon (39). Overall, our transcriptome analysis supported that *L. monocytogenes* SpxA1 plays a similar role to *B.*

subtilis Spx in regulating a response to oxidative stress, although with some interesting differences.

Our data provide strong evidence that heme production is directly regulated by SpxA1. Heme is a tetrapyrrole ring complexed to a central iron atom, making it a versatile redox-active molecule used as a cofactor by many enzymes, including catalase, cytochrome oxidase, and heme peroxidase. Heme can be taken up from the environment or synthesized *de novo* via the Hem proteins (HemALBCDEYHQ) that have recently been renamed to reflect their enzymatic activity (56). Heme biosynthesis has been extensively studied in *S. aureus,* and in that organism, the majority of genes encoding heme biosynthesis enzymes appear to be constitutively expressed (64). The exception is HemA/GtrA, the first committed enzyme in the biosynthetic pathway, which is post-transcriptionally regulated and acts as a switch to increase or decrease heme synthesis (64). Given the change in *hemEH* expression observed in the Δ*spxA1* strain in broth, we hypothesize that *hemEH* is the switch that is directly regulated by SpxA1 to control heme synthesis in response to redox stress in *L. monocytogenes*.

SpxA1 positively regulates *kat* and *hemEH* and both catalase and heme are required for aerobic growth. We initially hypothesized that heme was required as a cofactor for catalase and/or cytochrome *bd* oxidase, however the data did not support this. Specifically, over-expressing *kat* or *cydABCD* in the presence of exogenous heme did not restore Δ*spxA1* growth compared to adding heme alone. Conversely, over-expressing *kat* in the absence of exogenous heme rescued some Δ*spxA1* death. These data indicated Δ*spxA1* is capable of producing enough heme to produce functional catalase when *kat* is over-expressed. Prior studies demonstrated that *L. monocytogenes*

lacking *cydAB* uses fermentative metabolism and thus, displays only a modest reduction in aerobic growth (60). While we therefore do not predict that the lack of cytochrome *bd* plays a significant role in the Δ*spxA1* aerobic growth defect, it may be contributing to ROS production. Indeed, *Enterococcus faecalis* strains with non-functional cytochrome *bd* produce extracellular superoxide due to the nonenzymatic reaction of quinones with oxygen (65). Taken together, we propose a model in which *L. monocytogenes* Δ*spxA1* produces less cytochrome *bd* than wt, generating ROS from the incomplete electron transport chain. In addition, Δ*spxA1* produces less catalase than wt and therefore, is more sensitive to peroxide-mediated toxicity. The mechanism by which exogenous heme rescued Δ*spxA1* aerobic growth remains to be determined. Free heme is toxic due to its propensity to generate superoxide and cause oxidative damage to DNA and proteins (58, 59). Therefore, we speculate that exogenous heme is bound by a protein or proteins that relieve oxidative stress in Δ*spxA1*. The identity of these proteins is under investigation.

SpxA1-mediated activation of heme biosynthesis was required for aerobic growth of *L. monocytogenes*. While free heme is toxic, heme is also necessary for many biological processes and bacteria that cannot synthesize heme are impaired for growth. This phenomenon is most well-studied in regard to *S. aureus* small colony variants (SCVs) that are deficient in respiration due to a lack of heme (61). *S. aureus* SCVs arise spontaneously during chronic infections and can be recapitulated in the laboratory by deleting *hemB*. Here, we found that *L. monocytogenes* Δ*hemEH* mutants also form small colonies when grown aerobically in the absence of exogenous heme. We harnessed this phenotype to investigate the role of the SpxA1 recognition sequence in the promoter of *hemEH*. Disruption of the *hemEH* promoter GC-motif abolished aerobic growth and

resulted in a small colony phenotype on solid media similar to the Δ*hemEH* mutant. Surprisingly, these small colonies spontaneously reverted to large colonies when exposed to oxygen. Sequencing revealed that the large colonies had mutated back to the parental GC-motif sequence, underscoring the strong selective pressure for SpxA1-mediated *hemEH* expression during aerobic growth. In the *hemEH* promoter region, the GC-motif is shifted to the -45/-44 position relative to the TSS, rather than the canonical -44/-43 position (42). Our data suggest that either the actual TSS is one nucleotide upstream of the annotated TSS (51), or that the *L. monocytogenes* SpxA1 recognition sequence is more flexible than that of *B. subtilis* Spx. Ongoing studies are aimed at disentangling these possibilities.

Bacterial pathogens are exposed to 5-10 μM hydrogen peroxide in the host phagosome (66). To combat this stress, many bacteria encode more than one catalase enzyme; however, *L. monocytogenes* encodes only one catalase that predicted to be a cytosolic protein. Interestingly, prior studies found that low levels of extracellular peroxide kill wt *L. monocytogenes* and a *kat*-deficient strain is equally as sensitive as wt to exogenous peroxide (67). Further, catalase-deficient transposon mutants are fully virulent in both a chicken embryo model and an intravenous murine model of infection and catalase-deficient strains have been isolated in the clinic (67–69). Together with the results presented here, these data suggest that *L. monocytogenes* catalase is necessary to detoxify endogenous peroxide generated during aerobic growth, but is dispensable *in vivo*. Similarly, *hemEH* was required for aerobic replication but expendable during intracellular growth. These data demonstrate that distinct sets of SpxA1-regulated genes are required *in vitro* and *in vivo*.

Based on the similarities of Spx proteins and DNA recognition sequences, we propose a model of SpxA1-mediated transcriptional regulation similar to what has been described for Spx in *B. subtilis* (35). Spx was originally described as an 'anti-α factor' that negatively regulates gene expression by binding RNAP and disrupting activator-stimulated transcription (39). However, the mechanism by which Spx-family proteins activate gene expression is less well-understood. Our data are consistent with the model that SpxA1 directs RNAP to promoters with a GC-motif near the -44/-43 positions relative to the TSS (53). Further, our results suggest the GC-motif is necessary for direct SpxA1-mediated activation in those promoters that contain it, but the minimal sequence sufficient for SpxA1 recognition is not yet known.

The results described herein revealed the transcriptional regulation mediated by SpxA1 in *L. monocytogenes*, but many questions remain regarding the regulation of SpxA1 abundance and activity both in broth and during infection. *B. subtilis* Spx senses disulfide stress to regulate genes required for redox homeostasis (70). However, the precise redox stressors sensed by *L. monocytogenes* SpxA1 are not yet known. Importantly, the results from this study demonstrate that the Δ*spxA1* growth phenotype *in vitro* can be genetically uncoupled from the virulence defect observed in host cells, suggesting that SpxA1 may sense and respond to distinct stressors in each environment. Defining the stressors that modulate SpxA1 activity and the corresponding SpxA1-dependent genes required will ultimately clarify the complexity of environments experienced by intracellular pathogens during infection.

Chapter 3: Investigating the roles of *Listeria monocytogenes* peroxidases in growth and virulence

Introduction

Bacteria employ many defense mechanisms to defend themselves against ROS-mediated oxidative stress, the most impactful being the production of scavenging enzymes (50). Superoxide dismutase detoxifies superoxide, generating molecular oxygen and hydrogen peroxide that is then efficiently scavenged by peroxidases and catalases. Peroxidases are enzymes that reduce hydrogen peroxide and are the primary scavengers at low concentrations of peroxide. At high concentrations of peroxide when peroxidases become saturated, catalases disproportionate peroxide and become the dominant scavengers (66). Bacteria typically produce multiple functionally redundant enzymes to protect against peroxides. In fact, peroxide toxicity is not detected in the model organism *Escherichia coli* unless three peroxide scavenging enzymes are deleted simultaneously (*ahpCF*, *katG*, and *katE*) (71).

While the mechanisms of peroxide detoxification have been studied for decades in the model organisms *E. coli* and *Bacillus subtilis* (17, 50, 66), the mechanisms by which *Listeria monocytogenes* defends against ROS are less clear. *L. monocytogenes* is a facultative foodborne pathogen that invades host cells, replicates in the cytosol, and spreads to neighboring cells using actin-based motility (1). The virulence factors employed by *L. monocytogenes* to successfully infect a host are all transcriptionally regulated by the master virulence regulator PrfA, which is itself redox-regulated (11). In addition to virulence factors, PrfA regulates genes that enhance *L. monocytogenes* resistance to peroxide (72), further indicating that peroxide stress is relevant during

infection. We became particularly interested in the peroxide detoxification strategy employed by *L. monocytogenes* during infection when our previous work revealed that the single catalase (encoded by *kat*) produced by the bacterium is required for aerobic growth, but dispensable during infection (73). These results led to the hypothesis that *L. monocytogenes* produces other redundant peroxidases in order to survive the respiratory burst of the macrophage phagosome. Here, we evaluated the expression and essentiality of all peroxidase-encoding genes during *L. monocytogenes* growth *in vitro* and during infection of murine cells in tissue culture.

This chapter describes a paper co-authored by Monica Cesinger and Nicole Schwardt, in collaboration with Cortney Halsey, Maureen Thomason, and Michelle Reniere. My contributions to this paper included performing experiments described in Figures 17 and 19, as well as writing and preparation of the final manuscript.

Results

L. monocytogenes encodes 9 predicted peroxidases

In silico analysis of the *L. monocytogenes* proteome identified 9 proteins with predicted peroxidase activity (Table 3). According to the RedoxiBase database, peroxidase proteins belong to two families: heme-peroxidases and non-heme peroxidases (74). We performed a search of the *L. monocytogenes* proteome based on these categories. Of the heme peroxidases, *L. monocytogenes* encodes a heme-dependent catalase (Kat), a coproheme decarboxylase (ChdC, formerly HemQ), and a DyP-type peroxidase (Lmo0367). The non-heme peroxidases include the peroxiredoxin family (Thiol Prx superfamily), which is characterized by highly conserved peroxidatic

cysteine residues (66). In this family, *L. monocytogenes* encodes Lmo0983, AhpA (formerly AhpC or Prx), Tpx, Lmo1609, and OhrA. Finally, Fri is a non-heme bacterial ferritin classified as an oxidoreductase by the RedoxiBase database (74).

Prior research on the role of *L. monocytogenes* peroxidases is limited. The most well-studied is the ferritin protein Fri (formerly Dps), which was shown to be important for the acute peroxide stress response, long term stationary phase survival, and adaptation to shifting growth conditions (75, 76). A *L. monocytogenes* strain lacking *ohrA* is more sensitive to a variety of oxidative stressors and is attenuated during infection (13). The most dramatic phenotype associated with a *L. monocytogenes* peroxidase mutant is exhibited by strains lacking *kat*, which replicate aerobically to mid-log at the same rate as wild type (wt) but then succumb to endogenously produced peroxide toxicity (73). However, *kat* is not required for intracellular replication in macrophages or for virulence in a murine model of infection and catalase-deficient strains have been isolated from infected humans (69, 73, 77). Based on the important role of peroxide in the innate immune response and the limited research on *L. monocytogenes* peroxidases, we sought a more holistic picture of the role of peroxidases in aerobic growth and virulence.

Table 3. Predicted peroxidases encoded by *L. monocytogenes*

Gene	Name	Predicted Function	Reference(s)
lmo0367	-	heme-dependent dyp-type peroxidase	-
lmo0943	*fri, dps*	bacterioferritin, oxidoreductase	(75, 76)
lmo0983	-	glutathione peroxidase	-
lmo1583	*tpx*	thiol peroxidase	-

lmo1604	*ahpA*	2-cys peroxiredoxin	(78, 79)
lmo1609	-	thioredoxin	-
lmo2113	*chdC, hemQ*	putative heme peroxidase, involved in heme biosynthesis	(80)
lmo2199	*ohrA*	organic hydroperoxidase	(13)
lmo2785	*kat*	heme-dependent catalase	(73)

Expression of peroxidase-encoding genes

To investigate which peroxidase enzymes may be important during *L. monocytogenes* aerobic growth, we first evaluated gene expression in rich media by quantitative reverse transcriptase PCR (qPCR). In these experiments, bacteria were grown in tryptic soy broth (TSB) which lacks glutathione and heme, both of which influence the redox environment of bacterial cultures. Expression of each putative peroxidase-encoding gene was evaluated in wt and Δ*kat* strains and expression of transcripts was normalized to wt at 2 hours post-inoculation into shaking flasks. The Δ*kat* mutant replicated to mid-log, but stopped growing and began to die 8 hours post-inoculation (Fig. 15A). This requirement for Kat activity in early stationary phase corresponds to the peak expression of *kat* in wt *L. monocytogenes* (Fig. 15B). Accordingly, we found that gene expression could not be reliably measured in Δ*kat* 8 hours post-inoculation due to bacterial death. Analyzing transcript abundance of the other peroxidase-encoding genes revealed that lmo0367, lmo0983, ahpA, and lmo1609 did not increase appreciably over time in the wt or Δ*kat* background strains (Fig. 15C). In contrast, tpx expression was elevated early in *L. monocytogenes* lacking *kat* compared to wt,

although this was not statistically significant (Fig. 15D, p = 0.2). The gene encoding Fri was increased in wt *L. monocytogenes* 8 hours post-inoculation, similarly to *kat* expression. Expression of *chdC* exhibited a small, but statistically significant increase initially in *L. monocytogenes* lacking *kat* compared to wt and was significantly increased in wt after 6 hours of aerobic growth (Fig. 15D). The gene encoding OhrA exhibited maximal expression 2 hours post-inoculation and decreased dramatically over time in both strains. Taken together, these data demonstrated that *kat* and *fri* share similar expression dynamics during aerobic growth.

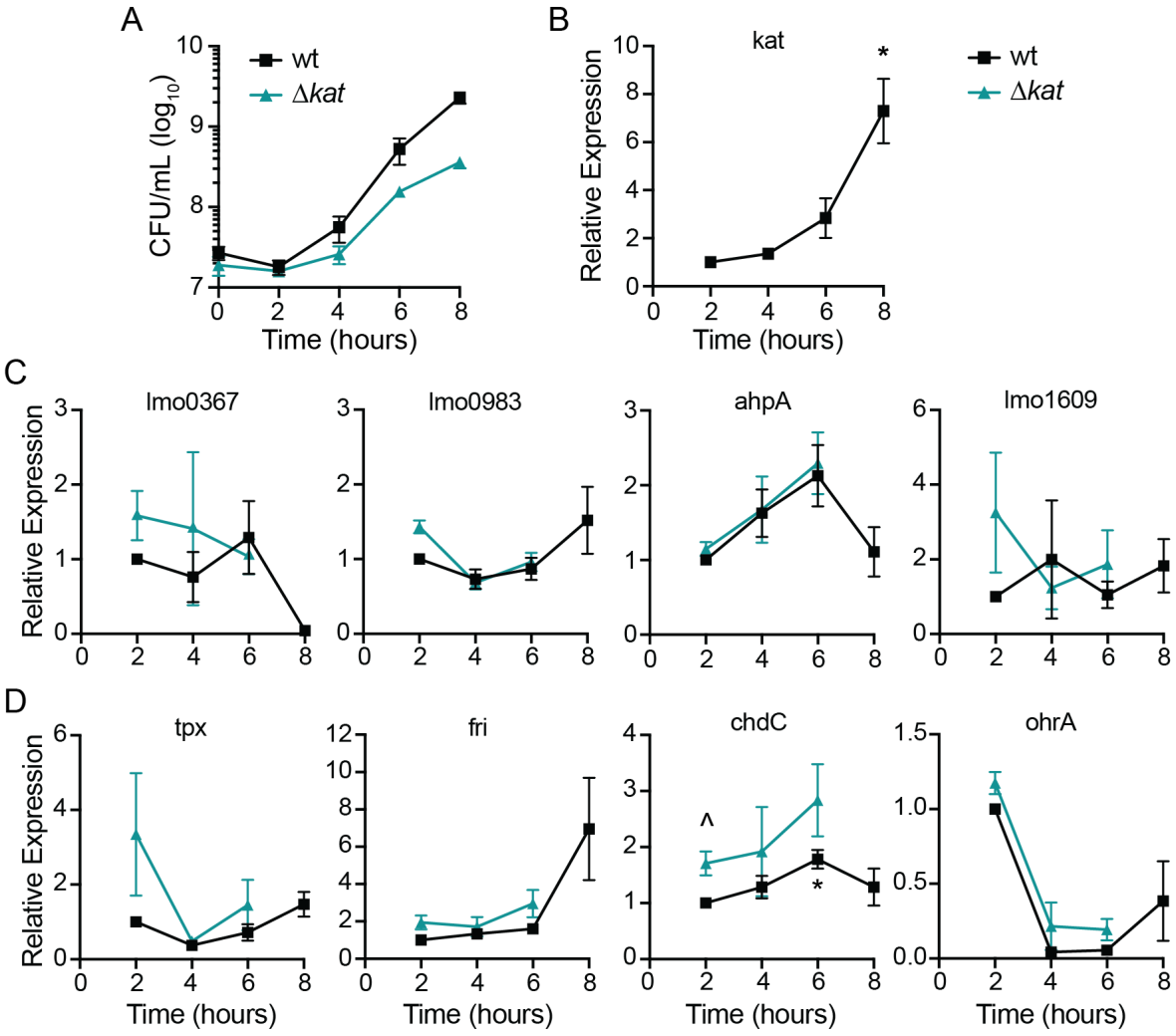

Figure 15. Expression of genes encoding putative peroxidases during aerobic growth. A. Aerobic growth of wt and Δ*kat* in shaking flasks was measured by plating for CFU and incubating the plates anaerobically. Data are the means and standard error of the means (SEM) for three biological replicates. B - D. Relative expression of putative peroxidase-encoding genes over time in both wt and Δ*kat,* as grown in *A*. Expression was normalized to wt expression at 2 hours. Data are the means and standard error of the means (SEMs) of at least three biological replicates. *p* values were calculated using a heteroscedastic Student's *t* test. * $p < 0.05$ expression compared to wt at 2 hours; ^ $p < 0.05$ expression in Δ*kat* compared to wt at that time point.

We next measured expression of these peroxidase-encoding genes during infection using fluorescent transcriptional reporters. Strains were engineered to express *rfp* from the native promoter of each peroxidase-encoding gene and *gfp* was expressed constitutively. J774 macrophages were infected for 1 hour before gentamicin was added to the media to eliminate extracellular bacterial growth. Flow cytometry was performed 6 hours post-infection and infected cells were identified by GFP fluorescence compared to an uninfected control. Cells infected with the reporter strains for expression of *fri*, *ahpA*, and *kat* exhibited significantly increased RFP production compared to the background (Fig. 16). These results suggested that only *fri, ahpA,* and *kat* are significantly expressed during macrophage infection and therefore might have a role in virulence.

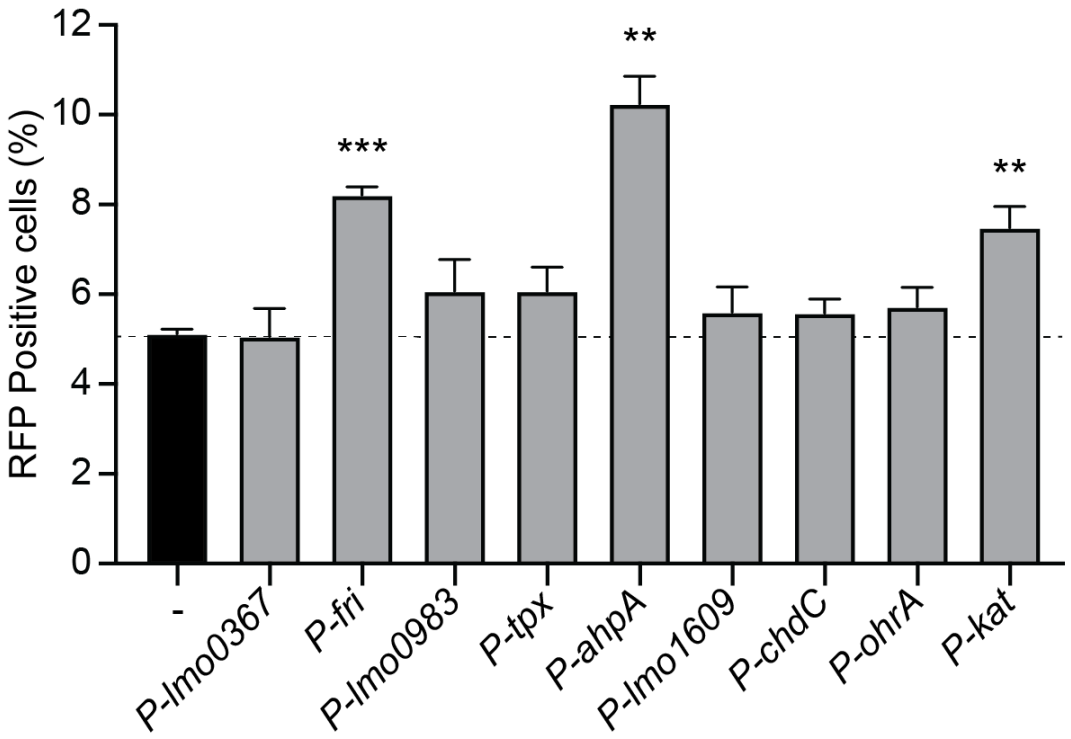

Figure 16. Intracellular expression of peroxidase-encoding genes. J774 macrophages were infected with each reporter strain, which expressed *rfp* from the indicated promoter and constitutive *gfp*. Cells were infected for six hours and then analyzed by flow cytometry. The dotted line indicates background RFP fluorescence. Data are the means and SEMs of three biological replicates. *p* values were calculated using a heteroscedastic Student's *t* test comparing each mutant to wt. ** $p < 0.01$; *** $p < 0.001$.

Growth of peroxidase mutants in broth

Previous work demonstrated that *L. monocytogenes* requires *kat* to detoxify endogenously-produced peroxide during aerobic growth (73). Here, we sought to test if additional peroxidases are important for aerobic growth. For this analysis, each potential peroxidase-encoding gene was deleted by allelic exchange while growing anaerobically to prevent oxygen-mediated toxicity. Based on the redundant roles of Kat and Ahp in other bacteria (71, 81), we also generated a Δ*kat*Δ*ahpA* double mutant. Anaerobic bacterial overnight cultures were diluted into rich media and grown aerobically in shaking

flasks. Serial dilutions were performed to enumerate CFU over time and the plates were incubated anaerobically to promote growth of potentially oxygen-sensitive strains.

Growth analyses revealed that several peroxidase-encoding genes were dispensable for aerobic replication, including: *lmo0367, lmo0983, tpx, ohrA, lmo1609,* and *ahpA* (Fig. 17A and 17B). In contrast, *kat* was required for aerobic growth and began to die upon entry into stationary phase (Fig. 17B), as previously reported (73). The Δ*kat*Δ*ahpA* double mutant was even more sensitive to oxygen, as we observed a significant attenuation in survival at 7 and 9 hours post-inoculation compared to the single mutant lacking *kat* (Fig. 17B). These data indicate that AhpA is functional and important for aerobic replication in the absence of catalase.

Interestingly, we observed a dramatic phenotype for the *L. monocytogenes* strain lacking *fri* (Fig. 17C). Despite normalizing the anaerobic overnight cultures by optical density, we consistently observed a 1- to 2-log defect in Δ*fri* CFU at the initial time point and this defect continued throughout growth until stationary phase (Fig. 16C). This aerobic growth defect could be complemented by providing a copy of *fri in trans* using the integrative plasmid pPL2 (p-*fri*) (82). Previous work suggested that *fri* is important for *L. monocytogenes* adaptation to stress conditions, including nutritional stress and temperature shifts (76). We therefore hypothesized that Δ*fri* was unable to rapidly adapt from hypoxia to aerobic growth. In support of this hypothesis, we found that Δ*fri* incubated aerobically overnight grew similarly to wt after diluting into shaking flasks (Fig. 17C, dotted lines). Consequently, the Δ*fri* mutant was incubated overnight aerobically for all subsequent experiments.

Finally, we observed the Δ*chdC* mutant did not replicate when diluted into shaking flasks and this growth defect was genetically complemented by expressing *chdC in trans* (p-*chdC*, Fig. 17D). This finding is in agreement with published work reporting that *chdC* is essential in *L. monocytogenes* (83). ChdC catalyzes the final step of heme biosynthesis and therefore the Δ*chdC* mutant lacks both peroxidase activity and endogenous heme (80). To distinguish which function is important for aerobic growth, we attempted to chemically complement Δ*chdC* growth by supplementing with exogenous heme. However, addition of exogenous heme is toxic unless bacterial cultures are pre-exposed to low levels of heme (84). Therefore, bacteria were first grown overnight in brain heart infusion (BHI) that contains heme and then diluted into TSB containing or lacking heme (5 μM). Exogenous heme fully restored growth of Δ*chdC* to that of wt (Fig. 17D, dotted lines), suggesting that the aerobic growth defect of *L. monocytogenes* lacking *chdC* is primarily due to a lack of heme.

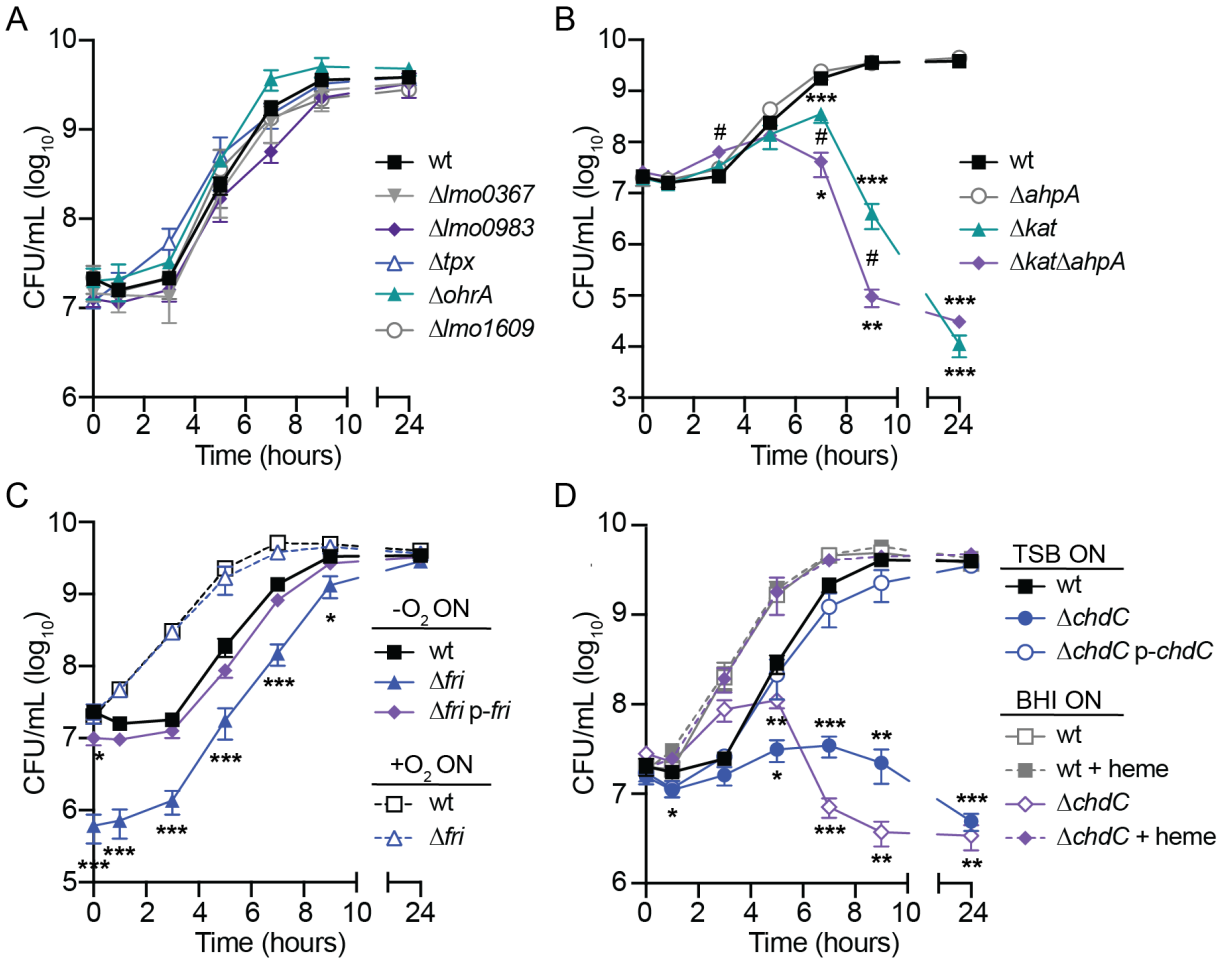

Figure 17. Aerobic growth of peroxidase mutants. A. Growth curves of strains that replicate at the same rate as wt ($p > 0.05$ at each time point). B. Growth curves comparing Δ*ahpA*, Δ*kat*, and Δ*kat*Δ*ahpA*. # indicates significant difference between Δ*kat* and Δ*kat*Δ*ahpA* ($p < 0.05$). C. Growth curves of strains grown anaerobically (solid lines) or aerobically (dotted lines) overnight before back-diluting into shaking flasks. D. Strains were grown anaerobically overnight in TSB or BHI and then diluted into TSB with or without exogenous heme (5 μM). In all panels, data are the mean and SEMs of three biological replicates. *p* values were calculated using a heteroscedastic Student's *t* test comparing each mutant to wt grown in the same conditions. * $p < 0.05$; ** $p < 0.01$; *** $p < 0.001$.

Peroxidases important for acute peroxide toxicity

We next investigated which peroxidases are required for detoxifying acute peroxide stress. Bacteria were grown overnight aerobically, as *L. monocytogenes* does not produce detectable peroxidase activity after anaerobic culture (73). Accordingly, only

the mutants which replicated aerobically could be tested in this experiment. Each strain was grown to early logarithmic phase (OD_{600} = 0.6) before hydrogen peroxide (120 mM) was added for 1 hour. At this concentration of peroxide, wt decreased 1.7-fold over one hour and most mutants exhibited similar resistance (Fig. 18). In contrast, both Δ*fri* and Δ*ahpA* were rapidly killed and no bacteria were detected at 30 or 60 minutes. These results are consistent with published reports demonstrating *fri* and *ahpA* are important for survival in the presence of peroxide (75, 78, 79), and reveal that none of the other peroxidases tested provide non-redundant protection from peroxide under these conditions.

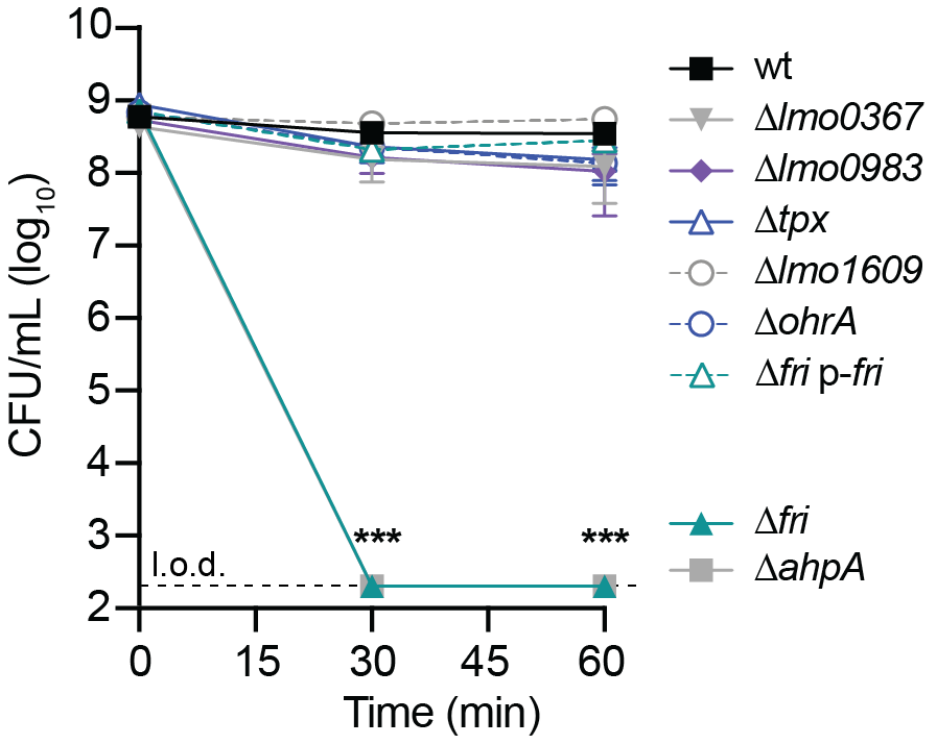

Figure 18. Acute peroxide toxicity. Bacteria were grown aerobically to mid-log before hydrogen peroxide (120 mM) was added. The dotted line indicates the limit of detection (l.o.d.). Data are the means and SEMs of four biological replicates. *p* values were calculated using a heteroscedastic Student's *t* test comparing each mutant to wt. *** $p < 0.001$.

Intracellular growth of peroxidase mutants

During infection of macrophages, *L. monocytogenes* resides briefly in the phagosome where it is bombarded by hydrogen peroxide produced by the host respiratory burst (12). Previous work demonstrated that Kat-mediated peroxide detoxification is not required for intracellular survival or growth in macrophages (73). To test which peroxidases are important intracellularly, we infected bone marrow-derived macrophages (BMDMs) with each strain at an MOI of 0.1 and enumerated CFU over time by plating anaerobically. All the mutants replicated similarly to wt in resting BMDMs (data not shown). To ensure a robust innate immune response, we next infected BMDMs that were pre-treated with interferon gamma (IFNg) to activate the host respiratory burst (85). In these experiments, the majority of peroxidase mutants grew similarly to wt (Fig. 19A). Surprisingly, the Δ*kat*Δ*ahpA* double mutant exhibited a significant 5-8-fold increase in CFU at each time point compared to wt (Fig. 19B). In contrast, the Δ*fri* strain was significantly attenuated for intracellular replication in activated BMDMs and this defect was genetically complemented by providing *fri in trans* (Fig. 19B).

Due to the role of Fri in iron storage, we sought to assess whether the growth defect of Δ*fri* was due to a lack of iron scavenging or peroxidase protection. To that end, intracellular growth curves were performed in gp91$^{phox-/-}$ (*phox*$^{-/-}$) macrophages which lack the NADPH oxidase responsible for the host oxidative bursts and thus mimics the most common genetic defect observed in humans with CGD (86). In these immunodeficient cells, the Δ*fri* mutant exhibited a significant defect 2 hours post-infection, but the intracellular bacterial burden was similar to that of wt and the complemented strain at every other time point (Fig. 19C). Taken together, these results demonstrate that while

the Δ*kat*Δ*ahpA* mutant has an unexpected advantage during infection, *fri* is required for efficient infection of activated macrophages and this is at least partially alleviated in the absence of the host respiratory burst.

One hypothesis to explain the dispensability of the majority of peroxidases for intracellular growth (Fig 19A) is that the host respiratory burst is ineffective against *L. monocytogenes* because the secreted pore-forming toxin LLO allows for rapid escape from the vacuole. To examine which peroxidases may be important specifically in the vacuolar environment, the gene encoding LLO (*hly*) was disrupted in each mutant background and survival in the vacuole of IFNg-activated BMDMs was evaluated over time. In agreement with the intracellular growth curves, the majority of peroxidase mutants survived in the vacuole for 6 hours at rates similar to wt (Fig. 19D). The exceptions were the Δ*kat*Δ*ahpA* mutant, which survived significantly better than wt, and Δ*fri*, which exhibited a ~1-log decrease in CFU at the earliest time point, although this was not statistically significant (p = 0.06). Together, these data demonstrate that the only peroxidase important for vacuolar survival and intracellular growth in activated BMDMs is *fri*.

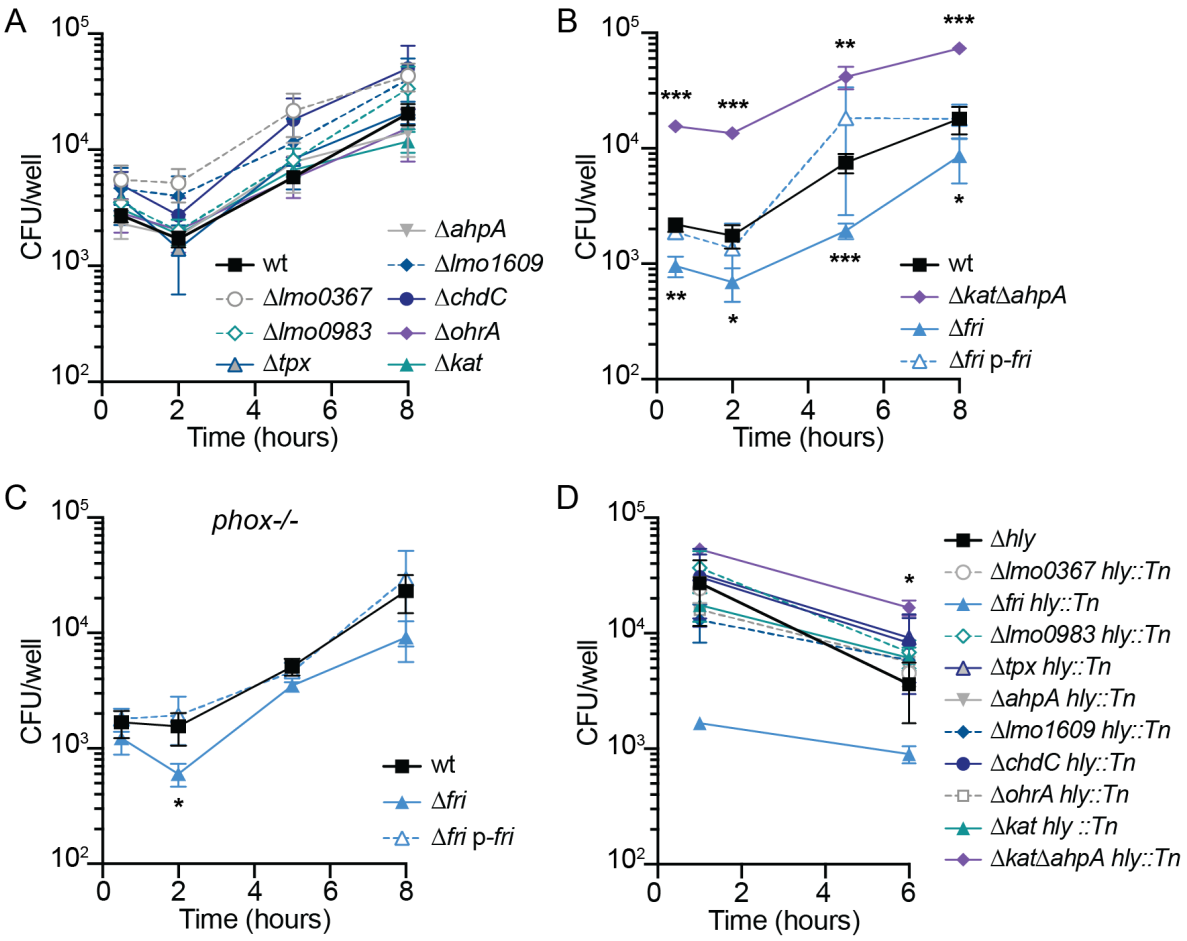

Figure 19. Intracellular survival and growth of peroxidase mutants in IFNg-activated BMDMs. A. Intracellular growth curves of mutant strains that replicated at the same rate as wt (p > 0.05 at each time point). B. Intracellular growth curves in activated BMDMs C. Intracellular growth curves in activated *phox*$^{-/-}$ BMDMs that lack NADPH oxidase. D. Survival of *hly* mutants trapped in the vacuoles of activated BMDMs. Although the error bars are too small to be visible, the Δ*fri hly::Tn* strain is not significantly different from wt at 1 hour (p = 0.06). In all panels, data are the mean and SEMs of at least three independent experiments. p values were calculated using a heteroscedastic Student's t test comparing each mutant to wt grown in the same conditions. * p < 0.05; ** p < 0.01; *** p < 0.001.

Intercellular spread

We next sought to test the role of each peroxidase in virulence using a plaque assay, which is a measure of intracellular growth and cell-to-cell spread that is highly correlated with virulence in a murine model of infection (13, 87). In this assay, a monolayer of L2 murine fibroblasts is infected and immobilized in agarose containing gentamicin to

kill extracellular bacteria. Three days post-infection the living cells are stained with neutral red and the area of the plaques formed by *L. monocytogenes* are analyzed as a measure of intercellular spread. In this assay, all of the mutant strains formed plaques similar in size or larger than those formed by wt (Fig. 20A). Although the Δ*kat*Δ*ahpA* double mutant formed plaques of a similar size as wt, the mutant exhibited a dramatic advantage at invading host cells. The Δ*kat*Δ*ahpA* formed approximately 5 times more numerous plaques than wt (Fig. 20B). This is consistent with the increased bacterial burden observed in IFNg-activated BMDMs at the earliest time points (Fig. 20B), and suggests that Δ*kat*Δ*ahpA* is better able to invade host cells.

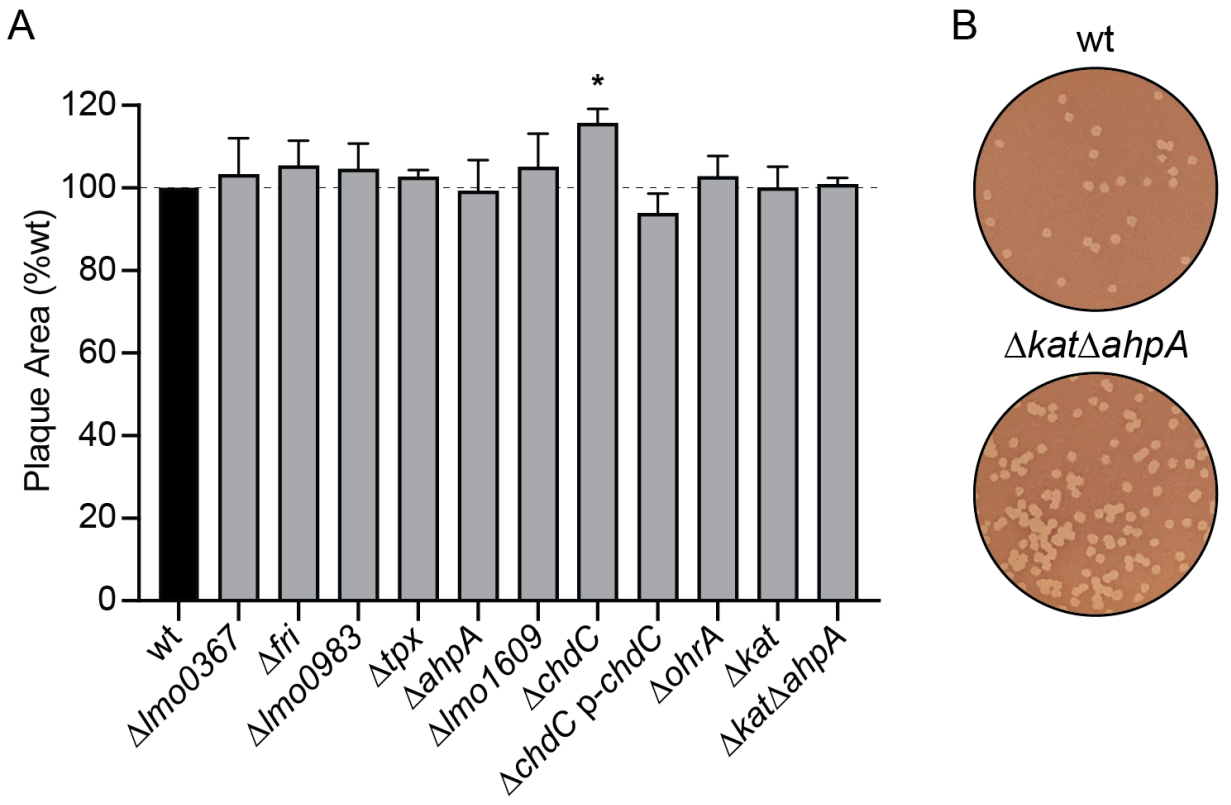

Figure 20. Intercellular spread of peroxidase mutants. A. Plaque formation in L2 fibroblasts was evaluated for each strain. Data are graphed as mean and SEMs. The dotted line signifies the 100% of wt. B. Representative images of plaques demonstrating the greater number of plaques formed by the Δ*kat*Δ*ahpA* mutant compared to wt.

Discussion

Bacterial pathogens must detoxify endogenously produced ROS and exogenous sources of oxidative stress during infection. Hydrogen peroxide is particularly dangerous, as it is an uncharged molecule that can penetrate membranes (50). In this study, we performed the first comparison of the expression and essentiality of all proteins with predicted peroxidase activity in *L. monocytogenes*. Importantly, of the nine peroxides examined here, only ChdC was previously biochemically characterized *in-vitro* for peroxidase activity (21). However, previous work has shown the importance of Fri, Kat, OrhA, and AhpA for *Listeria monocytogenes* survival of peroxide (12,14,15,16,19,20). Our results revealed that *kat* and *chdC* are required for aerobic growth in rich media, while *ahpA* and *fri* are required to detoxify acute peroxide stress *in vitro*. The strain lacking both *kat* and *ahpA* exhibited the most severe aerobic growth defect, but had a surprising advantage invading and surviving in host cells. While *fri*, *ahpA*, and *kat* were expressed during intracellular growth in macrophages, only *fri* was required for survival in INFg-activated BMDMs. Considering the host respiratory burst assaults invading bacteria with up to 100 μM peroxide in the phagosome (71), our results suggest a high degree of redundancy in the *L. monocytogenes* peroxide stress response.

Transcript analysis during aerobic growth revealed that *L. monocytogenes* expression of peroxidase-encoding genes was not dramatically altered in the *kat*-deficient strain compared to wt. This was unexpected, as *B. subtilis* strains lacking *katA* or *ahpC* experience peroxide stress during aerobic growth that induces the PerR (peroxide stress response) regulon (88, 89). Similarly, the *E. coli* OxyR regulon is activated by the peroxide that accumulates when Hpx- cells (Δ*katE*Δ*katG*Δ*ahpCF*) are grown aerobically (71, 90).

Thus, one interpretation of our results is that *L. monocytogenes* Δ*kat* succumbs to peroxide-mediated toxicity before the PerR regulon can be effectively activated (17). However, the Δ*kat*Δ*ahpA* double mutant is even more susceptible to endogenous redox stress *in vitro*, but undergoes undefined regulatory changes that result in increased invasion, survival, and replication in activated macrophages. Ongoing research is aimed at deciphering the regulatory changes that occur in the absence of *kat* and *ahpA* that lead to increased virulence.

Lmo1604 is annotated as an alkyl hydroperoxide reductase (Ahp) based on similarity to other enzymes. The classical Ahp system is comprised of two components: the peroxiredoxin (AhpC) and a dedicated reductase (AhpF) that reduces and recycles AhpC and is typically encoded by a sequence adjacent to *ahpC* (91). Many organisms encode multiple Ahp proteins, however *L. monocytogenes* encodes only Lmo1604 and there is no adjacent reductase. *L. monocytogenes* Lmo1604 shares 75% and 33% identity with *B. subtilis* AhpA and AhpC, respectively. While two previous publications referred to this protein as Prx (78, 79), herein we refer to Lmo1604 as AhpA to reflect its similarity to *B. subtilis* AhpA and the fact that it is a noncanonical Ahp that lacks a dedicated reductase. We found that *ahpA* is expressed during intracellular replication, but is not required for growth in IFNg-activated macrophages or prolonged survival in the vacuole. These results are consistent with published work showing the Δ*ahpA* mutant had no defect in macrophages or during infection of mice (79). However, *ahpA* was required for surviving acute peroxide stress *in vitro* and was important for detoxifying endogenous peroxide during aerobic replication in the absence of catalase. Together, these results suggest a role for *L. monocytogenes* AhpA in peroxide detoxification that is masked in wt

cells by the activity of catalase. Interestingly, the opposite is true in *E. coli* where Ahp is the primary scavenger of endogenous peroxide and catalase is important only in the presence of high concentrations of peroxide (90).

Hydrogen peroxide toxicity and iron are inextricably linked due to the Fenton reaction, in which ferrous iron reacts with hydrogen peroxide to generate hydroxyl radicals that damage DNA (71). Unsurprisingly, several of the putative peroxidases in this study are also involved in maintaining iron homeostasis in the cell, including: the heme-dependent peroxidase Lmo0367, the bacterial ferritin Fri, the terminal heme biosynthesis enzyme ChdC, and the heme-dependent catalase Kat. Additional studies are necessary to assess the roles of these enzymes in iron influx, oxidation, and storage in response to oxidative stress.

One method used by bacteria to mitigate the danger of free iron and the Fenton reaction is to sequester iron within bacterial ferritin proteins, which are multimeric protein shells that can store up to 4500 iron atoms. The amino acid sequence of *L. monocytogenes* Fri is identical to that of the *L. innocua* Dps protein, which has been biochemically characterized as a bacterial ferritin. *L. innocua* Dps was named due to its structural similarity to Dps family proteins (DNA-binding protein from starved cells), although it does not bind DNA (92). *L. innocua* Dps has a smaller internal diameter than typical ferritins and therefore can store only ~400 iron atoms per shell. The protection afforded by *L. innocua* Dps is due to the hydrogen peroxide-mediated iron oxidation that occurs rapidly and in a manner that prevents Fenton chemistry (92, 93). Based on the identity of the proteins, we predict *L. monocytogenes* Fri has a similar function and uses

peroxide to oxidize and store iron. It is therefore not possible to distinguish between the importance of the peroxidase activity of Fri and its role in iron homeostasis in the cell.

The role of Fri in *L. monocytogenes* has been investigated previously by several groups and in fact, the protein encoded by *lmo0943* has been given multiple different names, including: Flp (ferritin-like protein) (94), Frm (ferritin-like protein from *L. monocytogenes*) (95), and Frl (ferritin-like protein in *Listeria* species) (96). Here, we kept the more common name Fri (75, 76, 97). Our results are consistent with the literature showing that *fri* expression increases 8-fold upon entry into stationary phase and a Δ*fri* mutant is more sensitive to peroxide stress when treated in log phase (75, 97). In addition, we identified a critical role for Fri in the transition from anaerobiosis to aerobic replication. We also determined that *fri* expression is increased during intracellular growth and accordingly, *fri* is required for growth in activated BMDMs. This requirement was partially alleviated in host cells incapable of mounting an effective respiratory burst, suggesting that host-derived peroxide contributes to limiting Δ*fri* intracellular replication.

L. monocytogenes and *Staphylococcus aureus* mutants deficient in heme biosynthesis enzymes form small colonies on solid media and grow poorly in aerobic liquid cultures (61, 73). While *chdC* was previously reported to be essential (83), we generated a Δ*chdC* mutant in anaerobic growth conditions and observed that it was indeed unable to replicate aerobically in the absence of exogenous heme. This severe growth defect resembled that of *L. monocytogenes* Δ*hemEH*, which also cannot produce heme (73). As our data attribute the Δ*chdC* growth defect to the heme deficiency, it is unlikely that ChdC peroxidase activity plays a primary role in endogenous peroxide detoxification. However, our results raise an interesting question: why is heme

biosynthesis required for *L. monocytogenes* aerobic growth? Heme is an essential cofactor for cytochrome oxidases of the electron transport chain and therefore, *S. aureus hem* mutants are impaired for growth due to a lack of aerobic respiration (61, 98). However, *L. monocytogenes* lacking one or both terminal cytochrome oxidases are only moderately impaired for aerobic growth as compared to the complete lack of replication observed for Δ*chdC* and Δ*hemEH* mutants (73, 99). Interestingly, *S. aureus* requires heme biosynthesis for virulence in murine models of acute infection (64). In contrast, *L. monocytogenes* lacking *hemEH* or *chdC* are not defective for intracellular replication and in fact, exhibit increased intercellular spread compared to wt (reference 12 and N.H.S. unpublished observations). These results suggest that either heme biosynthesis is dispensable for *L. monocytogenes* pathogenesis or that exogenous host-derived heme can support growth of Δ*chdC* during infection. Ongoing research aims to determine the role of heme in *L. monocytogenes* aerobic growth and virulence.

In our assays, we did not observe phenotypes for *L. monocytogenes* lacking *lmo0367*, *lmo0983*, *tpx*, *lmo1609*, or *ohrA* and little is known about their functions. Lmo0367 shares 52% amino acid identity with the *B. subtilis* YwbN/EfeB protein, a DyP-type peroxidase that is transported as a folded protein across the cytoplasmic membrane via the twin-arginine translocation (Tat) pathway (100, 101). While protein localization and function of *L. monocytogenes* Lmo0367 have not been examined, the corresponding gene was found to be regulated by the ferric uptake regulator Fur and expression was consequently decreased in response to heme stress (102, 103). A screen for *L. monocytogenes* genes important for osmotic stress and desiccation identified a transposon in *lmo0983*, encoding a predicted glutathione peroxidase, although this

mutant was not further characterized (104). Tpx and Lmo1609 share 63% and 58% amino acid identity with their respective homologues in *B. subtilis* and both are activated by Spx in that organism, supporting their role in the oxidative stress response (39). The *L. monocytogenes ohrA* mutant was previously found to be attenuated in a plaque assay and for intracellular replication in BMDMs (13). In this study, the Δ*ohrA* strain was not attenuated and we hypothesize this discrepancy is due to the fact that herein, the bacteria were grown overnight anaerobically before infecting cells, whereas previous experiments grew bacteria aerobically. Future research will decipher the roles of these understudied putative peroxidases in *L. monocytogenes* and other Firmicutes.

Oxidative stress is abundant in the environment during aerobic growth and during infection. In this work we focused on peroxide stress, although superoxide is also generated endogenously and encountered exogenously in host phagocytes (12). *L. monocytogenes* produces a single manganese-dependent superoxide dismutase (MnSOD) that is required for infection (105, 106). MnSOD converts the superoxide produced by NADPH oxidase to hydrogen peroxide, which then needs to be detoxified by catalases and peroxidases. Our results demonstrate that the majority of peroxidases are individually dispensable for infection of mammalian cells and suggest redundancy in these antioxidants. Identifying expression changes in the Δ*kat*Δ*ahpA* strain will reveal the compensatory factors allowing this double mutant to more efficiently infect macrophages, despite the *in vitro* sensitivity of this strain to peroxide. Future investigations will build on the results described herein to provide further insight into the *L. monocytogenes* peroxide detoxification strategy during infection.

Chapter 4: The transcriptional regulator SpxA1 influences the morphology and virulence of Listeria monocytogenes

Introduction

Listeria monocytogenes is the causative agent of the foodborne disease listeriosis and a well-described model intracellular pathogen (107). *L. monocytogenes* lives as an environmental saprophyte until consumed by a susceptible mammalian host. Once ingested, *L. monocytogenes* is phagocytosed by professional phagocytes or induces its own uptake into non-phagocytic cells (108). Quickly after internalization, *L. monocytogenes* escapes the vacuole and replicates within the host cytosol (10). Here, *L. monocytogenes* produces the surface-associated protein ActA which recruits host actin to mediate intracellular motility and intercellular spread via characteristic actin comet tails (109). The asymmetric distribution of ActA along the bacterial cell surface is tightly coupled to the bacterial cell cycle and critical for motility initiation, comet tail formation, and bacterial movement within the host cytosol (110). While the complex set of biophysical steps necessary for efficient actin-dependent cytosolic motility of *L. monocytogenes* are not fully understood, the rod shape of this bacterium is thought to be essential to this process (22, 23).

Alterations to cell shape can have detrimental effects for many bacterial pathogens, as cell shape dictates motility, surface protein localization, innate immune activation, adherence, and invasion into host cells. For example, the helical shape of the foodborne pathogens *Helicobacter pylori* and *Campylobacter jejuni* is critical for flagellar motility in mucus and host colonization (111–113). Similarly, the curvature of the comma-shaped pathogen *Vibrio cholerae* enhances colonization of the small intestine (114). In *L.*

monocytogenes, mutants that form chains due to septation defects are deficient for invasion and virulence (115, 116). Further, the shape and geometry of *L. monocytogenes* influence actin tail formation and function while the mechanical stress of actin-based motility effects cell elongation and division (110, 116, 117).

Alternate morphologies can also provide survival advantages to bacterial pathogens. For example, many pathogenic organisms form filaments *in vivo* that are resistant to both phagocytosis and antimicrobials (118). Filamentation describes the process of continual longitudinal growth without formation of septa between newly replicated chromosomes. Increasing cell envelope volume absent separation results in cells much longer than their bacillary counterparts (119). Filamentous morphologies are induced in rod-shaped bacteria by a variety of stressors, such as metabolic changes, DNA damage (the SOS response), or alterations to the stoichiometry of cell division components (118). In addition to these stressors, *L. monocytogenes* filamentation is induced extracellularly in response to high or low pH, salt, cold, and heat stress (120–122). Despite these extracellular observations, the regulation of *L. monocytogenes* morphology *in vivo* and the relevance to pathogenesis is not well understood.

One *L. monocytogenes* regulator that is important for both extracellular and intracellular growth is the redox-responsive transcriptional regulator SpxA1 (17). SpxA1 belongs to the ArsC-like Spx family of proteins that is highly conserved in low G+C Firmicutes (34). *L. monocytogenes* SpxA1 is essential for aerobic growth in rich broth as well as virulence in a murine model of infection (13, 36). Similarly, *Staphylococcus aureus* Spx is essential for growth in rich media and Spx homologues are required for virulence in *Streptococcus* spp. and *Enterococcus faecalis* (38, 40, 41, 123, 124). Our previous

work found that *L. monocytogenes* lacking *spxA1* are unable to replicate aerobically due to toxic levels of endogenously produced hydrogen peroxide, resulting from a combination of dysregulated cytochrome oxidase and insufficient catalase production (73). However, the SpxA1-regulated genes necessary for aerobic growth are dispensable for infection and thus, the role of SpxA1 in pathogenesis remains to be defined.

In this work we sought to investigate the role of SpxA1 in *L. monocytogenes* virulence and made the surprising discovery that Δ*spxA1* mutant cells exhibit variable and elongated morphology during growth in the host cytosol. Quantitative microscopy further revealed Δ*spxA1* cells undergo filamentation extracellularly in anaerobic rich medium. A whole cell proteomics approach identified SpxA1-dependent changes in protein abundance, including motility and flagellar proteins that were depleted in the Δ*spxA1* mutant. Finally, we show that filamentation and decreased motility of Δ*spxA1* contribute to the virulence defect of Δ*spxA1* in tissue culture models of infection. Together, these results significantly advance our understanding of the role of SpxA1 in *L. monocytogenes* replication and pathogenesis.

This chapter presents the summary of my primary project in the Reniere lab, in collaboration with Oluwasegun Daramola, Lucy Kwiatkowski, and Michelle Reniere. I have performed experiments for every figure presented, and was the primary contributor to the writing and preparation of this manuscript.

Results

L. monocytogenes Δ*spxA1* exhibits an elongated morphology

The *L. monocytogenes* Δ*spxA1* strain is significantly impaired for intracellular replication and intercellular spread, although the SpxA1-regulated genes important for these processes have yet to be identified (36, 73). To further examine the role of SpxA1 in *L. monocytogenes* virulence, we took a microscopy-based approach and infected monolayers of murine fibroblasts grown on glass coverslips. Monolayers were fixed 10 hours post-infection and *L. monocytogenes*, DNA, and host actin were fluorescently labeled. As expected, wild type (wt) *L. monocytogenes* appeared as short rods in the host cytosol. Many bacteria colocalized with increased densities of host actin (red) and some appeared to be forming canonical actin comet tails (Fig. 21A). In contrast, intracellular Δ*spxA1* were more heterogeneous in shape, with some appearing as short rods and many appearing as chains of cells or elongated single cells. Furthermore, elongated Δ*spxA1* appeared to colocalize less frequently with highly dense areas of actin. Those cells that did colocalize with host actin displayed disorganized or non-polar actin recruitment and were rarely associated with actin comet tails (Fig. 21B). These results led us to question if the morphological defect of Δ*spxA1* was specific to growth in the mammalian cytosol.

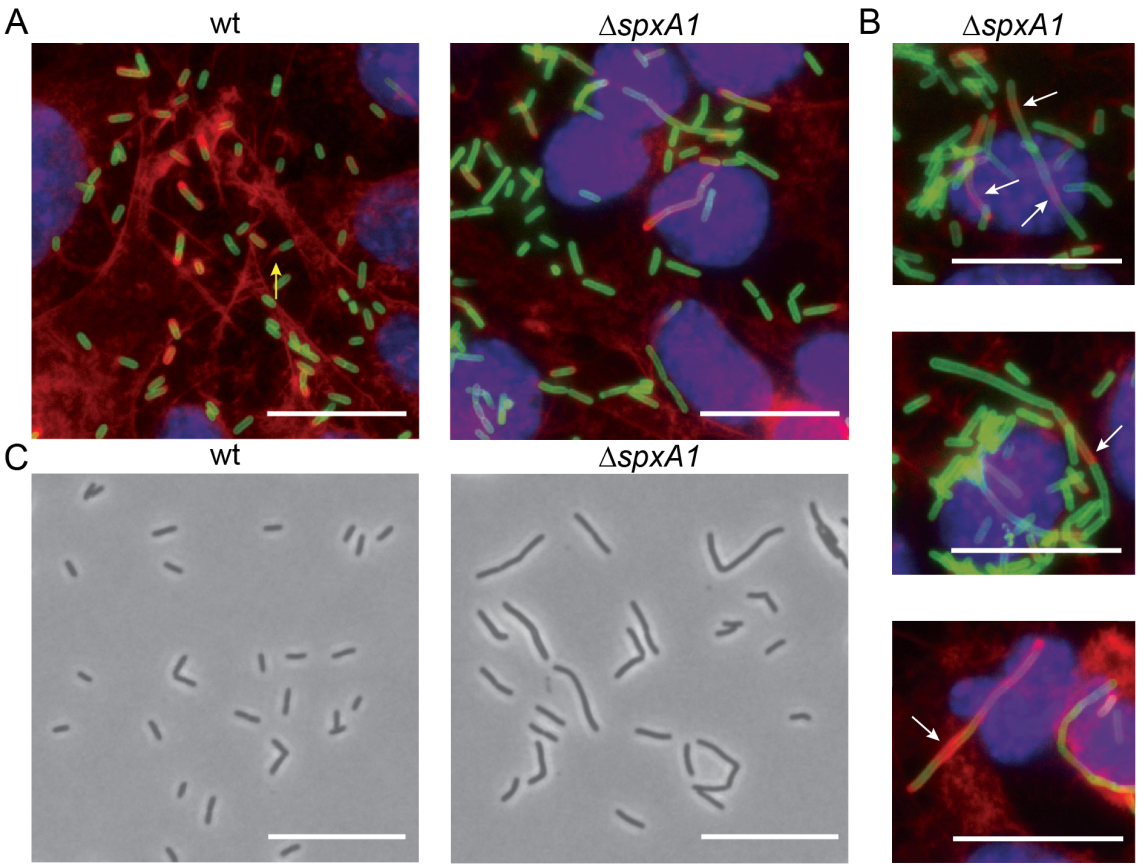

Figure 21. Microscopy of *L. monocytogenes* Δ*spxA1* during intracellular and extracellular growth. (A) L2 murine fibroblasts were infected for 10 h with wt or Δ*spxA1* cells and fluorescently labeled to visualize DNA (blue), *L. monocytogenes* (green), and host actin (red). The yellow arrow indicates a canonical actin comet tail. Images were taken using a 100× objective. (B) Additional examples of cells infected with the Δ*spxA1* mutant. White arrows indicate elongated bacteria with disorganized or nonpolar actin recruitment. (C) Phase-contrast images of wt and Δ*spxA1* cells grown to early exponential phase in rich anaerobic broth. Bacteria were imaged with a 40× objective. All scale bars represent 10 μm, and all images represent three biological replicates and at least 10 fields of view.

To determine if the observed Δ*spxA1* morphological heterogeneity was specific to intracellular growth, bacteria were grown to early exponential phase in a rich medium (brain heart infusion, BHI) in an anaerobic chamber and spotted onto PBS agar pads for phase contrast microscopy. In these conditions, wt *L. monocytogenes* were almost exclusively rod-shaped and of uniform length, whereas the Δ*spxA1* mutant exhibited varied and elongated morphologies (Fig. 21C). Together, these images suggested that

SpxA1 regulation of cell shape could play a significant role in *L. monocytogenes* growth in both intracellular and extracellular environments.

Quantification of Δ*spxA1* elongation

To quantitively evaluate Δ*spxA1* morphology, phase contrast images of wt and Δ*spxA1* grown anaerobically in BHI were analyzed with the cell segmentation software Celltool (125). Cell perimeter was used as the primary metric to describe cell size and account for the irregular shape and curvature of some Δ*spxA1* cells. Despite demonstrating no significant difference in growth rate compared to wt (Fig. 22), Δ*spxA1* cells had an increased mean, median, range, and variance of cell perimeters (Fig. 23A).

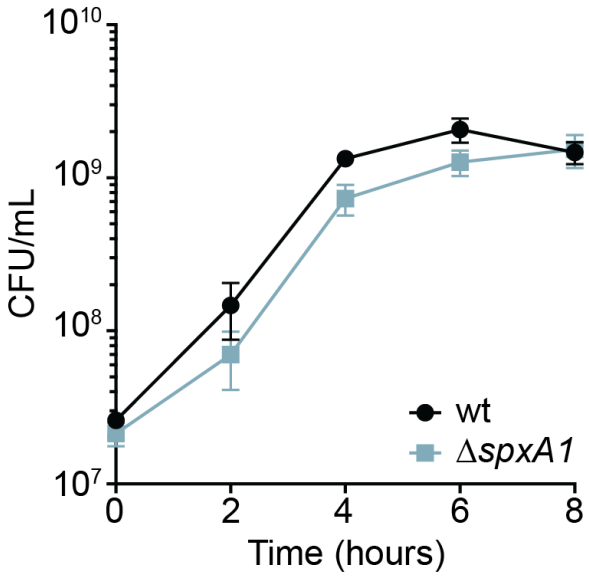

Figure 22. Anaerobic growth kinetics of L. monocytogenes wt and Δ*spxA1*. Anerobic cultures were diluted to an OD600 of 0.02 in BHI and grown anaerobically. Every two hours, bacterial cultures were serially diluted and plated to enumerate CFU. Data are the means and SEM of three biological replicates. The differences between wt and Δ*spxA1* were not statistically different at any time point, as determined by unpaired t-test.

The cell perimeters of wt and Δ*spxA1* differed most at early exponential phase, with the mean of wt cells measuring 8.5 μm compared to 16.9 μm for Δ*spxA1* cells. In addition, the maximum cell perimeter observed for the Δ*spxA1* mutant was 146 μm, nearly triple the size of the largest wt cell. While the average cell perimeter of both wt and Δ*spxA1* decreased over time, Δ*spxA1* cells were not restored to wt size at any point during the eight hour time course. In order to accurately assess the biological relevance of the observed elongation, we calculated the percentage of elongated bacteria. Elongated cells were defined as having a perimeter greater than one standard deviation (SD) above the mean of wt cells at each time point. Approximately 10% of wt cells were elongated at each time point examined (Fig. 23B). Throughout growth, Δ*spxA1* cultures contained a much higher percentage of elongated cells, with elongated cells comprising 54% of the population at 2 hours. This phenotype was rescued via genetic complementation by providing a copy of *spxA1* with its native promoter at an ectopic site on the chromosome using the integrative plasmid *pPL2* (Δ*spxA1 pPL2*.*spxA1*) (54). These data demonstrated that *L. monocytogenes* lacking *spxA1* form significantly longer cells, particularly at early exponential phase.

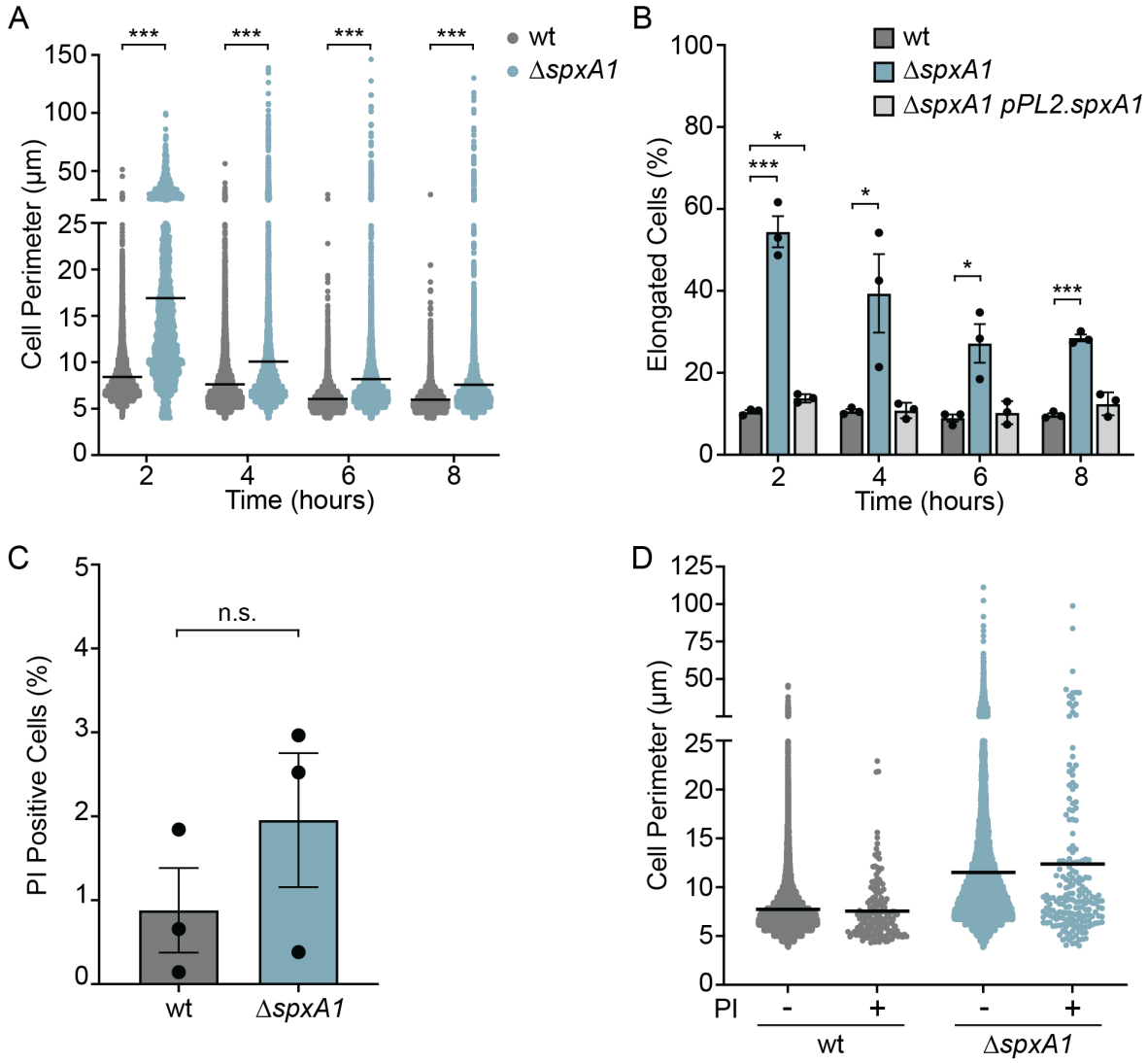

Figure 23. Quantification of *L. monocytogenes* Δ*spxA1* elongation and cell viability during broth growth. (A) Bacteria were grown anaerobically in rich broth, and cell perimeters were measured from phase-contrast images using Celltool. The lines indicate the means. Distributions were compared using Kolmogorov-Smirnov tests. ***, $P < 0.001$. (B) The percentages of elongated cells were measured for at least 10 fields of view or 1,000 cells. Elongated cells were defined as perimeter lengths greater than one SD above the wt mean at each time point. Each symbol represents a biological replicate, the bars indicate the mean, and the error bars denote the SEM. P values were calculated using an unpaired Student t test compared to wt. *, $P < 0.05$; ***, $P < 0.001$. (C) The percentages of propidium iodide (PI)-positive cells were calculated from at least 1,000 cells or 10 fields of view. The data are not significantly different, as determined by an unpaired Student t test (n.s. $P > 0.3$). (D) The cell perimeters of bacteria from PI-negative (–) and PI-positive (+) populations were measured. Graphs represent cell perimeters measured from three biological replicates where at least 1,000 cells or 10 fields of view were quantified per replicate. The lines indicate the means.

Due to the observed morphological irregularities, we hypothesized that highly elongated Δ*spxA1* cells may have irregular or damaged membranes and therefore decreased viability. To determine the viability and membrane integrity of the Δ*spxA1* mutant, early log phase cultures were stained with propidium iodide (PI), a live-dead stain which cannot penetrate intact lipid bilayers. We observed an approximate 2-fold increase in the percentage of PI-positive Δ*spxA1* cells compared to wt, although this difference was not statistically significant (Fig. 23C). Neither strain exhibited significant PI staining, with the percentage of PI-positive cells never reaching 2% for wt or 3% for Δ*spxA1*. To evaluate the viability of elongated cells specifically, the cell perimeters of the PI-positive and PI-negative populations were measured for each strain. The distributions of PI-positive and PI-negative Δ*spxA1* cells appeared nearly identical, indicating that the elongated Δ*spxA1* cells were not more likely to be PI-positive (Fig. 23D). Taken together, these results demonstrated that Δ*spxA1* cells are morphologically heterogenous and a significant portion of the cells are dramatically elongated. However, this elongation does not correlate to a critical defect in viability or membrane integrity.

Fluorescence microscopy of membranes

Phase contrast microscopy revealed that the majority of Δ*spxA1* cells were significantly elongated compared to wt, but the quantitative analysis of these images could not distinguish between incompletely separated chains of cells or filamentous single cells. To examine the specific nature of elongated Δ*spxA1* cells, bacteria were labeled with the fluorescent membrane dye TMA-DPH, which intercalates into lipid bilayers containing fatty acyl chains (126). *L. monocytogenes* wt cells appeared as typical rods at

various stages of division with sites of septation localized to the cell midpoint (Fig. 24A). In contrast, Δ*spxA1* exhibited a range of elongated filamentous morphologies which rarely contained septa at cell midpoints and often exhibited a complete lack of septa. These results suggested that the significant elongation of the Δ*spxA1* mutant was likely the result of filamentation rather than chaining.

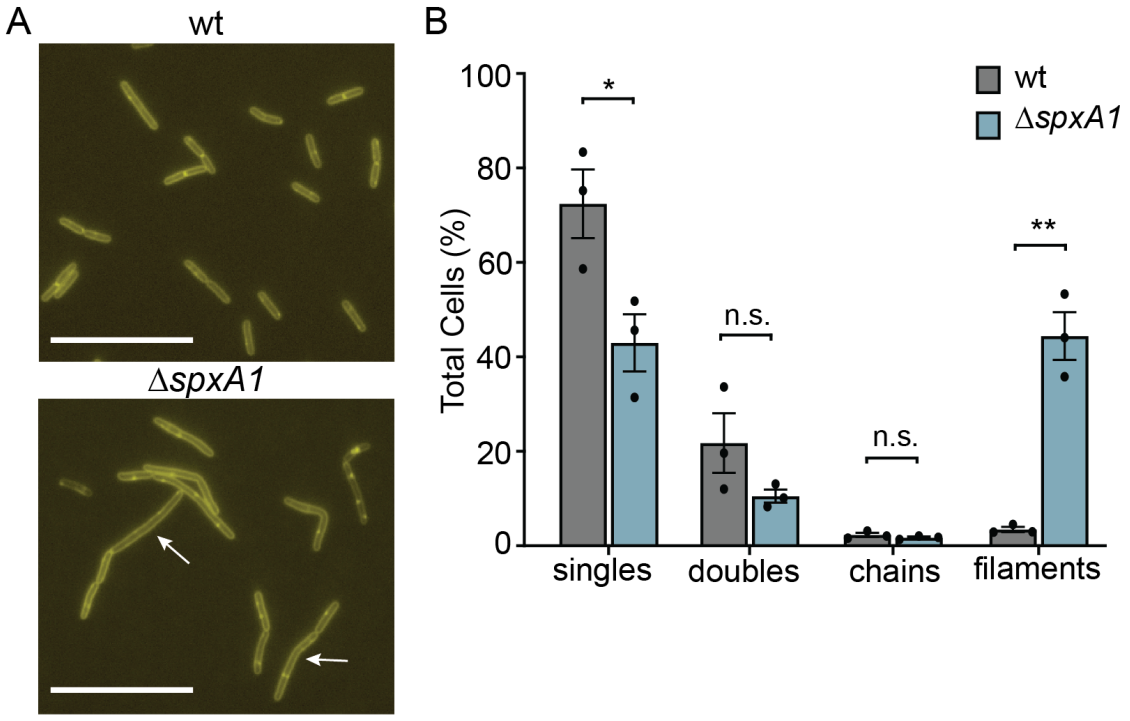

Figure 24. Fluorescent labeling of membranes indicates the prevalence of Δ*spxA1* filamentation. (A) L. monocytogenes wt and Δ*spxA1* cells grown to early exponential phase were labeled with the fluorescent membrane stain TMA-DPH. Arrows indicate elongated cells without regular septa, and scale bars represent 10 μm. (B) Quantification of elongated cells observed in panel A. Data displayed are the means and the SEM of three biological replicates of 1,000 cells each. P values were calculated using an unpaired Student t test compared to wt cells. *, $P < 0.05$; **, $P < 0.01$; n.s., not significant.

To quantify the frequency of Δ*spxA1* filamentation, we visually evaluated the TMA-DPH images and categorized over 1,000 cells per replicate for each strain. Single cells were defined as cells lacking fully formed septa that were approximately the length of the

wt mean (2-5 μm). Doublets and chains were defined as two or more linked bacteria, respectively, composed of 2-5 μm cells attached by evenly placed septa. Filaments were defined as cells longer than 2-5 μm that either lack septa completely, have irregular numbers of septa relative to the length of the cell, or contain septa placed outside the midpoint of the cell. As expected, approximately 94% of wt bacteria were either single cells or doublets, with a small minority of chains and filaments (Fig. 24B). In contrast, over 44% of Δ*spxA1* cells were elongated filaments with aberrant septum localization. These results confirmed that the majority of elongated Δ*spxA1* are filamentous single cells.

Scanning Transmission Electron Microscopy

After determining that the majority of Δ*spxA1* cells were filaments, we next sought to investigate the observed differences in membrane architecture at higher resolution. To that end, we performed Scanning Transmission Electron Microscopy (STEM) on wt, Δ*spxA1*, and the complemented Δ*spxA1* strain. Early exponential phase cultures were negatively stained with uranyl acetate, which incorporates into organic materials with a high affinity for phosphorylated molecules, enabling resolution of dense and highly phosphorylated components, such as membranes, nucleic acids, and some proteins (127). In many respects, the Δ*spxA1* cell envelope appeared indistinguishable from that of wt and the complemented strain (Fig. 25). For example, all three strains had a similarly thick outer layer of peptidoglycan covering a thin layer of highly contrasting phospholipid membrane, with no obvious differences in phospholipid or peptidoglycan abundance (Fig. 25A). Additionally, the division septa appeared to have similar architecture and composition in all three strains. However, several differences in the spatial organization

of the Δ*spxA1* envelope were observed. Consistent with our phase contrast and fluorescence microscopy images, Δ*spxA1* cells appeared elongated compared to wt (Fig. 25B-D). Multiple septa were observed at various stages of development within Δ*spxA1* filaments, and these were unevenly distributed along the cell (Fig. 25C). We observed Δ*spxA1* cells in the process of initiating septum formation in aberrant locations outside the cell midpoint, sometimes irregularly spaced and atypically close together (Fig. 25B and C). Formation of septa was not only initiated, but successfully completed outside of cell midpoints (Fig. 25D). Finally, Δ*spxA1* cells could initiate full separation of segmented cells at sites of mis-localized septation (Fig. 25D). Taken together, these images suggested that Δ*spxA1* filamentation is due to both improper localization and frequency of septum formation.

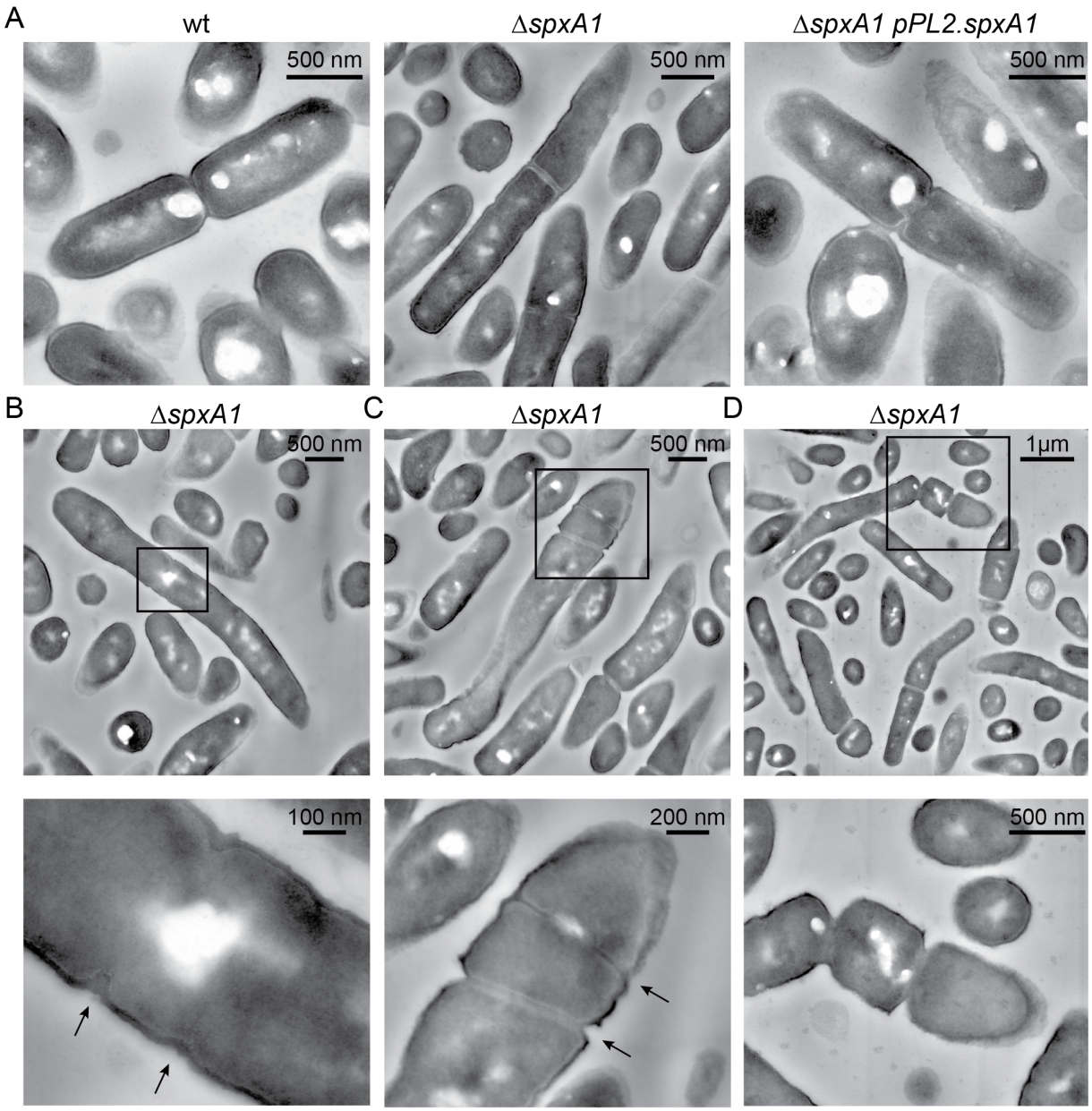

Figure 25. STEM images of L. monocytogenes. (A) L. monocytogenes strains grown to early exponential phase were fixed and imaged by STEM. (B to D) Representative examples of Δ*spxA1* filaments. Boxed portions of each image are shown magnified below. Black arrows indicate septa forming outside the cell midpoint, irregularly spaced, and atypically close together. Scale bars are indicated in each panel.

Whole cell proteomics

To identify SpxA1-dependent factors influencing cell morphology, we performed whole cell proteomics on early exponential phase bacterial cultures. Previous work demonstrated that SpxA1 impacts the transcription of 217 genes, activating 145 and repressing 72, including several proteins involved in protein degradation (73). Thus, a proteomics approach has the advantage of identifying the proteins that are changed directly via SpxA1 transcriptional regulation and indirectly via SpxA1 regulation of protein turnover. Bacteria were grown in triplicate to early exponential phase and proteins were isolated and quantified using unlabeled mass spectrometry coupled to liquid chromatography. We identified 1,692 proteins from 23,219 peptides, accounting for 60.1% of all protein coding regions. Proteins that differed at least 2-fold from wt abundance (p <0.05), or were absent in one strain and abundant (greater than 5 peptides detected) in the other, were considered for further analysis. Using these criteria, we identified 122 proteins that were significantly decreased in abundance in Δ*spxA1* compared to wt (Table 4), and 46 proteins that were significantly increased in abundance in Δ*spxA1* (Table 5).

Table 4. Proteins decreased in Δ*spxA1*

EGD-e	Gene name	Protein function	wt LFQ average	Δ*spxA1* LFQ average	Fold decrease (wt/Δ*spxA1*)	*P* value
Redox & respiration						
lmo2785	*kat*	catalase	2.8E+08	5.6E+06	50.1	1.4E-02
lmo2390		hypothetical thioredoxin reductase	3.9E+07	3.2E+06	12.3	1.1E-03
lmo2113	*chdC*	heme peroxidase	1.7E+08	1.9E+07	9.4	4.4E-05

lmo0983		glutathione peroxidase	4.2E+07	4.9E+06	8.7	6.0E-03
lmo2426	*spxA2*	ArsC-family protein	1.2E+08	1.6E+07	7.8	5.7E-04
lmo2478	*trxB*	thioredoxin reductase	2.2E+08	6.9E+07	3.2	6.6E-05
lmo0611	*azoR*	FMN-dependent NADH-azoreductase	3.9E+07	1.3E+07	3.0	9.7E-06
lmo2247		hypothetical oxidoreductase of aldo/keto reductase family	6.4E+07	2.2E+07	2.8	1.1E-04
lmo2389		NADH dehydrogenase	1.5E+08	5.2E+07	2.8	1.3E-03
lmo1439	*sodA*	manganese superoxide dismutase	9.3E+08	3.3E+08	2.8	7.1E-04
lmo1233	*trxA*	thioredoxin	2.9E+08	1.2E+08	2.4	1.4E-03
lmo2694		hypothetical arginine decarboxylase	2.9E+07	1.3E+07	2.1	4.6E-04
lmo0103		putative oxidoreductase	1.6E+07	7.3E+06	2.1	2.9E-02
lmo2152		putative thioredoxin	5.8E+07	2.8E+07	2.0	3.5E-02
lmo1609		thioredoxin	4.5E+07	2.2E+07	2.0	5.2E-03
lmo1673	*menB*	naphthoate synthase	8.3E+08	4.1E+08	2.0	4.4E-04
lmo2072	*rex*	redox-sensitive transcriptional repressor	2.8E+08	1.4E+08	2.0	1.2E-03
lmo2211	*hemH*	ferrochelatase	2.9E+08	0	-	1.6E-07
lmo2212	*hemE*	uroporphyrinogen decarboxylase	7.6E+07	0	-	1.2E-04
lmo1583	*tpx*	thiol peroxidase	7.2E+07	0	-	1.2E-07
lmo2191	*spxA1*	redox-responsive transcriptional regulator	6.4E+07	0	-	6.7E-06
lmo0823		hypothetical oxidoreductase of aldo/keto reductase family	3.6E+07	0	-	2.0E-03
lmo2715	*cydD*	ABC transporter	5.5E+07	2.0E+06	27.5	1.3E-03
lmo2718	*cydA*	cytochrome d ubiquinol oxidase subunit I	6.3E+07	4.9E+06	12.9	9.2E-04

lmo2716	*cydC*	transport ATP-binding protein	5.7E+07	0	-	1.2E-04
Motility						
lmo0697	*flgE*	flagellar hook protein	6.9E+07	3.0E+06	23.3	1.4E-03
lmo0690	*flaA*	flagellin	2.5E+09	3.6E+08	7.1	4.1E-04
lmo0723		methyl-accepting chemotaxis protein	6.1E+08	9.2E+07	6.7	2.9E-03
lmo0713	*fliF*	flagellar M-ring protein	9.0E+07	1.5E+07	6.2	2.3E-05
lmo0706	*flgL*	flagellar hook-associated protein	4.9E+07	8.1E+06	6.1	2.1E-02
lmo1699		methyl-accepting chemotaxis protein	2.3E+08	4.0E+07	5.9	3.3E-03
lmo0705	*flgK*	flagellar hook-associated protein	1.3E+08	2.2E+07	5.7	2.4E-03
lmo0692	*cheA*	signal transduction histidine kinase	2.4E+08	5.0E+07	4.7	3.5E-04
lmo0707	*fliD*	flagellar hook-associated protein	7.0E+07	1.5E+07	4.6	1.8E-02
lmo0691	*cheY*	chemotaxis regulator	2.5E+08	6.1E+07	4.2	3.9E-05
lmo0714	*fliG*	flagellar motor switch protein	1.2E+08	3.1E+07	3.8	6.5E-04
lmo0685	*motA*	flagellar motor rotation protein	5.6E+07	1.8E+07	3.2	7.5E-03
lmo0689	*cheV*	chemotaxis protein	4.1E+08	1.3E+08	3.0	1.9E-04
lmo0688	*gmaR*	flagellin glycosyltransferase	2.3E+08	8.4E+07	2.8	2.7E-04
lmo0699	*fliM*	flagellar motor switch protein	2.8E+07	0	-	6.2E-04
lmo0700	*cheC*	chemotaxis protein	2.7E+07	0	-	2.9E-04
Protein Turnover						
lmo2256		hypothetical peptidase	1.0E+08	2.5E+07	4.1	5.8E-03
lmo2188	*pepF*	oligoendopeptidase F	2.9E+08	9.2E+07	3.1	2.1E-04
lmo1578		hypothetical proline dipeptidase	2.5E+08	8.2E+07	3.0	3.5E-05
lmo1780	*pepT*	tripeptide aminopeptidase	2.8E+08	1.0E+08	2.7	2.1E-04
lmo0982		hypothetical deblocking aminopeptidase	1.8E+08	6.8E+07	2.6	5.6E-05

lmo1392		hypothetical zinc protease	8.6E+07	3.6E+07	2.4	1.5E-03
lmo1354		hypothetical aminopeptidase	4.0E+08	1.7E+08	2.3	1.3E-03
lmo1585		hypothetical protease IV	3.7E+07	1.6E+07	2.3	4.0E-03
lmo2338	*pepC*	aminopeptidase C	5.6E+07	2.7E+07	2.1	3.8E-04
lmo1393		metallopeptidase, M16 family	1.7E+08	8.6E+07	2.0	2.1E-04
Signal Transduction, Transcription, & Translation						
lmo2692	*pstA*	c-di-AMP binding signal transduction protein	1.1E+08	2.4E+07	4.7	7.2E-07
lmo0965		adenylate cyclase	2.4E+07	7.4E+06	3.3	1.8E-02
lmo2673	*uspA2*	universal stress protein	4.3E+07	1.6E+07	2.8	7.8E-04
lmo2016	*cspD*	cold shock protein	1.5E+09	5.6E+08	2.7	1.2E-04
lmo1378	*lisK*	two-component sensor histidine kinase	4.7E+07	1.9E+07	2.5	4.9E-02
lmo1935		protein tyrosine phosphatase	8.7E+07	3.7E+07	2.4	2.6E-04
lmo1466	*pgpH*	cyclic-di-AMP phosphodiesterase	2.7E+07	1.2E+07	2.1	2.1E-02
lmo1878	*mntR*	Mn-dependent transcriptional regulator	6.4E+07	2.8E+06	23.1	7.3E-05
lmo0483		transcriptional regulator, AraC family	4.4E+07	1.5E+07	3.0	3.7E-05
lmo0436		Rrf2 family transcriptional regulator, group III	2.9E+07	0	-	4.3E-04
lmo2557		transcription regulator	6.8E+06	0	-	2.0E-04
lmo0211	*rplY*	ribosomal protein L25p	5.9E+08	2.0E+08	2.9	2.8E-03
lmo2511	*hpf*	ribosomal subunit interface protein	9.3E+08	3.2E+08	2.9	1.1E-03
lmo2719	*tadA*	tRNA-specific adenosine deaminase	1.7E+07	0	-	7.4E-06
Metabolism						

lmo1579	*ald*	alanine dehydrogenase	2.4E+08	6.8E+07	3.6	1.8E-04
lmo1630	*trpC*	indole-3-glycerol phosphate synthase, tryptophan biosynthesis	1.9E+07	9.1E+06	2.1	1.4E-05
lmo2825	*serC*	phosphoserine aminotransferase, serine biosynthesis	2.8E+07	0	-	2.7E-05
lmo0282	*amiE*	aliphatic amidase	3.2E+07	8.3E+06	3.9	4.7E-02
lmo0664		maltose O-acetyltransferase	4.5E+07	1.9E+07	2.4	3.2E-03
lmo0907		phosphoglycerate mutase family protein	1.3E+08	6.0E+07	2.1	1.0E-03
lmo1667		L-lactate dehydrogenase, heterolactic fermentation	2.1E+07	1.0E+07	2.0	5.6E-03
lmo2477	*galE*	UDP-glucose 4-epimerase	4.7E+07	2.0E+07	2.4	4.2E-03
lmo2720		acyl-coenzyme A synthetases/AMP-(fatty) acid ligases	2.0E+08	5.6E+06	36.1	4.9E-05
lmo2425	*gcvH*	glycine cleavage system H protein	1.8E+08	3.0E+07	5.9	7.0E-05
lmo1877	*fhs*	formate-tetrahydrofolate ligase	2.7E+08	5.0E+07	5.4	5.0E-06
lmo1933	*folE*	GTP cyclohydrolase I	7.4E+07	2.9E+07	2.5	1.4E-03
lmo0931	*lplA1*	lipoate-protein ligase A	1.4E+08	6.2E+07	2.2	5.2E-03
lmo0110		esterase/lipase	3.3E+07	2.6E+06	12.5	7.8E-04
lmo2089		esterase/lipase	4.3E+08	8.8E+07	4.9	2.6E-05
lmo1688	*fabL*	enoyl-acyl carrier protein reductase I	2.6E+07	5.6E+06	4.7	2.7E-02
lmo0774		diacylglycerol kinase-related protein	1.5E+08	5.2E+07	2.9	2.8E-05
lmo1370	*buk*	butyrate kinase	3.4E+07	0	-	3.9E-05
Transport						

lmo1226		MMPL family transporter	6.0E+07	2.0E+06	30.4	7.6E-03
lmo0841	*lmcA1*	calcium-transporting ATPase	5.8E+07	9.0E+06	6.5	3.5E-03
lmo2372		ABC transporter, ATP-binding protein	1.5E+08	2.8E+07	5.3	5.5E-04
lmo2371		ABC transporter, permease protein	1.2E+08	3.2E+07	3.8	7.2E-07
lmo1017		PTS system, glucose-specific IIA component	1.5E+08	4.4E+07	3.3	3.4E-04
lmo2215	*ecsA*	ABC transporter, ATP-binding protein	2.1E+07	6.8E+06	3.1	1.5E-02
lmo1014	*gbuA*	glycine betaine ABC transport system, ATP-binding protein	2.7E+08	1.0E+08	2.7	7.3E-03
lmo0667		ABC transporter, ATP-binding protein	4.4E+07	1.7E+07	2.6	4.0E-02
lmo2139		ABC transporter, ATP-binding protein	1.2E+07	0	-	1.1E-04
DNA repair & metabolism						
lmo1564	*mutM*	formamidopyrimidine-DNA glycosylase (Base excision repair)	3.1E+07	9.5E+06	3.3	2.3E-03
lmo2050		excinuclease ABC subunit A	2.0E+07	0	-	2.9E-05
lmo1463		cytidine deaminase	1.1E+08	5.2E+07	2.2	4.4E-04
Unknown & Other						
lmo0454		MoxR family ATPase	3.0E+07	1.1E+06	26.8	1.3E-03
lmo0592		hypothetical protein	3.7E+08	3.9E+07	9.3	4.5E-04
lmo0684		hypothetical protein	3.5E+07	4.9E+06	7.3	8.6E-03
lmo0451		hypothetical protein	2.2E+07	3.4E+06	6.4	1.2E-02
lmo0718		hypothetical protein	1.3E+08	3.3E+07	3.8	3.7E-04
lmo0791		hypothetical protein	1.4E+08	3.9E+07	3.7	4.5E-05
lmo0704		hypothetical protein	6.0E+07	1.8E+07	3.3	2.7E-03
lmo2083		hypothetical protein	6.8E+07	2.0E+07	3.3	8.1E-05
lmo1065		hypothetical protein	7.2E+07	2.2E+07	3.3	4.7E-04
lmo1608		hypothetical protein	2.4E+08	8.6E+07	2.8	1.3E-02
lmo0208		hypothetical protein	1.1E+08	4.7E+07	2.4	4.4E-03
lmo0267		glyoxalase family protein	2.1E+07	8.9E+06	2.4	3.0E-02

lmo2079		hypothetical protein	1.3E+08	5.5E+07	2.3	4.0E-04
lmo2759		putative ADP-ribose-binding protein	7.4E+07	3.2E+07	2.3	4.4E-03
lmo2167		hypothetical protein	1.5E+08	6.8E+07	2.2	1.8E-02
lmo1601		general stress protein	8.5E+08	4.0E+08	2.1	1.0E-03
lmo2216		HIT domain-containing protein	5.9E+07	2.8E+07	2.1	4.6E-02
lmo2166		cyclic nucleotide-binding protein	7.3E+07	3.4E+07	2.1	1.9E-04
lmo2792		non-specific DNA-binding protein	5.3E+08	2.5E+08	2.1	2.3E-03
lmo1602		general stress protein	5.1E+08	2.5E+08	2.1	3.5E-04
lmo0158		Cof-like hydrolase	2.8E+07	1.4E+07	2.1	1.0E-02
lmo1059		hypothetical protein	3.6E+08	1.8E+08	2.0	2.3E-03
lmo1381		putative acylphosphatase	5.2E+07	0	-	9.0E-06
lmo0811		carbonic anhydrase	4.8E+07	0	-	5.6E-06
lmo2406		uncharacterized conserved protein	2.9E+07	0	-	1.3E-06
lmo0844		hypothetical protein	1.1E+07	0	-	3.9E-06
lmo1121		hypothetical protein	1.1E+07	0	-	2.1E-06

Table 5. Proteins increased in Δ*spxA1*

EGD-e	Gene name	Protein function	wt LFQ average	Δ*spxA1* LFQ average	Fold increase (Δ*spxA1/wt*)	*P* value
Protein synthesis & turnover						
lmo2190	*mecA*	putative proteolysis adaptor protein	3.8E+07	7.4E+08	19.3	1.8E-04
lmo0997	*clpE*	ATP-dependent Clp protease, ATP-binding subunit	2.3E+08	2.3E+09	9.9	1.1E-03
lmo0292	*htrA*	serine protease	2.3E+08	6.5E+08	2.8	2.2E-02
lmo1469	*rpsU*	SSU ribosomal protein S21p	2.7E+08	7.9E+08	2.9	2.9E-03
lmo2656	*rpsL*	SSU ribosomal protein S12p	1.4E+09	3.9E+09	2.7	3.8E-03
lmo0257	*rtcB*	tRNA splicing RNA laigase	1.6E+07	4.1E+07	2.6	2.3E-02

lmo2619	*rpsZ*	SSU ribosomal protein S14p	2.4E+08	4.9E+08	2.1	3.3E-02
Cell wall/membrane biogenesis						
lmo2526	*murA*	UDP-N-acetylglucosamine 1-carboxyvinyltransferase	6.3E+08	1.6E+09	2.5	4.7E-05
lmo0582	*cwhA/iap*	P60 autolysin	2.8E+08	6.1E+08	2.1	1.0E-03
Metabolism						
lmo1998		putative glucosamine-fructose-6-phosphate aminotransferase	2.0E+07	5.2E+07	2.6	8.4E-04
lmo0027		PTS system component EIIB	1.2E+07	3.3E+07	2.8	1.7E-03
lmo0182		glycosyl hydrolase	4.1E+07	1.1E+08	2.6	1.9E-02
lmo0183		alpha-glucosidase	4.0E+07	9.2E+07	2.3	3.2E-02
lmo0401		alpha-mannosidase	0.0E+00	3.3E+07	-	3.3E-07
lmo1031		unknown pentose isomerase	0.0E+00	3.0E+07	-	1.1E-03
lmo2660	*tkt*	transketolase, pentose phosphate pathway	0.0E+00	1.5E+07	-	5.1E-05
lmo1902	*panB*	phosphopantothenate biosynthesis	2.8E+08	1.6E+09	5.6	4.1E-06
lmo1901	*panC*	phosphopantothenate biosynthesis	8.7E+07	3.2E+08	3.6	6.9E-05
Transport						
lmo1739		amino acid ABC transporter, ATP-binding protein	2.5E+06	1.9E+07	7.6	7.7E-03
lmo2752		ABC transporter, ATP-binding/permease protein	4.8E+07	1.7E+08	3.5	2.8E-03
lmo1847	*mntA*	manganese ABC transporter, periplasmic-binding protein	6.8E+07	2.2E+08	3.3	4.8E-06
lmo2751		ABC transporter, ATP-binding protein	8.0E+07	2.6E+08	3.2	1.6E-03
lmo1738		amino acid ABC transporter, amino acid-binding protein	9.1E+06	2.4E+07	2.6	2.8E-03

lmo1849	*mntB*	manganese ABC transporter, ATP-binding protein	6.6E+07	1.7E+08	2.6	1.3E-04
lmo0641	*frvA*	heme-transporting ATPase	8.3E+07	2.1E+08	2.6	1.0E-04
lmo1422		glycine betaine ABC transport system	1.3E+07	2.8E+07	2.1	5.3E-03
DNA repair & metabolism						
lmo2221		DNA double-strand break repair rad50 ATPase	3.1E+06	1.5E+07	4.9	2.0E-02
lmo1775	*purE*	inosine-5'-phosphate biosynthesis II	4.1E+07	1.1E+08	2.7	1.0E-02
lmo1772	*purC*	inosine-5'-phosphate biosynthesis II	5.8E+07	1.4E+08	2.4	1.9E-02
lmo1769	*purL*	phosphoribosylformylglycinamidine synthase	7.7E+07	1.7E+08	2.2	4.9E-03
lmo1767	*purM*	phosphoribosylformylglycinamidine cyclo-ligase	2.9E+07	6.4E+07	2.2	2.2E-02
lmo1773	*purB*	adenylosuccinate lyase	2.8E+08	6.2E+08	2.2	2.9E-03
lmo1768	*purF*	amidophosphoribosyltransferase	1.5E+07	3.0E+07	2.0	2.9E-03
lmo1764	*purD*	phosphoribosylamine-glycine ligase	4.8E+07	9.8E+07	2.0	9.6E-03
lmo0055	*purA*	adenylosuccinate synthetase	9.6E+08	1.9E+09	2.0	1.1E-03
Unknown & Other						
lmo2533	*atpF*	ATP synthase B chain	5.4E+08	1.1E+09	2.1	1.3E-03
lmo0437		oxidoreductase	6.9E+07	6.8E+08	9.8	1.2E-05
lmo1475	*hrcA*	heat-inducible transcription repressor	2.7E+07	8.9E+07	3.3	3.4E-03
lmo0229	*ctsR*	transcriptional regulator	3.8E+07	8.9E+07	2.4	2.0E-04
lmo2224		hypothetical protein	4.2E+06	1.7E+07	4.2	4.2E-02
lmo0496		hypothetical protein	2.8E+07	8.2E+07	2.9	4.2E-03
lmo2254		permease	8.9E+06	2.3E+07	2.6	3.5E-02
lmo0802		hypothetical protein	1.1E+07	2.3E+07	2.2	2.1E-02
lmo0056		secreted protein	1.8E+07	3.8E+07	2.2	6.2E-03
lmo2407		hypothetical protein	3.6E+07	7.4E+07	2.1	1.0E-02

The largest category of proteins depleted in Δ*spxA1* compared to wt were proteins involved in redox homeostasis and respiration. Specifically, the largest decrease observed was for the protein catalase (50-fold), which detoxifies hydrogen peroxide and is produced during aerobic growth in an SpxA1-dependent manner (73). Further, proteomics detected thiol peroxidase (Tpx) and heme biosynthesis proteins (HemE and HemH) in wt cells at high abundance, but these proteins were below the limit of detection in Δ*spxA1* (Table 4). Other redox-related proteins depleted in Δ*spxA1* compared to wt included: ChdC (heme peroxidase), Lmo0983 (glutathione peroxidase), Lmo1609 (thioredoxin), Rex (redox-responsive regulator), and the SpxA1 paralogue SpxA2 (Lmo2426) (36). To test if the depletion of these proteins contributed to the morphology of Δ*spxA1* cells, we measured the cell perimeters of deletion mutants grown to early exponential phase in anaerobic BHI. *L. monocytogenes* cells lacking *kat, tpx, hemEH, chdC, lmo0983, lmo1609, rex,* or *spxA2* were not significantly elongated compared to wt cells (Fig. 26). Moreover, a mutant lacking both *spxA1* and *spxA2* exhibited filamentation at levels indistinguishable from Δ*spxA1* alone. These results indicated that the genes critical for Δ*spxA1* aerobic growth and redox homeostasis are not required for proper cell elongation and division.

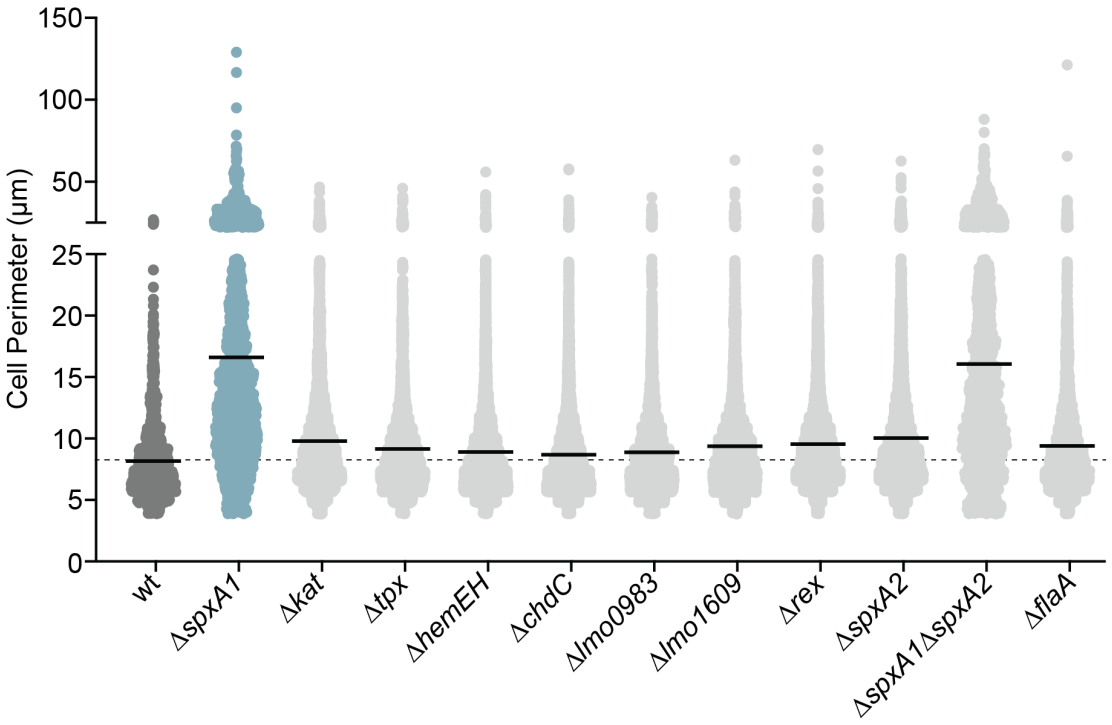

Figure 26. SpxA1-regulated redox homeostasis genes do not influence elongation. Bacteria were grown anaerobically in rich broth and cell perimeters were measured from phase contrast images using Celltool. The dotted line represents the wt mean, and solid black lines indicate the means of each strain.

We next evaluated protein turnover, as proteins in this category were the most dramatically enriched in Δ*spxA1* compared to wt (Table S2). Specifically, the protease adaptor proteins MecA and ClpE were the most increased in Δ*spxA1* (19- and 10-fold respectively). To explore the relevance of these proteins to *L. monocytogenes* morphology, mutants lacking *mecA* or *clpE* were generated via allelic exchange. Quantitative microscopy of *L. monocytogenes* Δ*mecA* and Δ*clpE* revealed no change in the frequency of cell elongation compared to wt (Fig. 27). Similarly, deletion of *mecA* and *clpE* in the Δ*spxA1* background did not rescue the elongation of Δ*spxA1*. Interestingly, the Δ*spxA1*Δ*clpE* double mutant was significantly more elongated than the Δ*spxA1*

parental strain. To extend our analysis of protein turnover, mutants lacking *yjbH* and *clpX* were generated in both wt and Δ*spxA1* backgrounds. SpxA1 abundance is regulated by YjbH- and ClpX-dependent degradation such that mutants deficient for *yjbH* or *clpX* have increased SpxA1 (17, 49). *L. monocytogenes* Δ*yjbH* and *clpX::Tn* mutants formed cells significantly smaller than wt (Fig. 27). Furthermore, double mutants that lack *spxA1* and *yjbH* or *clpX* did not differ in elongation compared to the Δ*spxA1* parental strain. Together, these data suggested that cell size maintenance requires precise regulation of SpxA1, as mutants with increased SpxA1 abundance form cells smaller than wt and *spxA1*-deficient cells are significantly elongated.

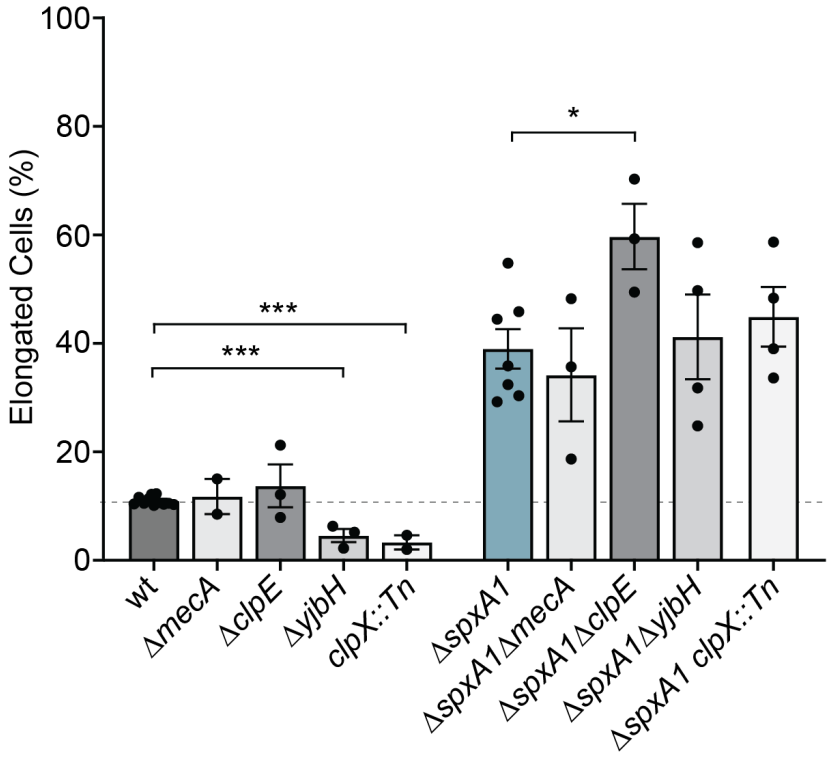

Figure 27. Proteolysis influences morphology of *L. monocytogenes*. The percentages of elongated cells were measured for at least 10 fields of view or 1,000 cells. Elongated cells were defined as perimeter lengths greater than one SD above the wt mean. Each symbol represents a biological replicate, the bars indicate the mean, and the error bars denote the SEM. P values were calculated using an unpaired Student t test compared to the parental strain, as indicated. *, $P < 0.05$; ***, $P < 0.001$.

We next examined whether *spxA1* elongation was mediated by well-described inducers of filamentation in other Firmicutes. Filamentation can arise due to changes in the abundance of proteins involved in cell envelope biosynthesis and modification, induction of the DNA damage response (the SOS response), or alterations to the stoichiometry of cell division proteins (118). Interestingly, none of the canonical factors critical for these processes were significantly changed in Δ*spxA1* compared to wt. Specifically, proteins involved in the synthesis and modification of wall teichoic acid (DltACD, TagABDH), lipoteichoic acid (LtaPS, LafAB, GtlAB) and peptidoglycan (MurBCDEFGIZ, PBPs, Ami, PgdA) were equally abundant in wt and Δ*spxA1* (Table S3). Furthermore, immunoblot detection of lipoteichoic acid revealed no changes in the size or composition of lipoteichoic acid between wt and Δ*spxA1* (data not shown). The SOS response induces filamentation in response to DNA damage through RecA-mediated transcriptional changes. RecA binds to single-stranded DNA and induces the auto-cleavage of the major SOS regulator LexA, leading to inhibition of septation (128). Whole cell proteomics identified no difference in the abundance of RecA or LexA in Δ*spxA1* compared to wt, and several other canonical SOS proteins were also unchanged (RecF, RecQ, RuvAB, and UvrABC). Lastly, critical cell shape determinants (MreBC, RodA1, RodZ), proteins necessary for the formation of the divisome (FtsAEHKYZ, SepF, ZapA,), and proteins required for septum localization to the cell midpoint (DivIB, EngB, EzrA, MinCDJ, Noc) were unchanged in the Δ*spxA1* mutant compared to wt. Together, we did not find evidence of cell envelope alterations, induction of the SOS response, or aberrant production of divisome proteins in Δ*spxA1* filamentous cells.

Finally, we examined whether Δ*spxA1* filamentation was the result of a deficiency in secreted factors such as autolysins, small peptides, or signaling molecules that would not be readily measured by whole cell proteomics. If this was the case, we hypothesized that co-culture with wt would rescue Δ*spxA1* filamentation *in trans*. Indeed, *L. monocytogenes* mutants lacking the secreted peptidoglycan hydrolases NamA or p60 form chains that are unable to divide unless exposed to wt culture supernatants (115, 116). However, anaerobic co-culture of wt constitutively expressing GFP with Δ*spxA1* expressing mCherry did not rescue the elongated phenotype of Δ*spxA1* (Fig. 28). Overall, our proteomic and microscopic analyses determined that SpxA1-dependent factor(s) regulate cell size, as proteolysis-deficient strains with increased SpxA1 abundance (Δ*yjbH* and Δ*clpX*) are significantly smaller than wt and *L. monocytogenes* lacking *spxA1* are significantly elongated. Moreover, we determined that SpxA1-dependent filamentation is not due to SOS response induction, altered synthesis or modification of teichoic acids or peptidoglycan, changes in cell division protein abundance, or defects in secreted factors such as autolysins or small molecules.

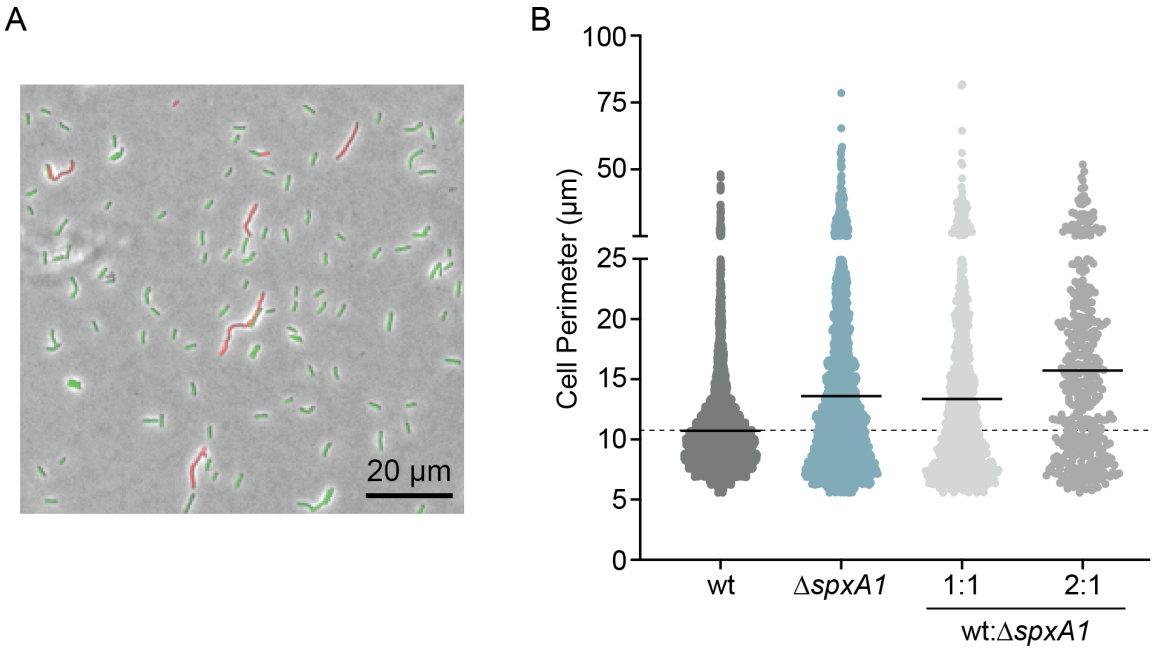

Figure 28. Co-culture with wt does not rescue Δ*spxA1* filamentation. L. monocytogenes wt constitutively producing GFP was co-cultured with Δ*spxA1* constitutively producing mCherry for 2 hours. (A) A representative image of a 2:1 (wt: Δ*spxA1*) co-culture is shown. (B) Cell perimeters of each condition were measured with Celltool and the data shown for the co-cultures indicate Δ*spxA1* cell perimeters. Data are from a single representative replicate where at least 1,000 cells or ten fields of view were quantified. The lines represent the means.

The roles of motility and morphology during infection

Upon examining our whole cell proteomics for protein changes that could impact virulence, we discovered that proteins associated with motility and chemotaxis were significantly decreased in abundance in Δ*spxA1* compared to wt (Table 6). Specifically, Δ*spxA1* was significantly deficient for 16 motility and chemotaxis proteins, including a 7-fold decrease in the flagellin monomer FlaA. While previous work demonstrated that *L. monocytogenes* strain 10403S significantly down-regulates *flaA* at 37ºC, flagella production and motility is not completely abrogated at this temperature . Indeed, we observed that wt *L. monocytogenes* was approximately 40% less motile at 37ºC compared to room temperature when incubated anaerobically (Fig. 29). Compared to wt,

the Δ*spxA1* mutant exhibited reduced motility at room temperature and was non-motile at 37ºC. This motility defect could be fully restored by in-trans complementation.

Table 6. Motility proteins decreased in Δ*spxA1*

10403S	EGD-e	Protein name	Protein function	wt average	Δ*spxA1* average	Fold decrease (wt/Δ*spxA1*)	*P* value
LMRG_00386	*lmo0697*	FlgE	flagellar hook protein	6.9E+07	3.0E+06	23.3	1.4E-03
LMRG_00378	*lmo0690*	FlaA	flagellin	2.5E+09	3.6E+08	7.1	4.1E-04
LMRG_00412	*lmo0723*	-	methyl-accepting chemotaxis protein	6.1E+08	9.2E+07	6.7	2.9E-03
LMRG_00402	*lmo0713*	FliF	flagellar M-ring protein	9.0E+07	1.5E+07	6.2	2.3E-05
LMRG_00395	*lmo0706*	FlgL	flagellar hook-associated protein	4.9E+07	8.1E+06	6.1	2.1E-02
LMRG_02773	*lmo1699*	-	methyl-accepting chemotaxis protein	2.3E+08	4.0E+07	5.9	3.3E-03
LMRG_00394	*lmo0705*	FlgK	flagellar hook-associated protein	1.3E+08	2.2E+07	5.7	2.4E-03
LMRG_00380	*lmo0692*	CheA	Signal transduction histidine kinase	2.4E+08	5.0E+07	4.7	3.5E-04
LMRG_00396	*lmo0707*	FliD	flagellar hook-associated protein	7.0E+07	1.5E+07	4.6	1.8E-02
LMRG_00379	*lmo0691*	CheY	Chemotaxis regulator	2.5E+08	6.1E+07	4.2	3.9E-05
LMRG_00403	*lmo0714*	FliG	flagellar motor switch protein	1.2E+08	3.1E+07	3.8	6.5E-04
LMRG_00373	*lmo0685*	MotA	Flagellar motor rotation protein	5.6E+07	1.8E+07	3.2	7.5E-03
LMRG_00377	*lmo0689*	CheV	chemotaxis	4.1E+08	1.3E+08	3.0	1.9E-04
LMRG_00376	*lmo0688*	GmaR	flagellin glycosyltransferase	2.3E+08	8.4E+07	2.8	2.7E-04

LMRG_ 00388	*lmo0699*	FliM	flagellar motor switch protein	2.8E+07	0	-	6.2E-04
LMRG_ 00389	*lmo0700*	CheC	chemotaxis	2.7E+07	0	-	2.9E-04

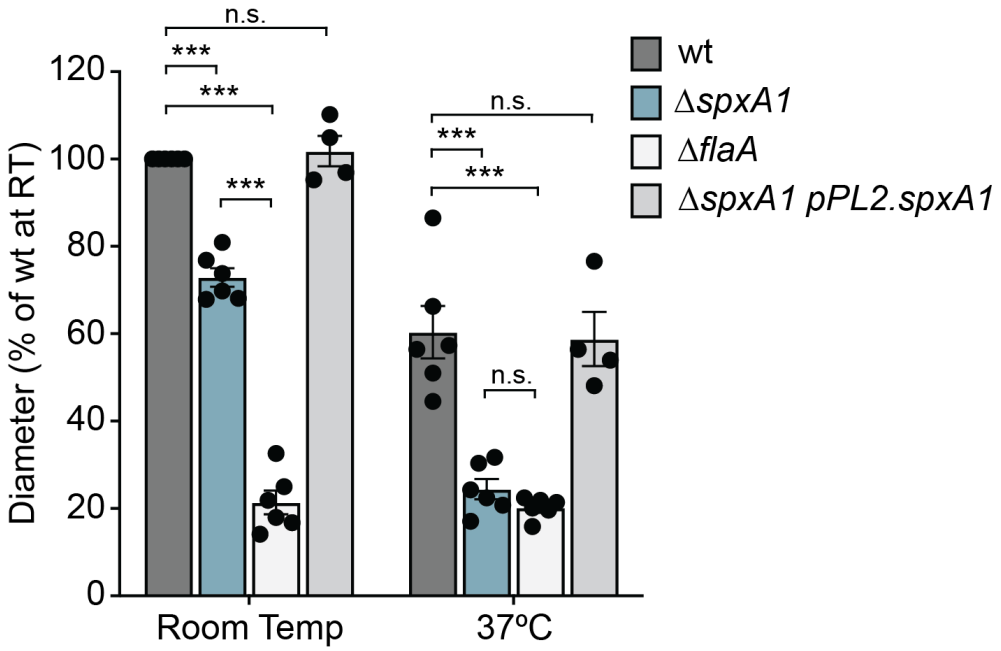

Figure 29. Motility of L. monocytogenes incubated anaerobically. BHI 0.4% agar motility plates were inoculated via stab with bacteria and incubated anaerobically at either room temperature or 37ºC for 4 days. The diameter of bacterial migration from the central stab was measured and compared to that of wt at room temperature. Data are from 4 or 6 biological replicates. The diameter of the non-motile ΔflaA mutant migration represents the diameter of the inoculation stab. Bars represent means and SEMs, and significance was determined by unpaired t-test. *** $p < 0.001$; n.s. $p > 0.05$.

We hypothesized that decreased motility contributes to the virulence defect of Δ*spxA1* in tissue culture infection models, as previous research demonstrated that non-motile mutants are unable to swim towards host cell monolayers and thus cannot efficiently invade (129, 130). To address this hypothesis, gentamicin protection assays were performed on infected immortalized murine bone marrow-derived macrophages (iBMMs) and uptake of Δ*spxA1* was compared to that of wt or a Δ*flaA* mutant that lacks

flagella (130). After a 30 minute infection with *L. monocytogenes*, cells were washed and incubated with media containing gentamicin for 30 minutes to kill extracellular bacteria. Host cells were then lysed, plated to enumerate CFU, and intracellular bacteria were calculated as a percentage of the total inoculum. The non-motile Δ*flaA* strain exhibited a ~3-fold reduction in intracellular bacteria compared to wt *L. monocytogenes* (Fig. 30A). The Δ*spxA1* mutants exhibited a similar ~4-fold reduction in intracellular bacteria, which was fully restored in the Δ*spxA1* pPL2.*spxA1* strain. To test if the Δ*spxA1* defect was due to impaired motility, centrifugation was applied immediately after infection to force the bacteria to contact the host cell monolayer. Following centrifugation, the Δ*flaA* and Δ*spxA1* mutants were taken up by iBMMs with the same efficiency as wt *L. monocytogenes* (Fig. 30B). These results suggested that the observed defect in phagocytosis of Δ*spxA1* can be attributed to decreased motility that limits interactions with the host cells.

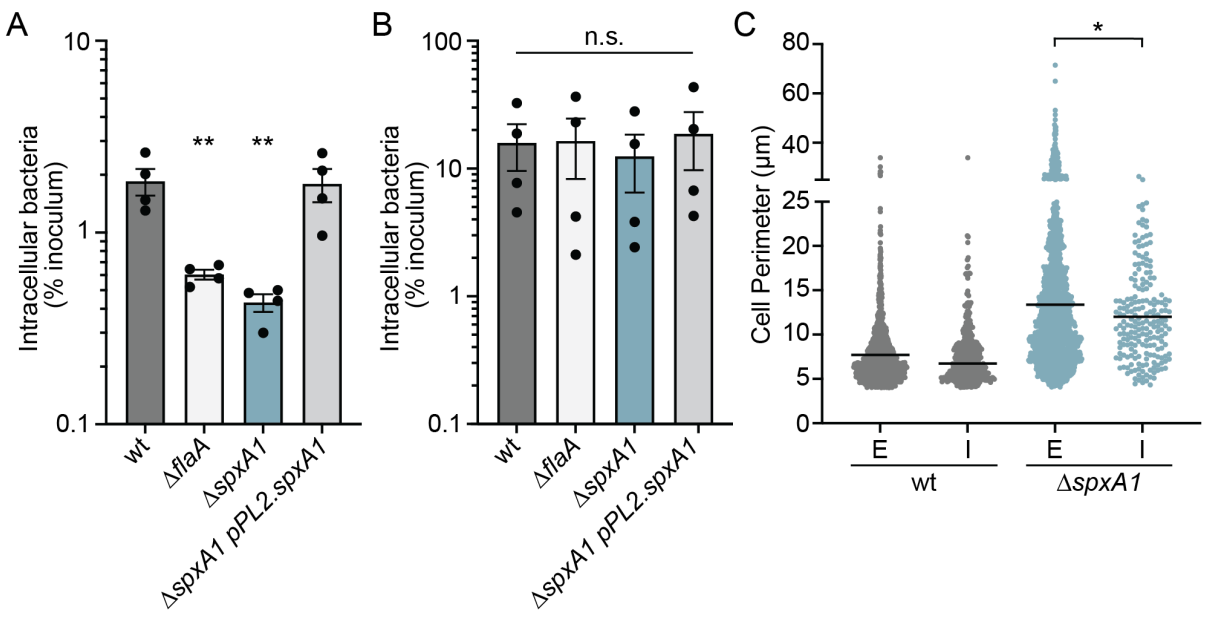

Figure 30. The roles of bacterial motility and morphology in macrophage phagocytosis of the Δ*spxA1* mutant. (A) Gentamicin protection assay measuring intracellular bacteria at 1 h postinfection of iBMMs. (B) Gentamicin protection assay after bacteria were centrifuged onto the host cells immediately after infection. The means and SEM of three biological replicates are shown for panels A and B. *P* values were calculated using an unpaired Student *t* test compared to wt cells. *, $P < 0.05$; n.s., $P > 0.05$. (C) iBMMs were infected with centrifugation for 15 min and stained to enable differentiation of extracellular (E) and intracellular (I) bacteria. The perimeters of cells in each compartment were measured using Celltool. Cell perimeters were measured from two biological replicates where at least 1,000 bacteria or 10 fields of view were quantified. The lines represent the means. Distributions were compared using Kolmogorov-Smirnov tests. *, $P < 0.05$.

While motility is clearly important for Δ*spxA1* cells to access the host cell monolayer, it is also well-known that filamentous bacteria and fungi are more resistant to phagocytosis than bacilli (118). To test if filamentation contributes to decreased host cell uptake of Δ*spxA1*, we performed quantitative immunofluorescence microscopy of infected iBMMs. *L. monocytogenes* wt or Δ*spxA1* constitutively expressing mCherry were added to cells with centrifugation and allowed to infect for 15 minutes. Cells were then washed, fixed, immunostained with a *L. monocytogenes*-specific antibody, and labeled with a green fluorophore. As the iBMMs were not permeabilized prior to immunostaining,

extracellular bacteria could be identified by the colocalization of red and green fluorescence, while intracellular bacteria could be differentiated by the absence of green fluorescence. Celltool was then used to measure the cell perimeters of intracellular and extracellular bacterial populations. We observed a significant decrease in the mean perimeter of intracellular Δ*spxA1* cells compared to extracellular cells and all filamentous Δ*spxA1* cells with a perimeter of 26 μm or larger remained extracellular (Fig. 30C). Together, these results suggested that macrophage uptake of Δ*spxA1* is impaired due to both decreased motility and impaired phagocytosis of Δ*spxA1* filaments.

Discussion

This study set out to define the role of the transcriptional regulator SpxA1 in *L. monocytogenes* pathogenesis. Surprisingly, we observed that Δ*spxA1* exhibits striking morphological heterogeneity during intracellular and extracellular growth, forming single rod-shaped bacteria, chains of cells, and filamentous single cells. Quantitative microscopic analysis of this morphology phenotype *in vitro* revealed that *L. monocytogenes* lacking *spxA1* primarily form filamentous cells with an average cell perimeter twice that of wt. These filamentous cells did not have compromised cell membranes and appeared to result from irregular frequency and localization of division septum formation. Using a whole cell proteomics approach, we determined that SpxA1 does not influence the abundance of proteins critical to cell division, the SOS response, or the synthesis or modification of cell envelope components. However, proteins important for motility and chemotaxis were significantly depleted in Δ*spxA1* compared to wt *L. monocytogenes* and bacterial motility was necessary for infection of macrophages

in tissue culture. Furthermore, highly filamentous Δ*spxA1* cells were more resistant to phagocytosis than their bacillary counterparts, supporting a multifaceted role of SpxA1 in virulence regulation. Together, our results provide novel insight into the function of SpxA1 in *L. monocytogenes* and its roles in regulating cell division, motility, and virulence.

To examine the morphological heterogeneity of Δ*spxA1* cells, we took several complimentary microscopy approaches. Phase contrast images revealed that approximately five-fold more Δ*spxA1* cells are elongated in early exponential phase than wt, but these elongated cells did not exhibit a significant loss in viability or membrane integrity. Membrane staining identified that Δ*spxA1* cultures are dominated by filamentous cells, the physiology of which we investigated more closely with STEM. Previous research successfully applied STEM to identify changes in the thickness and composition of peptidoglycan in the *L. monocytogenes* envelope (131). However, our STEM images suggested that the composition of the Δ*spxA1* cell envelope did not differ significantly from wt. Instead, we observed notable irregularities in division septum formation in Δ*spxA1* filamentous cells. Overall, these microscopic analyses suggested that the altered frequency and localization of division septa are likely responsible for Δ*spxA1* filamentation.

To elucidate the mechanism of Δ*spxA1* filamentation, quantitative label-free mass spectrometry of whole cell lysates was used to identify SpxA1-dependent changes in protein abundance. Results from this global proteomic analysis disproved many of our initial hypotheses about the potential mechanism of Δ*spxA1* filamentation. The largest category of proteins influenced by SpxA1 were those involved in redox homeostasis and respiration. However, the SpxA1-regulated redox genes essential for aerobic growth (*kat*

and *hemEH*) were dispensable for SpxA1 regulation of morphology. Furthermore, the experiments described herein were performed in strictly anaerobic conditions, eliminating redox stress as a potential cause of Δ*spxA1* filamentation. Our whole cell proteomics enforced observations from previous transcriptional analysis that SpxA1 plays a distinct role in regulating components of protein turnover. While the proteins most increased in Δ*spxA1* compared to wt were MecA and ClpE, both related to protein turnover, deleting these proteins did not rescue Δ*spxA1* filamentation. In fact, the increased filamentation of Δ*spxA1*Δ*clpE* compared to Δ*spxA1* suggests that ClpE over-production in Δ*spxA1* may be a direct response to the disrupted stoichiometries of SpxA1-regulated factors. Our data therefore support a novel model for SpxA1 influence over morphology which is independent of the other previously described roles for this protein.

Whole cell proteomics results excluded the influence of several canonical filamentation pathways on Δ*spxA1* morphology, including the SOS response, alterations to cell division machinery, and cell envelope modifications. Filamentation of bacteria is often associated with induction of the SOS response to DNA damage (118), but key SOS response proteins were unchanged in Δ*spxA1*. The production and modification of cell envelope components can also influence both morphology and pathogenesis in *L. monocytogenes* (132–134). However, proteins required for biosynthesis and modification of teichoic acids and peptidoglycan were not altered in the Δ*spxA1* mutant. Given the septation defects of the Δ*spxA1* mutant, it was most surprising that proteins important for cell division were unchanged in Δ*spxA1* compared to wt. The *Bacillus subtilis* homologue Spx directly regulates the divisome component ZapA, which interacts with the cell division Z-ring protein FtsZ to promote septum formation (135). In *L. monocytogenes*, neither FtsZ

nor ZapA were changed in abundance in the Δ*spxA1* mutant compared to wt. Overall, we found that Δ*spxA1* filamentation was occurring independently of the redox response, SOS response, cell division, and cell envelope biosynthesis. Current research is aimed at elucidating the SpxA1-dependent mechanism of filamentation.

Our data suggest that a combination of motility and morphology defects contribute to reduced phagocytosis of Δ*spxA1*. Whole cell proteomics revealed a significant depletion of proteins involved in motility and chemotaxis in Δ*spxA1* compared to wt. Indeed, we observed that Δ*spxA1* was nearly non-motile at 37ºC. We further demonstrate that flagellar motility is important for *L. monocytogenes* to interact with the host monolayer during tissue culture models of infection, as forcing Δ*spxA1* to contact host cells via centrifugation rescued the defect in uptake by macrophages. Immunofluorescence microscopy of the *L. monocytogenes*-host cell surface interaction revealed that the longest filaments were exclusively extracellular. Together, these results demonstrated roles for both motility and bacterial cell size in macrophage phagocytosis.

It is not yet clear which SpxA1-dependent factors are necessary during murine infection, during which Δ*spxA1* is attenuated over 500-fold in the spleen and 5-logs in the liver (36). Flagellar motility is important for adhesion and invasion of host cells *in vitro*, but dispensable for infection in both oral and intravenous models of murine infection (129, 136). While impaired phagocytosis of filamentous Δ*spxA1* cells may contribute to its virulence defect, entry into host cells is not the only barrier to virulence of Δ*spxA1*. Once in the host cytosol, the Δ*spxA1* mutant has a doubling time of 109 minutes as compared to 47 minutes for wt *L. monocytogenes* and is severely defective for intercellular spread (36). The rod shape of *L. monocytogenes* is required in the host cytosol for establishing

the asymmetric actin cloud necessary for canonical comet tail formation and motility (22, 23). Thus, the elongated shape and improper actin polarization observed for Δ*spxA1* filaments may limit cytosolic motility and intercellular spread, which would significantly impair host colonization (10, 137, 138). The impact of disorganized septum formation and filamentation on cytosolic growth, intercellular spread, and systemic infection is an area of ongoing investigation.

This study aimed to identify SpxA1-dependent factors important for *L. monocytogenes* pathogenesis. We discovered that Δ*spxA1* cells form elongated filaments that are impaired for motility and resistant to phagocytosis. While the mechanism of filamentation is not yet known, it is intriguing that the SpxA1-regulated genes necessary for aerobic growth *in vitro* are dispensable during infection and are not involved in cell size regulation or motility. SpxA1-dependent regulation thus independently impacts many areas of *L. monocytogenes* physiology. We predict that the complexity of SpxA1 regulation likely results from selective pressure to respond to a variety of signals in diverse environments. Future research will elucidate the cues that influence SpxA1 activity and the genes it regulates during both extracellular growth and pathogenesis.

Chapter 5: Future Directions and the SpxA1 Model

Summary of work

As a saprophyte and pathogen, *L. monocytogenes* is bombarded with varied stressors to which it must initiate protective responses. This dissertation examines the role of SpxA1, a redox-responsive transcriptional regulator critical for *L. monocytogenes* survival within the host as well as the aerobic environment. Together, the data generated here show that SpxA1 is of global importance for growth and virulence, impacting the regulation of a wide variety of processes including redox stress response, peroxide detoxification, cofactor biosynthesis, respiration, morphology, and motility. While this dissertation took a comprehensive omics approach to understanding the influence of SpxA1, there are still many unanswered questions about how the multiple facets of SpxA1 regulatory control uniquely impact the success of *L. monocytogenes* survival and pathogenesis. Overall, this work demonstrates several unique and previously undescribed roles for the highly conserved Spx-family proteins in our examination of *L. monocytogenes* SpxA1.

Final Questions

The role of SpxA1 in aerobic growth

Bacteria have necessarily evolved a protective arsenal of proteins to contend with redox stress caused by peroxides and other reactive oxygen species generated in aerobic environments. If not quickly addressed, an imbalance of cellular oxidants and reductants can disrupt cell homeostasis and result in death (66, 139). The redox-responsive regulator SpxA1 is essential for the aerobic growth of *L. monocytogenes*, but it was not clear how

SpxA1 regulation protected *L. monocytogenes* in aerobic environments prior to this study. This work found that SpxA1-activated genes encoding cytochrome bd oxidase (*cydABCD*), heme biosynthesis enzymes (*hemEH*) and catalase (*kat*) were required for *L. monocytogenes* aerobic growth in rich medium. Our working model for how regulation by SpxA1 protects *L. monocytogenes* from peroxide is described in Figure 31. An Spx-recognition motif previously defined in *Bacillus subtilis* was identified in the promoters of SpxA1-activated genes and proved necessary for the proper regulation of *hemEH*, indicating this regulation by SpxA1 is likely direct. However, neither heme biosynthesis nor catalase were necessary for virulence. Together, our findings suggest a model in which SpxA1 activation of peroxide-scavenging enzymes and the cofactor heme is essential for the surviving both exogenous and endogenously generated redox stress (73) (Fig. 31).

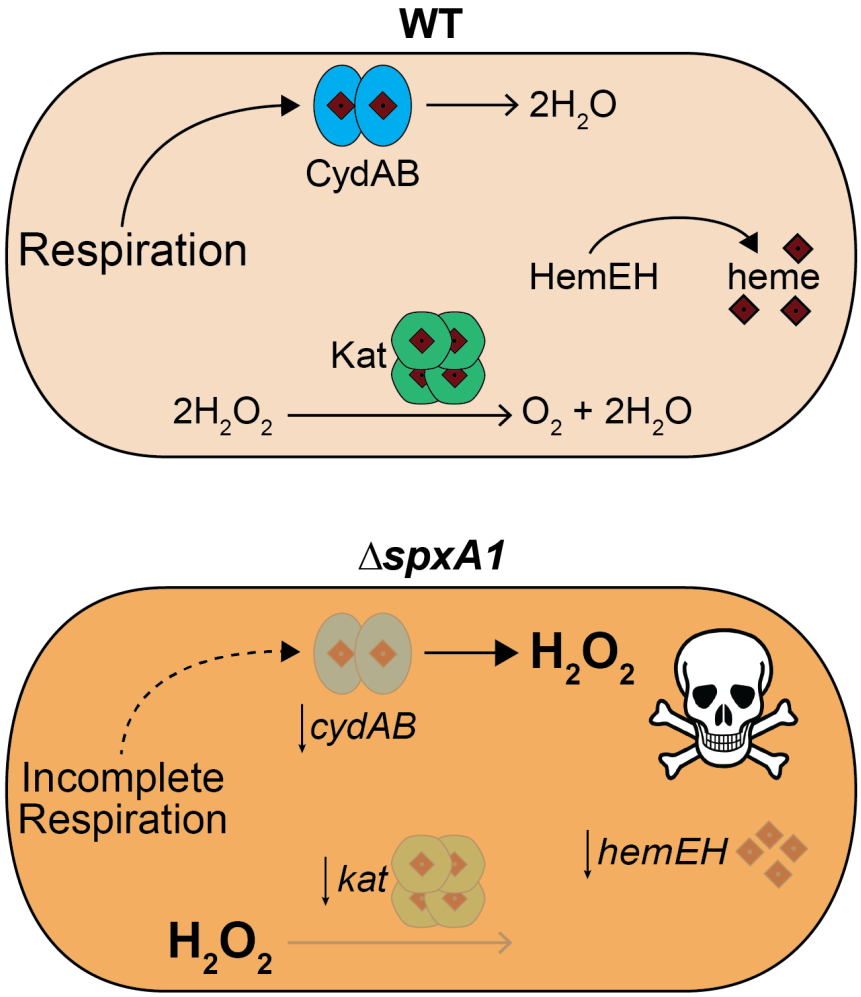

Figure 31. The model of SpxA1 aerobic essentiality. In the absence of *spxA1*, our data suggest that *L. monocytogenes* lacks sufficient abundance of terminal oxidase (CydAB) to support a fully functional oxidative respiration electron transport chain. The electron transport chain is further limited by a reduction in biosynthesis of the CydAB co-factor heme. Respiration generates a basal level of toxic ROS, but levels of peroxide are increased when respiration is incomplete. Mutants lacking *spxA1* do not make enough catalase or its cofactor heme to detoxify the increased generation of endogenous peroxide or any exogenous peroxide that *L. monocytogenes* might encounter.

The investigation of SpxA1 impact on aerobic growth generated several outstanding questions about the role of *L. monocytogenes* heme biosynthesis enzymes and peroxidases during infection. As catalase was not required for L. monocytogenes virulence, we sought to test the importance of other L. monocytogenes peroxidases during infection, and found that only the peroxidase Fri impacted intracellular growth. It

remains to be determined how, out of all the peroxidases in the *L. monocytogenes* arsenal, Fri is the only one necessary for virulence. One possibility is that Fri aids in the storage of iron necessary for the functionality of iron-dependent enzymes essential for infection. However, this theory is complicated by evidence from this study that that heme biosynthesis is unnecessary for cytosolic growth, and mutants lacking either *hemEH* or *chdC* show increased growth in host monolayers compared to wt. Interestingly, Iron starvation and iron saturation have been shown to impact the transcription of *Lm* virulence genes, including *actA, hly*, and *inlAB* (140–142). Thus, future work should address whether these virulence factors are impacted by iron storage proteins such as Fri. Fri has also been implicated in the regulation of the *dlt* operon, responsible for LTA modifications that promote adhesion and virulence (132). There is also evidence that Fri impacts cell morphology in response to cell wall stressors (143). Fri gene expression is modulated by PerR and Fur transcriptional regulators, both of which are important for successful infection of the host (144, 145). Our data suggest that the virulence impact of these regulators could be due in part to the regulation of *fri.* Further investigations will reveal the role of *fri*-dependent iron metabolism during rapidly changing redox conditions of infection.

During aerobic growth, the role of regulation in the redundancy of *L. monocytogenes* peroxidases remains to be investigated. The peroxidases examined in this study are known to be under complex transcriptional control by multiple redox-stress and metal-sensitive regulators. Of these peroxidases, *fri* and *lmo0367* are negatively regulated by Fur (ferric uptake regulator) and iron limiting conditions (146). Importantly, Fur itself is under the negative transcriptional control of PerR (peroxide stress response

regulator), along with the heme biosynthesis gene *hemA* and the genes *ahpA, fri,* and *kat* (62). Meanwhile, *kat, lmo1609, lmo0983, chdC*, and *tpx* are positively regulated by the redox-responsive regulator SpxA1 (73, 147). PerR, Fur, and SpxA1 play significant roles in survival of endogenous and exogenous peroxide stress, as well as *L. monocytogenes* virulence. Mutants lacking *spxA1* cannot grow aerobically, while Δ*perR* mutants have a significant aerobic growth defect (36, 62). Insufficient production of each of these regulators results in increased sensitivity to peroxide (13, 148). Deletion of each regulator also significantly reduces the capacity of *L. monocytogenes* to colonize murine modes. Interestingly, while mutants lacking *spxA1* are deficient for growth in host cytosol, those lacking *fur* and *perR* are not (148). Future investigations are necessary to clarify the important and complex crosstalk of these regulators in response to redox stress experienced in the environment and host.

The impact of SpxA1 on morphology

In this work, we set out to investigate the role of SpxA1 in a tissue culture model of infection and made the surprising discovery that Δ*spxA1* cells are dramatically elongated during growth in the host cytosol. Quantitative microscopy revealed Δ*spxA1* also forms elongated filaments extracellularly during early exponential phase in rich medium. Scanning and Transmission Electron Microscopy (STEM) analysis found the likely cause of this morphological phenotype is aberrantly placed division septa localized outside of cell midpoints. Quantitative mass spectrometry of whole cell lysates identified SpxA1-dependent changes in protein abundance, including a significant number of motility and flagellar proteins that were depleted in the Δ*spxA1* mutant. Accordingly, we found that

both the filamentation and the lack of motility contributed to decreased phagocytosis of Δ*spxA1* by macrophages. Overall, we identify a novel role for SpxA1 in regulating cell elongation and motility, both of which impact *L. monocytogenes* virulence (Fig. 32).

Our data suggest that SpxA1 does not adhere to the more characterized *B. subtilis* model of cell division regulation by Spx. First and foremost, the aberrant morphology exhibited in Δ*spxA1* has not been demonstrated in microscopy of mutants solely lacking Spx homologs in other species (37, 149). However*, B. subtilis* Spx influences the abundance of the critical division and septa development factor ZapA, a protein that stabilizes FtsZ-ring formation and subsequent division septa development. *B. subtilis* strains lacking *spx* contained decreased levels of ZapA, while Δ*yjbH* and Δ*clpX* strains have increased Spx and ZapA abundance (135). Interestingly, our whole-cell proteomics and previous RNA-seq did not reveal any difference in *L. monocytogenes* ZapA abundance in either Δ*spxA1* or Δ*yjbH,* and overexpressing *zapA* in Δ*spxA1* did not impact elongation (49, 73). While elongation was not observed in a *B. subtilis* mutant lacking Spx, minicell production increased 2-fold (135). However, minicells were nearly undetectable in *L. monocytogenes,* accounting for less than 0.1% of both wt and Δ*spxA1* (data not shown). These data are unsurprising considering that the generation of minicells is demonstrably rare in *L. monocytogenes*, even in critical cell division deletion mutants which present substantial minicell formation in other species (150). While still unknown, the mechanism that results in Δ*spxA1* elongation appears at this point unique to *L. monocytogenes*. Future research should investigate whether as-of-yet unexamined pathogens exhibit a similar model of SpxA1-regulated morphology.

Our whole cell proteomics stringently ruled out the influence of peptidoglycan,

lipoteichoic acid, and wall teichoic acid synthesis. However, the impact of both membrane lipid biosynthesis as well as a handful of integral membrane proteins of hypothetical function has not been investigated. It is possible that these proteins could play a role in Δ*spxA1* morphology. In our proteomics, we found changes in 6 different proteins critical for the synthesis of phosphatidic acid, the global precursor to bacterial membrane lipids (151). One protein in particular, the enoyl-acyl carrier protein reductase FabL, was decreased over 4-fold in Δ*spxA1*, corresponding to a global decrease in saturated fatty acids and some increases to unsaturated fatty acids based on lipidomics profiling (unpublished data). Importantly, given that FabL functions biochemically as a reductase of carbon bonds on unsaturated fatty acids, it would be exciting to test whether the changes observed in our lipidomics were FabL-dependent (152). FabL also generates precursors used by the protein divisome-associating enzyme PlsX, the first enzyme in the phosphatidic acid synthesis pathway (153). Interestingly, *B. subtilis* mutants with disrupted *plsX* have been shown to form aberrantly organized Z-rings, resulting in long and irregularly filamenting cells (154). Future studies should test whether, in a Δ*spxA1* mutant, reduced FabL produces less precursor for PlsX phosphatidic acid synthesis and phenotypically mimics a PlsX depletion in both cell lipid profile and morphology. In this study, we explored the impact of SpxA1 on each stage of the *L. monocytogenes* lifecycle (Fig. 38).

The role of SpxA1 in virulence

Our data suggest that both elongation and lack of flagellar motility influence uptake by immortalized murine phagocytes. However, the importance of elongation vs. flagellar

motility for uptake of L. monocytogenes by nonphagocytic cells remains unknown. Non-phagocytic cells require interactions with specific surface-presented bacterial factors called internalins for efficient uptake of *L. monocytogenes* (155–157). While SpxA1 does not influence the abundance of internalins A, B, or C, it will be very interesting to investigate whether the irregular morphology of Δ*spxA1* disrupts the function, presentation, or organization of these factors.

It is unknown whether elongation of Δ*spxA1* or any other factors play a role in the inability of this mutant to successfully colonize livers and spleens in a mouse model of infection. Previous Research on *L. monocytogenes* motility and chemotaxis proteins shows that decreased motility does not impact dissemination to the spleen and liver in whole-animal infection models (36, 129, 136, 158). Therefore, the motility defect of Δ*spxA1* most likely does not interfere with pathogenesis in a mouse, and more research should be focused on what other SpxA1-regulated factors might be important for whole-animal infection. For example, the transcription factor Rex is known to be important for colonizing gallbladders of mice, an important reservoir for dissemination, and was decreased in abundance in the Δ*spxA1* mutant. Therefore, future work should also characterize Δ*spxA1* colonization of the gallbladder and the impact of this colonization on deficient ΔspxA1 dissemination to other organs.

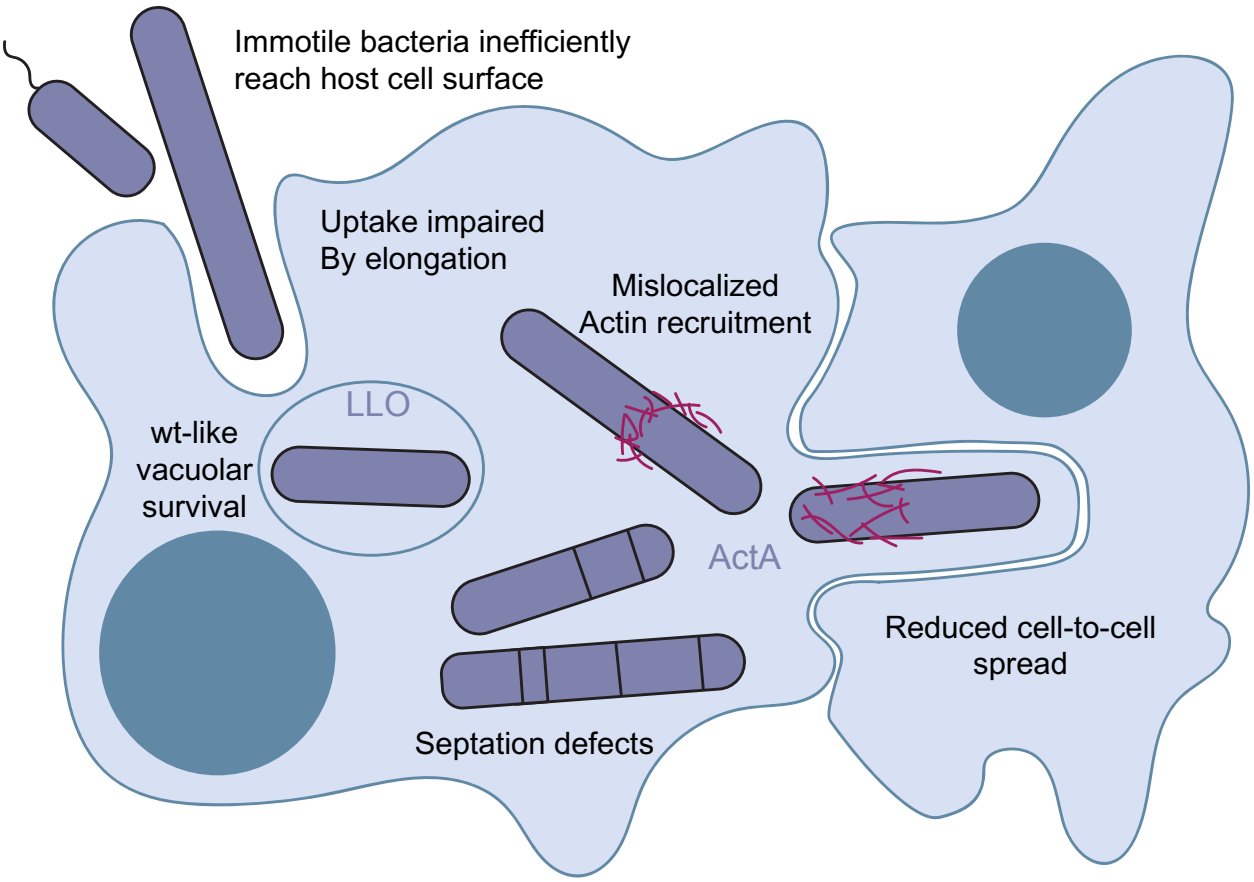

Figure 32. The working model of the impact of SpxA1 on virulence. The Δ*spxA1* mutant is immotile during infection conditions, resulting in fewer bacteria reaching host monolayers in laboratory settings. Once bacteria are in contact with host cells, phagocytes do not efficiently take up highly elongated bacteria. After entering the host cell, the Δ*spxA1* mutant can persist as well as wt in the vacuole until escaping to the cytosol (unpublished data). The Δ*spxA1* mutant divides irregularly in the cytosol, impacting bacterial shape and subsequently the organization of host actin recruitment on the bacterial surface. The Δ*spxA1* mutant is also deficient for ActA production, likely resulting in reduced actin recruitment overall (unpublished data). Together these phenotypes and other yet undescribed factors lead to defective cell-to-cell spread for the Δ*spxA1* mutant.

Concluding remarks

This work outlines the many functions of the highly conserved transcriptional regulator SpxA1 in *L. monocytogenes*, some of which have yet to be documented in other organisms. Like previously described Spx-family proteins, SpxA1 regulation is required to combat redox stress, specifically peroxide stress in oxygen-rich environments. We

have shown that SpxA1 accomplishes this through regulation of a set of functionally diverse peroxidases and heme biosynthesis enzymes. However, redox regulation of SpxA1 is completely independent of its roles in the regulation of virulence and morphology, both of which are under continued investigation. While the precise set of SpxA1-regulated genes that impact both virulence and morphology have yet to be described, our data shows that these phenotypes are likely connected. Elongation of the Δ*spxA1* mutant hinders uptake by host cells, and the variable cell shapes of this mutant appear to impact host actin organization on the bacterial surface, likely influencing cytosolic motility and cell to cell spread. Overall, our work affirms that conserved physiological systems described in model Gram positive organisms like *B. subtilis* do not always mimic those of important pathogens like *L. monocytogenes*, and studying these systems in pathogens can reveal novel and important connections between physiology and pathogenesis.

Chapter 6: Materials and Methods

Bacterial strains and culture conditions

L. monocytogenes strains were derived from the wt strain 10403S and are listed in Table 7. *E. coli* strains are listed in Table 8. *L. monocytogenes* was cultured in either tryptic soy broth (TSB) or brain heart infusion (BHI), aerobically in the dark shaking at 37°C unless other conditions were noted. Anaerobic conditions were established by growing bacteria in closed containers with GasPak EZ Anaerobe Gas Generating Pouches (Becton Dickinson) or placing cultures in degassed media inside of a closed-system anaerobic chamber (Don Whitley Scientific A35 Anaerobic Workstation). Unless otherwise stated, the chemicals used were purchased from Sigma Aldrich. The following concentrations of antibiotics were used: streptomycin, 200 μg mL^{-1}; chloramphenicol, 10 μg mL^{-1} (*E. coli*), 7.5 μg mL^{-1} (*L. monocytogenes*); carbenicillin, 100 μg mL^{-1}; erythromycin, 1μg mL^{-1}; and tetracycline, 1 μg mL^{-1}.

Table 7. *L. monocytogenes* strains used in this study

Strain name	Genotype	Reference
MLR-L001	wt	(159)
MLR-L0081	Δ*yjbH*	(13)
MLR-L0408	*yjbH::Tn*	(13)
MLR-L0448	*clpC::Tn*	(160)
MLR-L0449	*clpX::Tn*	(160)
MLR-L0470	Δ*spxA2*	(36)
MLR-L0551	*pPL3.mCherry*	(161)
MLR-L0552	*pPL3.GFP*	(162)
MLR-L0752	Δ*rex*	(163)
MLR-L1000	*Δfri hly::Tn*	(164)
MLR-L1001	*ΔkatΔahpA hly::Tn*	(164)
MLR-L1066	Δ*spxA1*	(147)

MLR-L1067	Δ*spxA1 pPL2.spxA1*	(147)
MLR-L1068	Δ*flaA*	Rochelle Glover, unpublished
MLR-L1069	Δ*clpE*	(147)
MLR-L1070	Δ*mecA*	(147)
MLR-L1072	Δ*spxA1* Δ*mecA*	(147)
MLR-L1073	Δ*spxA1* Δ*clpE*	(147)
MLR-L1074	Δ*spxA1 clpC::Tn*	(147)
MLR-L1075	Δ*spxA1 clpX::Tn*	(147)
MLR-L1076	Δ*spxA1 yjbH::Tn*	(147)
MLR-L1083	Δ*spxA1 pPL3.mCherry*	(147)
MLR-L174	*ΔohrA (lmo2199)*	(13)
MLR-L232	Δ*spxA1 pPL2t.spxA1.his*	(36)
MLR-L273	*P-spxA1::Tn*	(13)
MLR-L472	Δ*spxA1 pPL2.spxA1*	(36)
MLR-L637	Δ*spxA1 pPL2*	(36)
MLR-L705	*ΔspxA1 pOE-hemEH*	(73)
MLR-L707	*ΔspxA1 pOE-cydABCD*	(73)
MLR-L758	*ΔspxA1 pOE-gshF*	(73)
MLR-L759	*ΔspxA1 pOE-lmo0609*	(73)
MLR-L761	*ΔspxA1 pOE-lmo2467*	(73)
MLR-L770	*ΔspxA1 pOE-lmo0611*	(73)
MLR-L771	*ΔspxA1 pOE-lmo2176*	(73)
MLR-L772	*ΔspxA1 pOE-lmo2742-3*	(73)
MLR-L773	*ΔspxA1 pOE-lmo2719-cyd*	(73)
MLR-L779	*ΔspxA1 pOE-lmo0822*	(73)
MLR-L780	*ΔspxA1 pOE-lmo2060-2*	(73)
MLR-L793	*ΔspxA1 pOE-lmo0588*	(73)
MLR-L794	*ΔspxA1 pOE-lmo0656*	(73)
MLR-L795	*ΔspxA1 pOE-lmo0789-90*	(73)
MLR-L812	*ΔspxA1 pOE-spxA2*	(73)
MLR-L813	*ΔspxA1 pOE-trxA*	(73)
MLR-L816	*ΔspxA1 pOE-kat*	(73)
MLR-L826	Δ*kat*Δ*lmo2784*	(73)
MLR-L827	Δ*kat*Δ*lmo2784 pPL2.kat-lmo2784*	(73)
MLR-L828	Δ*kat (lmo2785)*	(73)
MLR-L829	Δ*kat*Δ*lmo2784 pPL2.lmo2784*	(73)
MLR-L830	Δ*kat*Δ*lmo2784 pPL2.kat*	(73)
MLR-L850	*pPL1.pHyper-gfp (pH-gfp)*	(164)

MLR-L879	*ΔahpA (lmo1604)*	(164)
MLR-L880	*ΔkatΔahpA*	(164)
MLR-L888	*ΔhemEH*	(73)
MLR-L896	*ΔhemEH pPL2.hemEH*	(73)
MLR-L897	*ΔhemEH pPL2.pCA-hemEH*	(73)
MLR-L899	*ΔkatΔlmo2784 pPL2.pCA-kat*	(73)
MLR-L900	*Δlmo2743*	(73)
MLR-L903	*Δlmo2743 pPL2.lmo2743*	(73)
MLR-L944	*ΔchdC (lmo2113)*	(164)
MLR-L948	*Δlmo0367*	(164)
MLR-L953	*Δlmo1609*	(164)
MLR-L954	*Δlmo0983*	(164)
MLR-L959	*Δtpx (lmo1583)*	(164)
MLR-L960	*Δfri (lmo0943)*	(164)
MLR-L971	*Δfri pPL2.fri*	(164)
MLR-L981	*pH-gfp P-kat-rfp*	(164)
MLR-L982	*pH-gfp P-chdC-rfp*	(164)
MLR-L983	*pH-gfp P-ahpA-rfp*	(164)
MLR-L984	*pH-gfp pHyper-rfp*	(164)
MLR-L985	*pH-gfp P-lmo0367-rfp*	(164)
MLR-L986	*pH-gfp P-fri-rfp*	(164)
MLR-L987	*pH-gfp P-lmo0983-rfp*	(164)
MLR-L988	*pH-gfp P-tpx-rfp*	(164)
MLR-L989	*pH-gfp P-lmo1609-rfp*	(164)
MLR-L990	*pH-gfp P-ohrA-rfp*	(164)
MLR-L991	*hly::himar1 (Tn)*	(11)
MLR-L992	*Δlmo0367 hly::Tn*	(164)
MLR-L993	*Δkat hly::Tn*	(164)
MLR-L994	*ΔchdC hly::Tn*	(164)
MLR-L995	*Δlmo0983 hly::Tn*	(164)
MLR-L996	*Δtpx hly::Tn*	(164)
MLR-L997	*Δlmo1609 hly::Tn*	(164)
MLR-L998	*ΔohrA hly::Tn*	(164)
MLR-L999	*ΔahpA hly::Tn*	(164)

Table 8. *E.coli* strains used in this study

Strain name	Genotype	Reference
MLR-E472	*pPL2.spxA1*	(36)
MLR-E558	*pPL3.mCherry*	(161)
MLR-E559	*pPL3.GFP*	(162)
MLR-E893	*pLIM*	Gift from Arne Rietsch (Case Western Reserve University)
MLR-E1078	*pLIMΔspxA1*	(147)
MLR-E1079	*pLIMΔmecA*	(147)
MLR-E1080	*pLIMΔclpE*	(147)
MLR-E1082	*pKSV7ΔflaA*	Rochelle Glover, unpublished
MLR-E233	*pPL2*	(54)
MLR-E543	*pOE-gshF*	(73)
MLR-E697	*pOE-hemEH*	(73)
MLR-E698	*pOE-cydABCD*	(73)
MLR-E725	*pOE-lmo0609*	(73)
MLR-E726	*pOE-lmo2467*	(73)
MLR-E744	*pOE-lmo0611*	(73)
MLR-E745	*pOE-lmo2176*	(73)
MLR-E746	*pOE-lmo2742-3*	(73)
MLR-E747	*pOE-lmo2719-cyd*	(73)
MLR-E766	*pOE-lmo0822*	(73)
MLR-E767	*pOE-lmo2060-2*	(73)
MLR-E781	*pOE-lmo0588*	(73)
MLR-E782	*pOE-lmo0656*	(73)
MLR-E783	*pOE-lmo0789-90*	(73)
MLR-E807	*pOE-spxA2*	(73)
MLR-E808	*pOE-trxA*	(73)
MLR-E810	*pOE-kat*	(73)
MLR-E824	*pPL2.kat-lmo2784*	(73)
MLR-E825	*pPL2.lmo2784*	(73)
MLR-E836	*pKSV7.kat-2784*	(73)
MLR-E837	*pPL2.kat*	(73)
MLR-E894	*pPL2.hemEH*	(73)
MLR-E895	*pPL2.pCA-hemEH*	(73)
MLR-E898	*pPL2.pCA-kat*	(73)
MLR-E901	*pPL2.lmo2743*	(73)
MLR-E902	*pPL2.pCA-lmo2743*	(73)

MLR-E970	*pPL2.fri*	(164)
MLR-E975	pPL2t.P-*lmo0367-rfp*	(164)
MLR-E978	pPL2t.P-*fri-rfp*	(164)
MLR-E976	pPL2t.P-*lmo0983-rfp*	(164)
MLR-E977	pPL2t.P-*tpx-rfp*	(164)
MLR-E974	pPL2t.P-*ahpA-rfp*	(164)
MLR-E979	pPL2t.P-*lmo1609-rfp*	(164)
MLR-E973	pPL2t.P-*chdC-rfp*	(164)
MLR-E980	pPL2t.P-*ohrA-rfp*	(164)
MLR-E972	pPL2t.P-*kat-rfp*	(164)

Tissue culture

Tissue culture cells were routinely cultured in high-glucose Dulbecco modified Eagle medium (DMEM) at 37°C with 5.5% CO_2. L2 fibroblasts were generated previously from L929 cells (13, 87). iBMMS were a gift from Josh Woodward, and MDCKs and HMEC-1s were generously gifted by Julie Theriot. L2s, MDCKs, Caco-2s, and J774 macrophages were maintained in media containing 10% FBS (HyClone), 2 mM L-glutamine (Gibco), and 1 mM sodium pyruvate (Gibco). H-MEC1s were grown in MCDB131 medium (Sigma) supplemented with 10 ng/mL epidermal growth factor (BD Biosciences), 1 µg hydrocortisone (Sigma Aldrich), 2 mM L-glutamine, and 10% FBS. Bone marrow-derived macrophages (BMDMs) were derived as previously described (13, 165). Bone marrow was from C57BL/6 mice purchased from The Jackson Laboratory or from B6.129S-*Cybb*^{tm1Din} (also known as gp91$^{phox-/-}$) mice, a generous gift from the Fang Laboratory (University of Washington) and originally from The Jackson Laboratory. BMDMs were cultured in 20% FBS, 2 mM L-glutamine, 1 mM sodium pyruvate, BME (55 µM) and 10% M-CSF (conditioned media from 3T3 cells expressing M-CSF).

Plasmid construction

In-frame deletions were carried out via either conjugatable suicide vector pLIM1 or pKSV7 and allelic exchange. Chromosomal mutations were confirmed by PCR and Sanger DNA sequencing when necessary. Complementation of in-frame deletions at ectopic loci were accomplished using pPL2 integration plasmids as previously described (138). Whole genes accompanied by promoter regions were amplified and ligated into pPL2. Constructs were transformed into *E. coli* SM10 cells and introduced into *L. monocytogenes* mutants via trans-conjugation. Complemented mutants were confirmed by antibiotic resistance and Sanger sequencing.

Knock-in of genes into *L. monocytogenes* was carried out using pPL2 and pPL2t integration plasmids (138, 188). Integration was confirmed by antibiotic resistance. The HyPer promoter used to generate over-expression vectors is a modified Pspac(hy) with a G-to-T mutation at the -1 position relative to the transcription start site (40, 189).

Fluorescent transcriptional reporters were engineered to express *gfp* constitutively from the HyPer promoter using the integrative plasmid pPL1 (13, 138). This was integrated into the chromosome of a phage-cured wt *L. monocytogenes* strain DP-L4056, or mutants phaged cured in this study (138). Next, the promoter regions of peroxidase genes were amplified and ligated to mTAG-RFP via NEBuilder HiFi DNA assembly. The mTAG-RFP was amplified from DP-L6508 (13). The promoter-*rfp* fusions were ligated into pPL2t and confirmed via PCR and Sanger sequencing. *E. coli* SM10 harboring the pPL2t.Promoter-*rfp* constructs were mated with MLR-L850 (pPL1.p*Hyper-gfp*) to generate the two-color transcriptional reporter strains. Integration was confirmed by antibiotic resistance and PCR.

Peroxidase mutants unable to escape from the vacuole were generated by transducing each mutant strain with a phage lysate produced in the *hly::himar1* background, as previously described (13). Briefly, U153 phage were mixed with the appropriate donor strain and incubated at 30 °C in LB soft agar overnight. Phage lysates were eluted from agar, filter-sterilized, and added to recipient strains for 30 minutes at room temperature. Transductions were plated on antibiotic containing agar and incubated at 37 °C. Insertions in *hly* were confirmed by PCR.

Generalized Transductions

Transducing lysates were prepared by mixing donor strain with U153 phage, as described previously (13). After overnight incubation at 30 °C in LB soft agar, phage were eluted from the agar, filter sterilized, and mixed with recipient *L. monocytogenes* (Δ*spxA1*) for 30 minutes at room temperature. Transductants were selected on antibiotic-containing agar at 37 °C anaerobically.

Phage Curing

In order to use the pPL1 construct, strains had to be phage cured (138). First *L. monocytogenes* 10403S strains with prophage comK-attBB' was grown in 5ml BHI at 37 ºC overnight. Next, *L. monocytogenes* were infected with phage U153 at MOI 20:1 in the presence of 5mM calcium chloride and incubated with shaking at 37 ºC for 75 min. Next, infected culture was diluted 1:100 and 1:10,000 in BHI, grown at 37 ºC until a 100-fold increase in OD600, and plated for viable colonies. Recovered colonies were then verified by PCR for excision of prophage.

L. monocytogenes strain construction

In-frame deletions were carried out by allelic exchange using a conjugation-proficient version of the suicide vector pKSV7 (190) or pLIM. We were not able to generate a pKSV7 construct to delete *kat* (catalase, *lmo2785*) which we hypothesize was due to toxicity of the neighboring gene in *E. coli*. Therefore, we simultaneously deleted both *kat* and the neighboring unannotated gene *lmo2784*. pKSV7.*kat-2784* was constructed by amplifying a 5' homologous region and a 3' homologous region, followed by synthesis by over-lapping extension (SOE) PCR to join the fragments together. This cassette was restriction-digested and ligated into pKSV7-oriT. A vector with the mutant Δ*kat-2784* allele was introduced into *L. monocytogenes* via trans-conjugation, integrated into the chromosome, colony-purified on selective nutrient-agar, and subsequently cured of the plasmid by conventional methods. Chromosomal mutations were confirmed by PCR and Sanger DNA sequencing when necessary. The resulting Δ*kat-2784* mutant was then complemented with pPL2.kat, pPL2.lmo2784, or pPL2.kat-2784 to ensure that the observed phenotypes were due to loss of *kat* and not *lmo2784.* We did not observe a role for *lmo2784* in aerobic growth or pathogenesis. Therefore, in this manuscript we have referred to Δ*kat-2784* pPL2.lmo2784 simply as '*Δkat*' and Δ*kat-2784* pPL2.kat-2784 as the complemented strain, for simplicity.

Knock-in of genes into *L. monocytogenes* was carried out using pPL2 and pPL2t integration plasmids (1, 2). Integration was confirmed by antibiotic resistance. The HyPer promoter used to generate over-expression vectors is a modified *Pspac*(hy) with a G-to-T mutation at the -1 position relative to the transcription start site (13, 189).

Fluorescent transcriptional reporters were engineered to express *gfp* constitutively from the HyPer promoter using the integrative plasmid pPL1 (13, 82). This was integrated into the chromosome of a phage-cured wt *L. monocytogenes* strain DP-L4056 (82). Next, the promoter regions of peroxidase genes were amplified and ligated to mTAG-RFP via NEBuilder HiFi DNA assembly. The mTAG-RFP was amplified from DP-L6508 (13). The promoter-*rfp* fusions were ligated into pPL2t and confirmed via PCR and Sanger sequencing. *E. coli* SM10 harboring the pPL2t.Promoter-*rfp* constructs were mated with MLR-L850 (pPL1.p*Hyper-gfp*) to generate the two-color transcriptional reporter strains. Integration was confirmed by antibiotic resistance and PCR.

Peroxidase mutants unable to escape from the vacuole were generated by transducing each mutant strain with a phage lysate produced in the *hly::himar1* background, as previously described (13). Briefly, U153 phage were mixed with the appropriate donor strain and incubated at 30 °C in LB soft agar overnight. Phage lysates were eluted from agar, filter-sterilized, and added to recipient strains for 30 minutes at room temperature. Transductions were plated on antibiotic containing agar and incubated at 37 °C. Insertions in *hly* were confirmed by PCR.

Whole genome sequencing

gDNA was isolated from overnight cultures using the Zymogene bacterial gDNA isolation kit and sent to MiGS , Microbial Sequencing and Analysis Center at University of Pittsburgh, for whole genome sequencing. All downstream processing and analysis was completed by MiGS using the NCBI *L. monocytogenes* 10403S reference genome.

Broth growth curves

For anaerobic growth, colonies were inoculated into broth and incubated at 37 °C in closed containers containing anaerobic gas-generating pouches (GasPak EZ; BD) or in an anaerobic chamber. In general, overnight cultures were normalized to OD_{600} 0.02 in 25 mL of rich broth in 250 mL flasks with shaking (250 rpm) for 24 hours. OD_{600} was measured every hour unless otherwise specified. For certain experiments, Δ*spxA1* bacterial cultures were plated 24 hours post-inoculation and incubated anaerobically to enumerate CFU.

In growth curves testing for the photochemical generation of peroxides (55), cultures were inoculated, and media was prepared in a biosafety hood in a windowless anteroom with all overhead lights turned off, severely limiting ambient light. TSB powder was dissolved in water in the dark and used within 24 hours of being made. TSB was treated with catalase (1 mg/mL) for two hours at room temperature and then filter-sterilized. Degassed TSB was incubated in an anaerobic chamber overnight before inoculation. To generate autoclaved catalase-treated TSB, a 1.5x solution of TSB without glucose was first mixed in the dark with 1 µg/mL catalase. Media was then filter-sterilized into tinfoil-wrapped bottles in the dark and left at 4° C overnight detoxify. Media was autoclaved to inactivate catalase 4 to12 hours before inoculation and mixed with a sterile solution of glucose in the dark to make 1x TSB immediately before inoculation.

To assess the response to acute peroxide toxicity, bacteria grown overnight in TSB at 37°C, shaking were back-diluted to OD_{600} = 0.1 and incubated for 2 hours to OD_{600} ~ 0.6. Hydrogen peroxide (120 mM, Sigma) was added and cultures were incubated with

shaking for 1 hour. At each time point, bacterial cultures were serially diluted and plated on BHI to enumerate CFU.

Intracellular growth curves

Primary BMDMs were seeded at a concentration of 6 x 10^5 cells per well in TC-treated 24-well plates the day before infection. BMDMs were activated by incubating the monolayer with recombinant murine IFNg (100 ng/mL, PeproTech) overnight and during infection. Overnight bacterial cultures were grown anaerobically in TSB or BHI(Δ*fri* aerobically) at 30°C statically, washed twice with PBS, and resuspended in warmed BMDM media (13). BMDMs were infected at an MOI of 0.1 for 30 minutes before cells were washed twice with PBS and then BMDM media containing gentamicin (50 μg/mL) was added to each well. For MDCKs and HMEC-1s, were seeded at a concentration of 2.5 x 10^5 cells per well in TC-treated 24-well plates the day before infection. Cells were infected at an MOI of 10 for 1 hour before cells were washed twice with PBS and then cell-specific media containing gentamicin (50 μg/mL) was added to each well. To measure bacterial growth, cells were washed twice with PBS and then lysed by incubating with 250 μL cold PBS with 0.1% Triton X-100 for 5 min at room temperature, followed by serial dilutions and plating on BHI agar to enumerate CFU. For the *phox*$^{-/-}$ growth curves all strains were incubated aerobically in TSB.

RNA isolation

Nucleic acids were purified from bacteria harvested from broth culture or from infected macrophages, as previously described (11, 191). Briefly, bacteria were grown

overnight anaerobically in BHI at 37 °C and sub-cultured 1:20 into BHI. After 4 hours of anaerobic growth at 37 °C, bacteria were mixed 1:1 with ice-cold methanol, pelleted, and stored at -80 °C. For infections, J774 cells were plated at a density of 2 x 10^7 cells in 150 mm TC-treated dishes and infected with an MOI of 20. After thirty minutes, the cells were washed twice with sterile PBS and media containing gentamicin was added. Eight hours post-infection, cells were washed with PBS and lysed by addition of ice-cold nuclease-free water. Cells were collected by scraping, vortexed quickly, and pelleted. The bacteria were harvested by filtering the supernatant and freezing the filter at -80 °C. RNA was then purified from the frozen bacterial samples via phenol-chloroform extraction and DNase treatment according to published methods (191).

RNA-seq

Ribosomal RNA was removed from broth sample total RNA using the Ribo-Zero rRNA Removal kit (Bacteria kit), according to manufacturer's recommendations (Illumina, Inc., San Diego, CA, USA). The Ribo-Zero Gold rRNA Removal Kit (Epidemiology kit) was used to deplete both bacterial and mammalian rRNA from samples of infected cells. Depleted samples were then analyzed by the Genomics & Bioinformatics Shared Resources at Fred Hutchinson Cancer Research Center. Ribosomal-depleted RNA integrity was confirmed using an Agilent 4200 TapeStation (Agilent Technologies, Inc., Santa Clara, CA) and quantified using a Trinean DropSense96 spectrophotometer (Caliper Life Sciences, Hopkinton, MA).

RNA-seq libraries were prepared from rRNA-depleted using the TruSeq RNA Sample Prep Kit v2, omitting the poly-A selection step, (Illumina, Inc.) and a Sciclone

NGSx Workstation (PerkinElmer, Waltham, MA, USA). Library size distributions were validated using an Agilent 4200 TapeStation. Additional library QC, blending of pooled indexed libraries, and cluster optimization were performed using Life Technologies' Invitrogen Qubit® 2.0 Fluorometer (Life Technologies-Invitrogen, Carlsbad, CA, USA). RNA-seq libraries were pooled (10-plex) and clustered onto a flow cell lane. Sequencing was performed using an Illumina HiSeq 2500 in rapid mode employing a paired-end, 50 base read length (PE50) sequencing strategy. Image analysis and base calling were performed using Illumina's Real Time Analysis v1.18 software, followed by 'demultiplexing' of indexed reads and generation of FASTQ files, using Illumina's bcl2fastq Conversion Software v1.8.4.

Reads of low quality were filtered prior to alignment to the reference genome (*Listeria monocytogenes* 10403S) using TopHat v2.1.0 (166). Counts were generated from TopHat alignments for each gene using the Python package HTSeq v0.6.1. Genes with low counts across all samples were removed, prior to identification of differentially expressed genes using the Bioconductor package edgeR v3.12.1. A false discovery rate (FDR) method was employed to correct for multiple testing, with differential expression defined as $|\log_2 (\text{ratio})| \geq 1$ (± 2-fold) with the FDR set to 5%. Results were then evaluated using CLC Genomics Workbench (Qiagen) and transcripts that were changed >2-fold ($P < 0.001$) were included in our analysis.

Quantitative RT-PCR of bacterial transcripts

Bacteria grown anaerobically overnight in degassed TSB or BHI were normalized to OD_{600} = 0.02 in 50 mL media in 500 mL flasks and incubated at 37°C in the dark, with

shaking. At each time point, 5-7 mL of bacterial culture were removed, mixed with ice-cold methanol (1:1), pelleted by centrifugation, flash frozen, and stored at -80°C. Nucleic acids were harvested as previously described using phenol:chloroform extraction and bead beating. RNA was precipitated overnight, washed in ethanol, and RT-PCR was performed with iScript Reverse Transcriptase (Bio-Rad). Quantitative PCR was performed with iTaq Universal SYBR Green Supermix (Bio-Rad) according to manufacturers' recommendations. Transcripts were normalized to that of 16S rRNA and fold-change was calculated using the comparative C_T method.

Infections and flow cytometry

J774 cells were plated in 12-well TC-treated dishes at 10^6 cells per well. Generally, *L. monocytogenes* transcriptional reporter strains were grown to mid-log phase at 37°C with shaking. After being washed twice and resuspended in PBS, bacterial suspensions were added to the cells at an MOI=10. One hour post-infection, cells were washed twice with PBS and media containing gentamicin (50 μg/mL) was added to each well. 4 or 7 hours post-infection the cells were washed twice with PBS, treated with 0.25% trypsin (Gibco), and resuspended in an equal volume of media. The cells were then fixed with 2% formaldehyde, washed twice with flow buffer (PBS containing 5% FBS), and resuspended in 300 μL flow buffer. Flow cytometry was performed on an LSRII flow cytometer (BD) and analyzed using FlowJo (FlowJo, LLC). Cells were discriminated from debris by forward scatter area (FSC-A) and side scatter area (SSC-A). Single cells were gated using FSC-A and forward scatter height (FSC-H).

Plaque assays

Plaque assays were performed as previously described (26). Briefly, TC-treated 6-well dishes were seeded with 1.2 x 10^6 L2 murine fibroblasts per well. *L. monocytogenes* strains were incubated in BHI overnight at 30°C, static. Overnight cultures were diluted 1:10 in sterile PBS, and 5-10 µL was used to infect each well. One hour post-infection, cells were washed twice with PBS and 3 mL of molten agarose-DMEM solution was added to each well. This solution consisted of a 1:1 mixture of 2X DMEM (Gibco) and 1.4% SuperPure agarose LE (U.S. Biotech Sources, LLC) containing gentamicin (10 µg/mL). Three days post-infection, 2 mL of molten agarose-DMEM solution containing neutral red was added to each well to visualize plaques. After 24 hours, the plates were scanned, and the plaque areas measured using ImageJ software (167). The area of at least 20 plaques was measured for each strain and normalized to that of wt.

Motility assays

A degassed BHI 0.4% agar plate was inoculated via stab with a single colony from each strain. Plates were then incubated at the designated temperature for 4 days in anaerobic chamber?. Motility was determined by the measuring the diameter of observed bacterial spread through the agar.

Immunofluorescence microscopy

To visualize intracellular bacteria, L2 fibroblasts were seeded at 1.5 x 10^6 cells per well in 6-well tissue culture-treated plates containing collagen-coated glass coverslips (Thermo Fisher Scientific) and inoculated with *L. monocytogenes* the next day at an MOI

of 50. Bacterial cultures were grown overnight in anaerobic BHI at 37°C and washed twice in PBS prior to inoculation. One hour post-infection, monolayers were washed twice with PBS and media containing 30 μg/ mL gentamicin was added to kill extracellular bacteria. 10 hours post infection, coverslips were washed twice with PBS, fixed for 10 minutes in 4% formaldehyde (Pierce), washed in TBS-Tx (0.1% Triton, 50 mM Tris pH 7.6, 150 mM NaCl), and incubated in antibody buffer (TBS-Tx, 1% BSA) at 4°C overnight. Coverslips were then incubated for 30 minutes with rabbit anti-Listeria O antigen antiserum (Difco) at a concentration of 1:100 in antibody buffer and washed in TBS-Tx followed by a secondary incubation with a 1:200 solution of goat anti-rabbit-Alexa488 (Life Tech) in antibody buffer and Alexa555-Phalloidin (Life Tech) at a concentration of 1:1000. After immunolabeling and washing in TBS-Tx a final time, coverslips were attached to glass slides with ProLong Anti-fade Diamond with DAPI, (Life Tech), left to cure at room temperature overnight, and imaged with a 100x objective.

For fluorescence microscopy of extracellular bacteria, overnight cultures of selected strains were diluted in BHI to an OD_{600} of 0.02 and grown for 2 hours to early exponential phase (OD ~0.2) in an anaerobic chamber at 37°C. Prior to staining, 1 mL of culture was pelleted at 10,000 x *g* for 1 minute in a tabletop centrifuge and resuspended in PBS which halts further bacterial growth and cell death (36). To label cell membranes, cultures were incubated with 20 μg/mL membrane intercalating agent TMA-DPH for 10 minutes in the dark and then washed twice in PBS prior to spotting on PBS-agar pads. To visualize membrane integrity and viability of bacterial cells, cultures were mixed with 5 μg/mL propidium iodide solution, incubated in the dark for 15 minutes, and then spotted immediately onto agar pads.

All imaging was performed using a Keyence BZ-X710 All-in-one Fluorescence Microscope with either a 40x objective or 100x oil immersion objective and corresponding filter cubes (Keyence). Phase contrast images were taken using bright field settings. Propidium iodide and mCherry were detected using BZ-X Filter TexasRed. TMA-DPH was detected using BZ-X Filter DAPI. GFP and Alexa488 were detected using BZ-X Filter GFP.

Quantitative analysis of bacterial morphology using Celltool

Phase contrast and fluorescence microscopy was performed on *L. monocytogenes* grown anaerobically shaking in BHI and then resuspended in PBS. Culture resuspensions were immediately spotted on PBS-2% agarose pads, sealed under a glass coverslip and imaged. All quantified images were taken using the 40x objective. Fluorescence images were generated in the appropriate channel for each fluorescent label as specified per experiment. At least 10 fields of view were imaged such that at least 1,000 cells could be analyzed per biological replicate per sample. Binary masks were uniformly applied to each field of view using the MATLAB imbinarize function. Quantitative analysis of binarized images was performed using the Celltool software package (125). Image contours were extracted using the extract_contours functions and smoothed via interpolation to polygons with 100 evenly placed vertices. Fluorescence intensities of labeled bacteria were measured using the extract_images function which specifically extracts intensity per area of fluorescence microscopy images based on contours previously generated from phase contrast images. The measure_contours function was used for the final generation of data output. Perimeter length of contours was used as the

primary metric for analysis to account for curved and irregular morphologies. Unpaired t-tests were used to measure the difference in perimeter length distributions between populations of bacteria. Percent of elongated cells was calculated by measuring the number of cell perimeters in a population which were greater than one SD above the wt mean for each corresponding replicate and time point. SEM and means were displayed for three biological replicates of percent-elongation analysis.

Scanning Transmission Electron Microscopy

The appropriate strains were grown to early exponential phase anaerobically in 400 mL BHI. Cultures were centrifuged for 10 minutes at 4,500 RPM, and pellets were washed once in 1M PBS. Pellets of approximately 100 µL volume were mixed with an equal volume of fixative buffer consisting of 4% mass spectrometry grade paraformaldehyde and 0.1 M sodium cacodylate. After 30 minutes, cells were pelleted and mixed with equal volumes fresh fixative buffer for 1 hour at room temperature. Samples were then rinsed with 0.1 M sodium cacodylate buffer, post-fixed in osmium tetroxide buffered with 0.1 M sodium cacodylate for 2 hours, and then washed to remove osmium tetroxide. Samples were then progressively dehydrated with increasing concentrations of ethanol (50%, 70%, 90%, 100%), and twice with 100% acetone. Bacteria were then embedded in 50:50 acetone:resin (Epon) and incubated rotating for 4 hours. Incubation was next performed using 20:80 acetone:resin. After drying for 2 hours, samples were placed in a 100% resin gelatin capsule under light vacuum for 2 hours. Finally, samples were placed in fresh resin molds and incubated at 60°C overnight. Resin blocks were sectioned at 80 nm using a Leica Ultracut 6 Microtome and stained using

uranyl acetate and Reynolds lead citrate stains. Samples were imaged with an FEI Tecnai G2 F20 Twin transmission electron microscope at 200 kV.

Whole-cell proteomics

Protein isolation was performed as previously described (49). *L. monocytogenes* were grown anaerobically in BHI for 2 hrs. Bacteria were pelleted, washed once in PBS, and immediately flash frozen. Bacterial pellets were resuspended in lysis buffer containing 8M urea and lysed by sonification. Proteins in lysates were reduced via incubation with DTT and alkylated via incubation with iodoacetamide. After quantification of protein concentration via BCA, 300 µg of protein per sample were treated with Trypsin Gold (Promega) overnight. The pH was adjusted to pH 2 using trifluoroacetic acid and then proteins were purified using C18-300 peptide purification columns per manufacturer instructions (Nest Group). After elution, peptides were dried and resuspended in 0.1% formic acid. Autosampler vials were loaded with 100 µL sample at a concentration of 0.5 µg/mL. Mass spectrometry was performed on each sample using an Orbitrap Eclipse Mass Spectrometer (Thermo-Scientific) and liquid chromatography was performed using the Easy-nLC 1000 Liquid Chromatograph (Thermo-Scientific). Raw spectral data was processed using the MaxQuant suite of software with default settings and peptide sequences were searched against the *L. monocytogenes* 10403S reference proteome (UniProt).

The relative abundance of proteins was determined using the LFQ intensity metric generated by analysis with the MaxLFQ algorithm, a generic label-free quantification technology available in MaxQuant (193, 194). The LFQ intensity metric was chosen as it

does not depend on normalization with housekeeping proteins for accurate abundance prediction sample-to-sample, relying instead on the assumption that most proteins are minimally changed between experimental conditions. Furthermore, LFQ intensities are the result of calculations using the maximum possible information extracted from samples and retain the absolute scale of original peptide intensities, giving a highly accurate proxy for absolute protein abundance (193). Proteins changed in abundance between wt and Δ*spxA1* were considered for further analysis if they met the following criteria: 1. Proteins differed in average abundance between wt and Δ*spxA1* by at least 2-fold. 2. An unpaired t-test comparing the LFQ intensities of three wt and Δ*spxA1* biological replicates yielded a P-value less than 0.05. To increase the stringency of our hit identification and reduce possible false positives, protein abundance calculations were based on the identification of at least 5 peptides per protein in the sample with higher abundance.

Measuring phagocytosis via gentamicin protection assay and microscopy

Gentamicin protection assays were performed as previously described (141). Immortalized murine bone marrow-derived macrophages (iBMMs), primary macrophages, and J774 phagocytes were seeded in 24-well plates at a density of 6 x 10^5 cells per well. The next day, overnight anaerobic cultures were washed twice with sterile PBS. Macrophages were infected with an MOI of 10 and the inocula were serially diluted and plated on BHI-strep agar to enumerate CFU. For MDCKs and HMEC-1s, were seeded at a concentration of 2.5 x 10^5 cells per well in TC-treated 24-well plates the day before infection. Cells were infected at an MOI of 50 for 1 hour before cells were washed twice with PBS and then cell-specific media containing gentamicin (50 μg/mL). To force

bacteria to the cell surface, select 6-well plates were then centrifuged at 300 x g for 2 minutes after inoculation. After 30 minutes or 1 hour, monolayers were washed twice in sterile PBS. New media with 30 μg/mL gentamicin was added for 30 min to eliminate any extracellular bacteria and then monolayers were washed twice and lysed in 250 μL cold 0.1% Triton X-100 in PBS. Lysates were serially diluted and plated on BHI-strep agar to enumerate CFU. Percent uptake was calculated by dividing the number of bacteria recovered from each well by the starting inoculum CFU.

To image uptake of bacteria, iBMMs were seeded in 24-well plates containing ethanol-sterilized glass coverslips at a density of 6 x 10^5 cells per well. Overnight anaerobic cultures were washed twice with sterile PBS. Macrophages were infected with mCherry-expressing bacteria at an MOI of 10 and centrifuged for 2 minutes at 300 x g to normalize strain contact with the monolayer. Infections were incubated for 15 minutes and then washed twice in sterile PBS. Coverslips were removed and fixed for 10 minutes in 4% formaldehyde (Pierce), washed in PBS, and blocked in PBS with 1% BSA at 4°C overnight. PBS replaced TBST-Tx for all buffers used to prevent the permeabilization and immunolabel infiltration of host cells. Thus, only extracellular bacteria were labeled. Coverslips where then incubated successively with the described immunostaining agents diluted in PBS with 1% BSA, with PBS washes between incubations: 1:20 Fc Block (BD), 1:100 rabbit anti-*Listeria* O antigen antiserum (Difco), 1:200 goat anti-rabbit-Alexa488 (Life Tech). After washing with PBS a final time, coverslips were attached to glass slides with ProLong Anti-fade Diamond, (Life Tech), left to cure at room temperature overnight, and imaged with a 100x objective. Celltool was used to extract contours from mCherry images (125). Cells were determined to be extracellular based on the intensity of

fluorescence extracted from GFP images within the same area as Celltool-derived contours.

Chapter 7: Referenced Literature

1. Freitag NE, Port GC, Miner MD. 2009. *Listeria monocytogenes* - from saprophyte to intracellular pathogen. Nat Rev Microbiol 7:623–628.

2. Gray ML, Killinger AH. 1966. *Listeria monocytogenes* and listeric infections. Bacteriol Rev 30:309–382.

3. Murray EGD, Webb RA, Swann MBR. 1926. A disease of rabbits characterised by a large mononuclear leucocytosis, caused by a hitherto undescribed bacillus *Bacterium monocytogenes* (n.sp.). J Pathol Bacteriol 29:407–439.

4. Todd ECD, Notermans S. 2011. Surveillance of listeriosis and its causative pathogen, *Listeria monocytogenes*. Food Control 22:1484–1490.

5. McLauchlin J, Mitchell RT, Smerdon WJ, Jewell K. 2004. *Listeria monocytogenes* and listeriosis: a review of hazard characterisation for use in microbiological risk assessment of foods. Int J Food Microbiol 92:15–33.

6. Allerberger F, Wagner M. 2010. Listeriosis: a resurgent foodborne infection. Clin Microbiol Infect 16:16–23.

7. Charlier C, Perrodeau É, Leclercq A, Cazenave B, Pilmis B, Henry B, Lopes A, Maury MM, Moura A, Goffinet F, Dieye HB, Thouvenot P, Ungeheuer M-N, Tourdjman M, Goulet V, de Valk H, Lortholary O, Ravaud P, Lecuit M, Hausfater P, Pourriat J-L, Casalino E, Riou B, Pateron D, Yéni P, Bricaire F, Ville Y, Azria E, Dommergues M, Bergmann J-F, Wolff M, Mira J-P, Guillevin L, Zuber M … Zumbo C. 2017. Clinical features and prognostic factors of listeriosis: the MONALISA national prospective cohort study. Lancet Infect Dis 17:510–519.

8. Tack DM. 2020. Preliminary Incidence and Trends of Infections with Pathogens Transmitted Commonly Through Food — Foodborne Diseases Active Surveillance Network, 10 U.S. Sites, 2016–2019. MMWR Morb Mortal Wkly Rep 69.

9. Myers JT, Tsang AW, Swanson JA. 2003. Localized Reactive Oxygen and Nitrogen Intermediates Inhibit Escape of *Listeria monocytogenes* from Vacuoles in Activated Macrophages. J Immunol 171:5447–5453.

10. Tilney LG, Portnoy DA. 1989. Actin filaments and the growth, movement, and spread of the intracellular bacterial parasite, *Listeria monocytogenes*. J Cell Biol 109:1597–1608.

11. Reniere ML, Whiteley AT, Hamilton KL, John SM, Lauer P, Brennan RG, Portnoy DA. 2015. Glutathione activates virulence gene expression of an intracellular pathogen. Nature 517:170–173.

12. Reniere ML. 2018. Reduce, Induce, Thrive: Bacterial Redox Sensing during Pathogenesis. J Bacteriol 200:e00128-18.

13. Reniere ML, Whiteley AT, Portnoy DA. 2016. An In Vivo Selection Identifies *Listeria monocytogenes* Genes Required to Sense the Intracellular Environment and Activate Virulence Factor Expression. PLOS Pathog 12:e1005741.

14. de las Heras A, Cain RJ, Bielecka MK, Vázquez-Boland JA. 2011. Regulation of *Listeria* virulence: PrfA master and commander. Curr Opin Microbiol 14:118–127.

15. Marr AK, Joseph B, Mertins S, Ecke R, Müller-Altrock S, Goebel W. 2006. Overexpression of PrfA Leads to Growth Inhibition of *Listeria monocytogenes* in Glucose-Containing Culture Media by Interfering with Glucose Uptake. J Bacteriol 188:3887–3901.

16. Ripio MT, Domínguez-Bernal G, Lara M, Suárez M, Vazquez-Boland JA. 1997. A Gly145Ser substitution in the transcriptional activator PrfA causes constitutive overexpression of virulence factors in *Listeria monocytogenes*. J Bacteriol 179:1533–1540.

17. Ruhland BR, Reniere ML. 2019. Sense and sensor ability: redox-responsive regulators in *Listeria monocytogenes*. Curr Opin Microbiol 47:20–25.

18. Bonazzi M, Lecuit M, Cossart P. 2009. *Listeria monocytogenes* Internalin and E-cadherin: From Bench to Bedside. Cold Spring Harb Perspect Biol 1:a003087.

19. Hamon M, Bierne H, Cossart P. 2006. *Listeria monocytogenes*: a multifaceted model. Nat Rev Microbiol 4:423–434.

20. Travier L, Lecuit M. 2014. *Listeria monocytogenes* ActA: a new function for a 'classic' virulence factor. Curr Opin Microbiol 17:53–60.

21. Freitag NE, Jacobs KE. 1999. Examination of *Listeria monocytogenes* intracellular gene expression by using the green fluorescent protein of Aequorea victoria. Infect Immun 67:1844–1852.

22. Bernheim-Groswasser A, Wiesner S, Golsteyn RM, Carlier M-F, Sykes C. 2002. The dynamics of actin-based motility depend on surface parameters. 6886. Nature 417:308–311.

23. Cameron LA, Robbins JR, Footer MJ, Theriot JA. 2004. Biophysical Parameters Influence Actin-based Movement, Trajectory, and Initiation in a Cell-free System. Mol Biol Cell 15:2312–2323.

24. Dabiri GA, Sanger JM, Portnoy DA, Southwick FS. 1990. *Listeria monocytogenes* moves rapidly through the host-cell cytoplasm by inducing directional actin assembly. Proc Natl Acad Sci 87:6068–6072.

25. Khademian M, Imlay JA. 2020. How Microbes Evolved to Tolerate Oxygen. Trends Microbiol 0.

26. Imlay JA. 2019. Where in the world do bacteria experience oxidative stress? Environ Microbiol 21:521–530.

27. Korshunov S, Imlay JA. 2006. Detection and quantification of superoxide formed within the periplasm of *Escherichia coli*. J Bacteriol 188:6326–6334.

28. Li X, Imlay JA. 2018. Improved measurements of scant hydrogen peroxide enable experiments that define its threshold of toxicity for *Escherichia coli.* Free Radic Biol Med 120:217–227.

29. Keyer K, Imlay JA. 1996. Superoxide accelerates DNA damage by elevating free-iron levels. Proc Natl Acad Sci U S A 93:13635–13640.

30. Winterbourn CC, Kettle AJ. 2013. Redox reactions and microbial killing in the neutrophil phagosome. Antioxid Redox Signal 18:642–660.

31. Nauseef WM, Clark RA. 2019. Intersecting Stories of the Phagocyte NADPH Oxidase and Chronic Granulomatous Disease. Methods Mol Biol Clifton NJ 1982:3–16.

32. Dinauer MC. 2005. Chronic granulomatous disease and other disorders of phagocyte function. Hematol Am Soc Hematol Educ Program 89–95.

33. van den Berg JM, van Koppen E, Ahlin A, Belohradsky BH, Bernatowska E, Corbeel L, Español T, Fischer A, Kurenko-Deptuch M, Mouy R, Petropoulou T, Roesler J, Seger R, Stasia M-J, Valerius NH, Weening RS, Wolach B, Roos D, Kuijpers TW. 2009. Chronic granulomatous disease: the European experience. PloS One 4:e5234.

34. Zuber P. 2004. Spx-RNA polymerase interaction and global transcriptional control during oxidative stress. J Bacteriol 186:1911–1918.

35. Zuber P. 2009. Management of oxidative stress in *Bacillus*. Annu Rev Microbiol 63:575–597.

36. Whiteley AT, Ruhland BR, Edrozo MB, Reniere ML. 2017. A Redox-Responsive Transcription Factor Is Critical for Pathogenesis and Aerobic Growth of *Listeria monocytogenes*. Infect Immun 85.

37. Pamp SJ, Frees D, Engelmann S, Hecker M, Ingmer H. 2006. Spx Is a Global Effector Impacting Stress Tolerance and Biofilm Formation in *Staphylococcus aureus.* J Bacteriol 188:4861–4870.

38. Chen L, Ge X, Wang X, Patel JR, Xu P. 2012. SpxA1 Involved in Hydrogen Peroxide Production, Stress Tolerance and Endocarditis Virulence in *Streptococcus sanguinis.* PLOS ONE 7:e40034.

39. Nakano S, Küster-Schöck E, Grossman AD, Zuber P. 2003. Spx-dependent global transcriptional control is induced by thiol-specific oxidative stress in *Bacillus subtilis*. Proc Natl Acad Sci 100:13603–13608.

40. Kajfasz JK, Rivera-Ramos I, Abranches J, Martinez AR, Rosalen PL, Derr AM, Quivey RG, Lemos JA. 2010. Two Spx proteins modulate stress tolerance, survival, and virulence in *Streptococcus mutans*. J Bacteriol 192:2546–2556.

41. Kajfasz JK, Mendoza JE, Gaca AO, Miller JH, Koselny KA, Giambiagi-Demarval M, Wellington M, Abranches J, Lemos JA. 2012. The Spx regulator modulates stress responses and virulence in *Enterococcus faecalis.* Infect Immun 80:2265–2275.

42. Rochat T, Nicolas P, Delumeau O, Rabatinová A, Korelusová J, Leduc A, Bessières P, Dervyn E, Krásny L, Noirot P. 2012. Genome-wide identification of genes directly regulated by the pleiotropic transcription factor Spx in *Bacillus subtilis*. Nucleic Acids Res 40:9571–9583.

43. Newberry KJ, Nakano S, Zuber P, Brennan RG. 2005. Crystal structure of the *Bacillus subtilis* anti-alpha, global transcriptional regulator, Spx, in complex with the α C-terminal domain of RNA polymerase. Proc Natl Acad Sci 102:15839–15844.

44. Borezee E, Msadek T, Durant L, Berche P. 2000. Identification in *Listeria monocytogenes* of MecA, a homologue of the *Bacillus subtilis* competence regulatory protein. J Bacteriol 182:5931–5934.

45. Larsson JT, Rogstam A, Von Wachenfeldt C. 2007. YjbH is a novel negative effector of the disulphide stress regulator, Spx, in *Bacillus subtilis*. Mol Microbiol 66:669–684.

46. Chan CM, Garg S, Lin AA, Zuber P. 2012. Geobacillus thermodenitrificans YjbH recognizes the C-terminal end of *Bacillus subtilis* Spx to accelerate Spx proteolysis by ClpXP. Microbiol Read Engl 158:1268–1278.

47. Garg SK, Kommineni S, Henslee L, Zhang Y, Zuber P. 2009. The YjbH protein of *Bacillus subtilis* enhances ClpXP-catalyzed proteolysis of Spx. J Bacteriol 191:1268–1277.

48. Engman J, von Wachenfeldt C. 2015. Regulated protein aggregation: a mechanism to control the activity of the ClpXP adaptor protein YjbH. Mol Microbiol 95:51–63.

49. Ruhland BR, Reniere ML. 2020. YjbH Requires Its Thioredoxin Active Motif for the Nitrosative Stress Response, Cell-to-Cell Spread, and Protein-Protein Interactions in *Listeria monocytogenes*. J Bacteriol 202:e00099-20.

50. Imlay JA. 2008. Cellular defenses against superoxide and hydrogen peroxide. Annu Rev Biochem 77:755–776.

51. Wurtzel O, Sesto N, Mellin JR, Karunker I, Edelheit S, Bécavin C, Archambaud C, Cossart P, Sorek R. 2012. Comparative transcriptomics of pathogenic and non-pathogenic *Listeria* species. Mol Syst Biol 8:583.

52. Reyes DY, Zuber P. 2008. Activation of transcription initiation by Spx: formation of transcription complex and identification of a Cis-acting element required for transcriptional activation. Mol Microbiol 69:765–779.

53. Lin AA, Walthers D, Zuber P. 2013. Residue Substitutions Near the Redox Center of *Bacillus subtilis* Spx Affect RNA Polymerase Interaction, Redox Control, and Spx-DNA Contact at a Conserved cis-Acting Element. J Bacteriol 195:3967–3978.

54. Lauer P, Chow MYN, Loessner MJ, Portnoy DA, Calendar R. 2002. Construction, characterization, and use of two *Listeria monocytogenes* site-specific phage integration vectors. J Bacteriol 184:4177–4186.

55. Sun AN, Camilli A, Portnoy DA. 1990. Isolation of *Listeria monocytogenes* small-plaque mutants defective for intracellular growth and cell-to-cell spread. Infect Immun 58:3770–3778.

56. Dailey HA, Dailey TA, Gerdes S, Jahn D, Jahn M, O'Brian MR, Warren MJ. 2017. Prokaryotic Heme Biosynthesis: Multiple Pathways to a Common Essential Product. Microbiol Mol Biol Rev MMBR 81:e00048-16.

57. Reniere ML, Torres VJ, Skaar EP. 2007. Intracellular metalloporphyrin metabolism in *Staphylococcus aureus.* BioMetals 20:333.

58. Anzaldi LL, Skaar EP. 2010. Overcoming the Heme Paradox: Heme Toxicity and Tolerance in Bacterial Pathogens. Infect Immun 78:4977–4989.

59. Wakeman CA, Hammer ND, Stauff DL, Attia AS, Anzaldi LL, Dikalov SI, Calcutt MW, Skaar EP. 2012. Menaquinone biosynthesis potentiates haem toxicity in *Staphylococcus aureus.* Mol Microbiol 86:1376–1392.

60. Corbett D, Goldrick M, Fernandes VE, Davidge K, Poole RK, Andrew PW, Cavet J, Roberts IS. 2017. *Listeria monocytogenes* Has Both Cytochrome bd-Type and Cytochrome aa3-Type Terminal Oxidases, Which Allow Growth at Different Oxygen Levels, and Both Are Important in Infection. Infect Immun 85.

61. Proctor RA, von Eiff C, Kahl BC, Becker K, McNamara P, Herrmann M, Peters G. 2006. Small colony variants: a pathogenic form of bacteria that facilitates persistent and recurrent infections. Nat Rev Microbiol 4:295–305.

62. Rea R, Hill C, Gahan CGM. 2005. *Listeria monocytogenes* PerR Mutants Display a Small-Colony Phenotype, Increased Sensitivity to Hydrogen Peroxide, and Significantly Reduced Murine Virulence. Appl Environ Microbiol 71:8314–8322.

63. Gaballa A, Antelmann H, Hamilton CJ, Helmann JDY 2013. Regulation of *Bacillus subtilis* bacillithiol biosynthesis operons by Spx. Microbiology 159:2025–2035.

64. Choby JE, Skaar EP. 2016. Heme Synthesis and Acquisition in Bacterial Pathogens. J Mol Biol 428:3408–3428.

65. Huycke MM, Moore D, Joyce W, Wise P, Shepard L, Kotake Y, Gilmore MS. 2001. Extracellular superoxide production by Enterococcus faecalis requires demethylmenaquinone and is attenuated by functional terminal quinol oxidases. Mol Microbiol 42:729–740.

66. Mishra S, Imlay J. 2012. Why do bacteria use so many enzymes to scavenge hydrogen peroxide? Arch Biochem Biophys 525:145–160.

67. Leblond-Francillard M, Gaillard JL, Berche P. 1989. Loss of catalase activity in Tn1545-induced mutants does not reduce growth of *Listeria monocytogenes* in vivo. Infect Immun 57:2569–2573.

68. Azizoglu RO, Kathariou S. 2010. Temperature-Dependent Requirement for Catalase in Aerobic Growth of *Listeria monocytogenes* F2365. Appl Environ Microbiol 76:6998–7003.

69. Cepeda JA, Millar M, Sheridan EA, Warwick S, Raftery M, Bean DC, Wareham DW. 2006. Listeriosis due to infection with a catalase-negative strain of *Listeria monocytogenes*. J Clin Microbiol 44:1917–1918.

70. Nakano S, Erwin KN, Ralle M, Zuber P. 2005. Redox-sensitive transcriptional control by a thiol/disulphide switch in the global regulator, Spx. Mol Microbiol 55:498–510.

71. Park S, You X, Imlay JA. 2005. Substantial DNA damage from submicromolar intracellular hydrogen peroxide detected in Hpx- mutants of *Escherichia coli.* Proc Natl Acad Sci U S A 102:9317–9322.

72. Mains DR, Eallonardo SJ, Freitag NE. 2021. Identification of *Listeria monocytogenes* genes contributing to oxidative stress resistance under conditions relevant to host infection. Infect Immun https://doi.org/10.1128/IAI.00700-20.

73. Cesinger MR, Thomason MK, Edrozo MB, Halsey CR, Reniere ML. 2020. *Listeria monocytogenes* SpxA1 is a global regulator required to activate genes encoding catalase and heme biosynthesis enzymes for aerobic growth. Mol Microbiol 114:230–243.

74. Savelli B, Li Q, Webber M, Jemmat AM, Robitaille A, Zamocky M, Mathé C, Dunand C. 2019. RedoxiBase: A database for ROS homeostasis regulated proteins. Redox Biol 26:101247.

75. Olsen KN, Larsen MH, Gahan CGM, Kallipolitis B, Wolf XA, Rea R, Hill C, Ingmer H. 2005. The Dps-like protein Fri of *Listeria monocytogenes* promotes stress tolerance and intracellular multiplication in macrophage-like cells. Microbiol Read Engl 151:925–933.

76. Dussurget O, Dumas E, Archambaud C, Chafsey I, Chambon C, Hébraud M, Cossart P. 2005. *Listeria monocytogenes* ferritin protects against multiple stresses and is required for virulence. FEMS Microbiol Lett 250:253–261.

77. Leblond-Francillard M, Gaillard JL, Berche P. 1989. Loss of catalase activity in Tn1545-induced mutants does not reduce growth of *Listeria monocytogenes* in vivo. Infect Immun 57:2569–2573.

78. Dons LE, Mosa A, Rottenberg ME, Rosenkrantz JT, Kristensson K, Olsen JE. 2014. Role of the *Listeria monocytogenes* 2-Cys peroxiredoxin homologue in protection against oxidative and nitrosative stress and in virulence. Pathog Dis 70:70–74.

79. Kim K-P, Hahm B-K, Bhunia AK. 2007. The 2-cys peroxiredoxin-deficient *Listeria monocytogenes* displays impaired growth and survival in the presence of hydrogen peroxide in vitro but not in mouse organs. Curr Microbiol 54:382–387.

80. Milazzo L, Hofbauer S, Howes BD, Gabler T, Furtmüller PG, Obinger C, Smulevich G. 2018. Insights into the Active Site of Coproheme Decarboxylase from *Listeria monocytogenes*. Biochemistry 57:2044–2057.

81. Cosgrove K, Coutts G, Jonsson I-M, Tarkowski A, Kokai-Kun JF, Mond JJ, Foster SJ. 2007. Catalase (KatA) and Alkyl Hydroperoxide Reductase (AhpC) Have Compensatory Roles in Peroxide Stress Resistance and Are Required for Survival, Persistence, and Nasal Colonization in *Staphylococcus aureus.* J Bacteriol 189:1025–1035.

82. Lauer P, Chow MYN, Loessner MJ, Portnoy DA, Calendar R. 2002. Construction, characterization, and use of two *Listeria monocytogenes* site-specific phage integration vectors. 184:4177–4186.

83. Collins B, Curtis N, Cotter PD, Hill C, Ross RP. 2010. The ABC transporter AnrAB contributes to the innate resistance of *Listeria monocytogenes* to nisin, bacitracin, and various beta-lactam antibiotics. Antimicrob Agents Chemother 54:4416–4423.

84. Torres VJ, Stauff DL, Pishchany G, Bezbradica JS, Gordy LE, Iturregui J, Anderson KL, Dunman PM, Joyce S, Skaar EP. 2007. A *Staphylococcus aureus* regulatory system that responds to host heme and modulates virulence. Cell Host Microbe 1:109–119.

85. Herskovits AA, Auerbuch V, Portnoy DA. 2007. Bacterial ligands generated in a phagosome are targets of the cytosolic innate immune system. PLoS Pathog 3:e51.

86. Dinauer MC. 2005. Chronic granulomatous disease and other disorders of phagocyte function. Hematol Educ Program Am Soc Hematol Am Soc Hematol Educ Program 2005:89–95.

87. Sun AN, Camilli A, Portnoy DA. 1990. Isolation of *Listeria monocytogenes* small-plaque mutants defective for intracellular growth and cell-to-cell spread. Infect Immun 58:3770–3778.

88. Bsat N, Chen L, Helmann JD. 1996. Mutation of the *Bacillus subtilis* alkyl hydroperoxide reductase (ahpCF) operon reveals compensatory interactions among hydrogen peroxide stress genes. J Bacteriol 178:6579–6586.

89. Chen L, Keramati L, Helmann JD. 1995. Coordinate regulation of *Bacillus subtilis* peroxide stress genes by hydrogen peroxide and metal ions. Proc Natl Acad Sci 92:8190–8194.

90. Seaver LC, Imlay JA. 2001. Alkyl hydroperoxide reductase is the primary scavenger of endogenous hydrogen peroxide in *Escherichia coli.* J Bacteriol 183:7173–7181.

91. Broden NJ, Flury S, King AN, Schroeder BW, Coe GD, Faulkner MJ. 2016. Insights into the Function of a Second, Nonclassical Ahp Peroxidase, AhpA, in Oxidative Stress Resistance in *Bacillus subtilis*. J Bacteriol 198:1044–1057.

92. Su M, Cavallo S, Stefanini S, Chiancone E, Chasteen ND. 2005. The So-Called *Listeria innocua* Ferritin Is a Dps Protein. Iron Incorporation, Detoxification, and DNA Protection Properties. Biochemistry 44:5572–5578.

93. Bozzi M, Mignogna G, Stefanini S, Barra D, Longhi C, Valenti P, Chiancone E. 1997. A novel non-heme iron-binding ferritin related to the DNA-binding proteins of the Dps family in *Listeria innocua*. J Biol Chem 272:3259–3265.

94. Hébraud M, Guzzo J. 2000. The main cold shock protein of *Listeria monocytogenes* belongs to the family of ferritin-like proteins. FEMS Microbiol Lett 190:29–34.

95. Mohamed W, Darji A, Domann E, Chiancone E, Chakraborty T. 2006. The ferritin-like protein Frm is a target for the humoral immune response to *Listeria monocytogenes* and is required for efficient bacterial survival. Mol Genet Genomics 275:344–353.

96. Mohamed W, Sethi S, Darji A, Mraheil MA, Hain T, Chakraborty T. 2010. Antibody Targeting the Ferritin-Like Protein Controls *Listeria* Infection. Infect Immun 78:3306–3314.

97. Polidoro M, De Biase D, Montagnini B, Guarrera L, Cavallo S, Valenti P, Stefanini S, Chiancone E. 2002. The expression of the dodecameric ferritin in *Listeria* spp. is induced by iron limitation and stationary growth phase. Gene 296:121–128.

98. Hammer ND, Reniere ML, Cassat JE, Zhang Y, Hirsch AO, Indriati Hood M, Skaar EP. 2013. Two heme-dependent terminal oxidases power *Staphylococcus aureus* organ-specific colonization of the vertebrate host. mBio 4:e00241-13.

99. Corbett D, Goldrick M, Fernandes VE, Davidge K, Poole RK, Andrew PW, Cavet J, Roberts IS. 2017. *Listeria monocytogenes* has both a bd-type and an aa3-type terminal oxidase which allow growth in different oxygen levels and both are important in infection. Infect Immun 85:e00354-17.

100. Jongbloed JDH, Grieger U, Antelmann H, Hecker M, Nijland R, Bron S, Dijl JMV. 2004. Two minimal Tat translocases in *Bacillus*. Mol Microbiol 54:1319–1325.

101. Miethke M, Monteferrante CG, Marahiel MA, van Dijl JM. 2013. The *Bacillus subtilis* EfeUOB transporter is essential for high-affinity acquisition of ferrous and ferric iron. Biochim Biophys Acta BBA - Mol Cell Res 1833:2267–2278.

102. Ledala N, Sengupta M, Muthaiyan A, Wilkinson BJ, Jayaswal RK. 2010. Transcriptomic response of *Listeria monocytogenes* to iron limitation and Fur mutation. Appl Environ Microbiol 76:406–416.

103. dos Santos PT, Larsen PT, Menendez-Gil P, Lillebæk EMS, Kallipolitis BH. 2018. *Listeria monocytogenes* Relies on the Heme-Regulated Transporter hrtAB to Resist Heme Toxicity and Uses Heme as a Signal to Induce Transcription of lmo1634, Encoding *Listeria* Adhesion Protein. Front Microbiol 9.

104. Hingston PA, Piercey MJ, Hansen LT. 2015. Genes Associated with Desiccation and Osmotic Stress in *Listeria monocytogenes* as Revealed by Insertional Mutagenesis. Appl Environ Microbiol 81:5350–5362.

105. Vasconcelos JA, Deneer HG. 1994. Expression of superoxide dismutase in *Listeria monocytogenes*. Appl Environ Microbiol 60:2360–2366.

106. Archambaud C, Nahori M-A, Pizarro-Cerda J, Cossart P, Dussurget O. 2006. Control of *Listeria* superoxide dismutase by phosphorylation. J Biol Chem 281:31812–31822.

107. Gray MJ, Freitag NE, Boor KJ. 2006. How the Bacterial Pathogen *Listeria monocytogenes* Mediates the Switch from Environmental Dr. Jekyll to Pathogenic Mr. Hyde. Infect Immun 74:2505.

108. Ireton K. 2007. Entry of the bacterial pathogen *Listeria monocytogenes* into mammalian cells. Cell Microbiol 9:1365–1375.

109. Pillich H, Puri M, Chakraborty T. 2017. ActA of *Listeria monocytogenes* and Its Manifold Activities as an Important Listerial Virulence Factor, p. 113–132. *In* Mannherz, HG (ed.), The Actin Cytoskeleton and Bacterial Infection. Springer International Publishing, Cham.

110. Rafelski SM, Theriot JA. 2006. Mechanism of polarization of *Listeria monocytogenes* surface protein ActA. Mol Microbiol 59:1262–1279.

111. Frirdich E, Biboy J, Adams C, Lee J, Ellermeier J, Gielda LD, DiRita VJ, Girardin SE, Vollmer W, Gaynor EC. 2012. Peptidoglycan-Modifying Enzyme Pgp1 Is Required for Helical Cell Shape and Pathogenicity Traits in *Campylobacter jejuni.* PLOS Pathog 8:e1002602.

112. Sycuro LK, Pincus Z, Gutierrez KD, Biboy J, Stern CA, Vollmer W, Salama NR. 2010. Peptidoglycan Crosslinking Relaxation Promotes *Helicobacter pylori*'s Helical Shape and Stomach Colonization. Cell 141:822–833.

113. Taylor JA, Bratton BP, Sichel SR, Blair KM, Jacobs HM, DeMeester KE, Kuru E, Gray J, Biboy J, VanNieuwenhze MS, Vollmer W, Grimes CL, Shaevitz JW, Salama NR. 2020. Distinct cytoskeletal proteins define zones of enhanced cell wall synthesis in *Helicobacter pylori.* eLife 9:e52482.

114. Bartlett TM, Bratton BP, Duvshani A, Miguel A, Sheng Y, Martin NR, Nguyen JP, Persat A, Desmarais SM, VanNieuwenhze MS, Huang KC, Zhu J, Shaevitz JW, Gitai Z. 2017. A Periplasmic Polymer Curves *Vibrio cholerae* and Promotes Pathogenesis. Cell 168:172-185.e15.

115. Kuhn M, Goebel W. 1989. Identification of an extracellular protein of *Listeria monocytogenes* possibly involved in intracellular uptake by mammalian cells. Infect Immun 57:55–61.

116. Alonzo F, McMullen PD, Freitag NE. 2011. Actin Polymerization Drives Septation of *Listeria monocytogenes* namA Hydrolase Mutants, Demonstrating Host Correction of a Bacterial Defect. Infect Immun 79:1458–1470.

117. Siegrist MS, Aditham AK, Espaillat A, Cameron TA, Whiteside SA, Cava F, Portnoy DA, Bertozzi CR. 2015. Host actin polymerization tunes the cell division cycle of an intracellular pathogen. Cell Rep 11:499–507.

118. Justice SS, Hunstad DA, Cegelski L, Hultgren SJ. 2008. Morphological plasticity as a bacterial survival strategy. Nat Rev Microbiol 6:162–168.

119. Yang DC, Blair KM, Salama NR. 2016. Staying in Shape: the Impact of Cell Shape on Bacterial Survival in Diverse Environments. Microbiol Mol Biol Rev 80:187–203.

120. Isom LL, Khambatta ZS, Moluf JL, Akers DF, Martin SE. 1995. Filament Formation in *Listeria monocytogenes*. J Food Prot 58:1031–1033.

121. Vail KM, McMullen LM, Jones TH. 2012. Growth and filamentation of cold-adapted, log-phase *Listeria monocytogenes* exposed to salt, acid, or alkali stress at 3°C. J Food Prot 75:2142–2150.

122. Rowan NJ, Anderson JG. 1998. Effects of Above-Optimum Growth Temperature and Cell Morphology on Thermotolerance of *Listeria monocytogenes* Cells Suspended in Bovine Milk. Appl Environ Microbiol 64:2065–2071.

123. Villanueva M, Jousselin A, Baek KT, Prados J, Andrey DO, Renzoni A, Ingmer H, Frees D, Kelley WL. 2016. Rifampin Resistance rpoB Alleles or Multicopy Thioredoxin/Thioredoxin Reductase Suppresses the Lethality of Disruption of the Global Stress Regulator spx in *Staphylococcus aureus*. J Bacteriol 198:2719–2731.

124. Port GC, Cusumano ZT, Tumminello PR, Caparon MG. 2017. SpxA1 and SpxA2 Act Coordinately To Fine-Tune Stress Responses and Virulence in *Streptococcus pyogenes*. mBio 8:e00288-17.

125. Pincus Z, Theriot JA. 2007. Comparison of quantitative methods for cell-shape analysis. J Microsc 227:140–156.

126. Prendergast FG, Haugland RP, Callahan PJ. 1981. 1-[4-(Trimethylamino)phenyl]-6-phenylhexa-1,3,5-triene: synthesis, fluorescence properties, and use as a fluorescence probe of lipid bilayers. Biochemistry 20:7333–7338.

127. Terzakis JA. 1968. Uranyl acetate, a stain and a fixative. J Ultrastruct Res 22:168–184.

128. Kawai Y, Moriya S, Ogasawara N. 2003. Identification of a protein, YneA, responsible for cell division suppression during the SOS response in *Bacillus subtilis*. Mol Microbiol 47:1113–1122.

129. Bigot A, Pagniez H, Botton E, Fréhel C, Dubail I, Jacquet C, Charbit A, Raynaud C. 2005. Role of FliF and FliI of *Listeria monocytogenes* in Flagellar Assembly and Pathogenicity. Infect Immun 73:5530–5539.

130. O'Neil HS, Marquis H. 2006. *Listeria monocytogenes* Flagella Are Used for Motility, Not as Adhesins, To Increase Host Cell Invasion. Infect Immun 74:6675–6681.

131. Kaplan Zeevi M, Shafir NS, Shaham S, Friedman S, Sigal N, Nir Paz R, Boneca IG, Herskovits AA. 2013. *Listeria monocytogenes* Multidrug Resistance Transporters and Cyclic Di-AMP, Which Contribute to Type I Interferon Induction, Play a Role in Cell Wall Stress. J Bacteriol 195:5250–5261.

132. Abachin E, Poyart C, Pellegrini E, Milohanic E, Fiedler F, Berche P, Trieu-Cuot P. 2002. Formation of D-alanyl-lipoteichoic acid is required for adhesion and virulence of *Listeria monocytogenes*. Mol Microbiol 43:1–14.

133. Rismondo J, Schulz LM, Yacoub M, Wadhawan A, Hoppert M, Dionne MS, Gründling A. 2021. EslB Is Required for Cell Wall Biosynthesis and Modification in *Listeria monocytogenes*. J Bacteriol 203:e00553-20.

134. Webb AJ, Karatsa-Dodgson M, Gründling A. 2009. Two-enzyme systems for glycolipid and polyglycerolphosphate lipoteichoic acid synthesis in *Listeria monocytogenes*. Mol Microbiol 74:299–314.

135. Yu Y, Dempwolff F, Oshiro RT, Gueiros-Filho FJ, Jacobson SC, Kearns DB. 2021. The division defect of a *Bacillus subtilis* minD noc double mutant can be suppressed by Spx-dependent and Spx-independent mechanisms. J Bacteriol JB0024921.

136. Way SS, Thompson LJ, Lopes JE, Hajjar AM, Kollmann TR, Freitag NE, Wilson CB. 2004. Characterization of flagellin expression and its role in *Listeria monocytogenes* infection and immunity. Cell Microbiol 6:235–242.

137. Smith GA, Portnoy DA, Theriot JA. 1995. Asymmetric distribution of the *Listeria monocytogenes* ActA protein is required and sufficient to direct actin-based motility. Mol Microbiol 17:945–951.

138. Rafelski SM, Theriot JA. 2005. Bacterial Shape and ActA Distribution Affect Initiation of *Listeria monocytogenes* Actin-Based Motility. Biophys J 89:2146–2158.

139. Clifford DP, Repine JE. 1982. Hydrogen peroxide mediated killing of bacteria. Mol Cell Biochem 49:143–149.

140. Conte MP, Longhi C, Polidoro M, Petrone G, Buonfiglio V, Santo SD, Papi E, Seganti L, Visca P, Valenti P. 1996. Iron availability affects entry of *Listeria monocytogenes* into the enterocytelike cell line Caco-2. Infect Immun 64:3925–3929.

141. Conte MP, Longhi C, Petrone G, Polidoro M, Valenti P, Seganti L. 2000. Modulation of actA gene expression in *Listeria monocytogenes* by iron. J Med Microbiol 49:681–683.

142. Böckmann R, Dickneite C, Middendorf B, Goebel W, Sokolovic Z. 1996. Specific binding of the *Listeria monocytogenes* transcriptional regulator PrfA to target sequences requires additional factor(s) and is influenced by iron. Mol Microbiol 22:643–653.

143. Krawczyk-Balska A, Lipiak M. 2013. Critical Role of a Ferritin-Like Protein in the Control of *Listeria monocytogenes* Cell Envelope Structure and Stability under β-lactam Pressure. PLOS ONE 8:e77808.

144. Olsen KN, Larsen MH, Gahan CGM, Kallipolitis B, Wolf XA, Rea R, Hill C, Ingmer H. 2005. The Dps-like protein Fri of *Listeria monocytogenes* promotes stress tolerance and intracellular multiplication in macrophage-like cells. Microbiology 151:925–933.

145. Fiorini F, Stefanini S, Valenti P, Chiancone E, De Biase D. 2008. Transcription of the *Listeria monocytogenes* fri gene is growth-phase dependent and is repressed directly by Fur, the ferric uptake regulator. Gene 410:113–121.

146. Ledala N, Sengupta M, Muthaiyan A, Wilkinson BJ, Jayaswal RK. 2010. Transcriptomic Response of *Listeria monocytogenes* to Iron Limitation and fur Mutation. Appl Environ Microbiol 76:406–416.

147. Cesinger MR, Daramola OI, Kwiatkowski LM, Reniere ML. 2022. The Transcriptional Regulator SpxA1 Influences the Morphology and Virulence of *Listeria monocytogenes*. Infect Immun 0:e00211-22.

148. Rea RB, Gahan CGM, Hill C. 2004. Disruption of Putative Regulatory Loci in *Listeria monocytogenes* Demonstrates a Significant Role for Fur and PerR in Virulence. Infect Immun 72:717–727.

149. Schäfer H, Heinz A, Sudzinová P, Voß M, Hantke I, Krásný L, Turgay K. 2019. Spx, the central regulator of the heat and oxidative stress response in *B. subtilis,* can repress transcription of translation-related genes. Mol Microbiol 111:514–533.

150. Kaval KG, Rismondo J, Halbedel S. 2014. A function of DivIVA in *Listeria monocytogenes* division site selection. Mol Microbiol 94:637–654.

151. Yao J, Rock CO. 2013. Phosphatidic Acid Synthesis in Bacteria. Biochim Biophys Acta 1831:495–502.

152. Yao J, Ericson ME, Frank MW, Rock CO. 2016. Enoyl-Acyl Carrier Protein Reductase I (FabI) Is Essential for the Intracellular Growth of *Listeria monocytogenes*. Infect Immun 84:3597–3607.

153. Sastre DE, Pulschen AA, Basso LGM, Benites Pariente JS, Marques Netto CGC, Machinandiarena F, Albanesi D, Navarro MVAS, de Mendoza D, Gueiros-Filho FJ. 2020. The phosphatidic acid pathway enzyme PlsX plays both catalytic and channeling roles in bacterial phospholipid synthesis. J Biol Chem 295:2148–2159.

154. Takada H, Fukushima-Tanaka S, Morita M, Kasahara Y, Watanabe S, Chibazakura T, Hara H, Matsumoto K, Yoshikawa H. 2014. An essential enzyme for phospholipid synthesis associates with the *Bacillus subtilis* divisome. Mol Microbiol 91:242–255.

155. Shen Y, Naujokas M, Park M, Ireton K. 2000. InlB-Dependent Internalization of *Listeria* Is Mediated by the Met Receptor Tyrosine Kinase. Cell 103:501–510.

156. Phelps CC, Vadia S, Arnett E, Tan Y, Zhang X, Pathak-Sharma S, Gavrilin MA, Seveau S. 2018. Relative Roles of Listeriolysin O, InlA, and InlB in *Listeria monocytogenes* Uptake by Host Cells. Infect Immun 86:e00555-18.

157. Drolia R, Bhunia AK. 2019. Crossing the Intestinal Barrier via *Listeria* Adhesion Protein and Internalin A. Trends Microbiol 27:408–425.

158. Dons L, Eriksson E, Jin Y, Rottenberg ME, Kristensson K, Larsen CN, Bresciani J, Olsen JE. 2004. Role of flagellin and the two-component CheA/CheY system of *Listeria monocytogenes* in host cell invasion and virulence. Infect Immun 72:3237–3244.

159. Bécavin C, Bouchier C, Lechat P, Archambaud C, Creno S, Gouin E, Wu Z, Kühbacher A, Brisse S, Pucciarelli MG, García-del Portillo F, Hain T, Portnoy DA, Chakraborty T, Lecuit M, Pizarro-Cerdá J, Moszer I, Bierne H, Cossart P. 2014. Comparison of widely used *Listeria monocytogenes* strains EGD, 10403S, and EGD-e highlights genomic variations underlying differences in pathogenicity. mBio 5:e00969-00914.

160. Zemansky J, Kline BC, Woodward JJ, Leber JH, Marquis H, Portnoy DA. 2009. Development of a mariner-based transposon and identification of *Listeria monocytogenes* determinants, including the peptidyl-prolyl isomerase PrsA2, that contribute to its hemolytic phenotype. J Bacteriol 191:3950–3964.

161. Vincent WJB, Freisinger CM, Lam P, Huttenlocher A, Sauer J-D. 2016. Macrophages mediate flagellin induced inflammasome activation and host defense in zebrafish. Cell Microbiol 18:591–604.

162. Chen C, Nguyen BN, Mitchell G, Margolis SR, Ma D, Portnoy DA. 2018. The Listeriolysin O PEST-like Sequence Co-opts AP-2-Mediated Endocytosis to Prevent Plasma Membrane Damage during *Listeria* Infection. Cell Host Microbe 23:786-795.e5.

163. Halsey CR, Glover RC, Thomason MK, Reniere ML. 2021. The redox-responsive transcriptional regulator Rex represses fermentative metabolism and is required for *Listeria monocytogenes* pathogenesis. PLoS Pathog 17:e1009379.

164. Cesinger MR, Schwardt NH, Halsey CR, Thomason MK, Reniere ML. 2021. Investigating the Roles of *Listeria monocytogenes* Peroxidases in Growth and Virulence. Microbiol Spectr e0044021.

165. Sauer J-D, Sotelo-Troha K, von Moltke J, Monroe KM, Rae CS, Brubaker SW, Hyodo M, Hayakawa Y, Woodward JJ, Portnoy DA, Vance RE. 2011. The N-Ethyl-N-Nitrosourea-Induced Goldenticket Mouse Mutant Reveals an Essential Function of Sting in the In Vivo Interferon Response to *Listeria monocytogenes* and Cyclic Dinucleotides. Infect Immun 79:688–694.

166. Trapnell C, Pachter L, Salzberg SL. 2009. TopHat: discovering splice junctions with RNA-Seq. Bioinforma Oxf Engl 25:1105–1111.

167. Schneider CA, Rasband WS, Eliceiri KW. 2012. NIH Image to ImageJ: 25 years of image analysis. Nat Methods 9:671–675.